Université d'Ottawa · University of Ottawa

Université d'Ottawa • University of Ottawa

FACULTÉ DE ÉTUDES SUPÉRIEURES
ET POSTDOCTORALES

FACULTY OF GRADUATE AND
POSTDOCTORAL STUDIES

Zhaobin SONG
AUTEUR DE LA THÈSE - AUTHOR OF THESIS

Ph.D. (Civil Engineering)
GRADE - DEGREE

Department of Civil Engineering
FACULTÉ, ÉCOLE, DÉPARTEMENT - FACULTY, SCHOOL, DEPARTMENT

TITRE DE LA THÈSE - TITLE OF THE THESIS

Fracture Analysis of Bridges by Spline Finite Strip Method

M.S. Cheung
DIRECTEUR DE LA THÈSE - THESIS SUPERVISOR

CO-DIRECTEUR DE LA THÈSE - THESIS CO-SUPERVISOR

EXAMINATEURS DE LA THÈSE - THESIS EXAMINERS

D. Lau

S. Mirza

M. Mohareb

H. Tanaka

J.-M. De Koninck, Ph.D.
LE DOYEN DE LA FACULTÉ DES ÉTUDES
SUPÉRIEURES ET POSTDOCTORALES

DEAN OF THE FACULTY OF GRADUATE
AND POSTDOCTORAL STUDIES

FRACTURE ANALYSIS OF BRIDGES BY SPLINE FINITE STRIP METHOD

by

Zhaobin Song

Thesis submitted to the

Faculty of Graduate and Postdoctoral Studies

In partial fulfilment of the requirements

For the **PhD** degree in Structural Engineering

Department of Civil Engineering *
Faculty of Engineering
University of Ottawa

* The Doctor of Philosophy Program in Civil Engineering
is a joint program with Carleton University
administered by the Ottawa-Carleton institute in Civil Engineering

Your file Votre référence
ISBN: 0-494-01764-3
Our file Notre référence
ISBN: 0-494-01764-3

Acknowledgments

I would first like to express sincere thanks to my advisor, Professor Moe Shing Cheung, for his thorough guidance, support and patience.

The financial support provided by the Natural Sciences and Engineering Research Council is greatly appreciated.

Special thanks to Dr. Wen Chang Li for his valuable helps.

Finally, I thank my family, my wife, Fan, and my daughter, Gena, for their love and understanding.

ABSTRACT

The primary objective of this thesis is to develop crack strip method and verify the convergency of the method, finally to perform fracture analysis of bridge structures using spline finite strip method. In this thesis, combining the shape function of spline finite strip with the eigenfunction expansions at a crack tip, three types of crack strips, namely anti-plane shear crack strip, plane crack strip and bending crack strip, have been developed, in which cracks are perpendicular to the longitudinal axis of strips and the stress intensity factors can be computed directly. Based on plane crack strips and bending crack strips, the flat shell crack strip is developed for the fracture analysis of box girder bridges. Several case studies have demonstrated the satisfactory convergence of the proposed method. The fracture analysis of different types of bridges have been successfully conducted using these crack strips.

In Chapter 3, the basic model of the crack strip is formed. Substructure technique and extra knots are employed to enhance the efficiency and the convergence of this model. Two Gaussian quadratures for improper integrals are introduced to calculate the singular integral in the crack strip. The efficiencies of these two methods are compared through case studies.

On the basis of anti-plane eigenfunction expansion derived by Tilley (1978), plane eigenfunction expansion by Williams (1957) and bending eigenfunction expansion by Williams (1961) in the area around the crack tip, anti-plane shear crack strip, plane crack strip and bending crack strip are developed in Chapter 4 to 6, respectively. The convergence of the proposed models is generally good as shown by case studies.

In Chapter 7, these crack strip models are applied to the fracture analysis of bridge structures. Based on the plane crack strip and the bending crack strip, flat shell crack strip is formed for the fracture analysis of box girder bridges. The fracture analysis of different types of bridges, such as slab bridge, continuous slab bridge, single - cell box girder bridge and continuous bridge with top-open box girder, are successfully conducted using these crack strips. The leading diagonal terms are replaced by large numbers to deal with those restraints in the continuous bridges.

The present method, i.e., combining the spline finite strip method with the analytical solution for the area around crack tip, provides a new and efficient approach for fracture analysis of structures, especially for the fracture analysis of bridge structures.

CONTENTS

LIST OF FIGURES

LIST OF TABLES

Notations and Definition

a	crack length
$\{A\}$	parameter vector of eigenfunction expansion
b	width of strip
$[B]$	matrix of strain or curvature
C_i	transverse shape function for nodal line ***i***
$[C]$	matrix of transverse shape function
$\{c\}\{d\}\{e\}\{f\}$	spline interpolation coefficient vector
D	$= Et^3 / 12(1-\upsilon^2)$, flexural rigidity
D_x, D_y, D_{xy}, D_1	rigidity parameters
$[D]$	elastic matrix or rigidity matrix
$[e]$, $[E]$	coordinate transformation matrix
E	elastic modulus
$[F]$	$=[L]^{-1}$
$\{\hat{F}\}$	equivalent load vector
G	shear modulus
h	length of longitudinal section
$[H]$	coefficient matrix in eigenfunction expansion
$[J]$	Jacobi matrix
K_I, K_{II}, K_{III}	stress intensity factors in opening mode (Mode I), sliding mode (Mode II) and tearing mode (Mode III)
K_c	material toughness
$[k^e]$	stiffness matrix of traditional spline strip
$[\hat{k}]$	stiffness matrix of crack strip
$[k]$	stiffness matrix corresponding to displacement vector
l	length of the finite strip
$[L]$	matrix of the values of the spline functions at knots
M_x, M_y, M_{xy}	x, y and xy components of bending moment
$[N]$	matrix of shape function
$[N']$	generalized shape function matrix for strains
q	distributed normal load
r	number of spline function knots

t	thickness of the plate
$[T]$	transformation matrix on nodal line between the displacements of nodes and the coefficients of spline function interpolation, or transformation matrix in crack special area between the displacements of knots and the parameters of eigenfunction expansions
u, v, w	displacements in x, y, and z directions
U	transformation matrix from the coefficients $\{A\}$ to the L nodal deflections $\{w\}$
$\{w\}$	L nodal deflections vector
ν	Poisson's ratio
$\{\varepsilon\}$	vector of strains or curvatures
$\kappa_x, \kappa_y, \kappa_{xy}$	x, y and xy curvatures
θ	transverse slope $\partial w/\partial x$
$[\lambda]$	matrix of coordinate transforming
$\{\sigma\}$	vector of stresses or moments
ϕ_i	B_3 spline function centered at y_i
$[\Phi]$	matrix of spline function

Chapter 1

Introduction

The numerical fracture analysis has been one of the most active areas in structural engineering, and the finite element method (FEM) plays an important role in this subject. The finite strip method (FSM) (Cheung, M.S. et al. 1996), as an extension of the finite element method, uses significantly less number of degrees-of-freedom in comparison with the finite element method, and thus is computationally more efficient than the FEM.

The finite strip method is one of the most efficient tools in numerical analysis of bridge structures due to its semi-analytical nature. The earlier finite strip method is limited to regular prismatic structures, whereas today, with development of the spline finite strip method, the application of this method has been extended to various fields, including fracture analysis of structures.

However, most earlier numerical models in fracture analysis experienced the difficulty of dealing

with stress singularity at the crack tip, because ordinary numerical models are ineffective in areas with high stress gradient. Later, some special elements with proper singularities have been developed for the area around crack tip. For example, Williams' eigenfunction expansion has been introduced to model displacements around crack tip in a special element (Wilson 1973, Holston 1976, Cai et al. 1983), and the efficiency of the numerical analysis has been enhanced significantly.

Li (Li et al. 1994) modified the semi-analytical Fourier expansions in the finite strip method for solving the problem of periodically occurring cracks in lay-ups laminates. The approximate model of displacements was formed basing on the conception of stiffness reduction by damage. However, some fracture characteristics such as stress intensity factor and displacement around the crack tips were not present in this formulation.

In 1996, Cheung and Jiang (1996) developed a cracked strip for plane problems by incorporating the Williams' expansion with the spline finite strip displacement model. Thus, the stress intensity factor could be directly computed. However, that model is only applicable to longitudinal cracks in plane spline finite strips.

In this thesis, through the combination of traditional spline finite strips with Tilley's anti-plane eigenfunction expansion (1978), Williams' plane eigenfunction expansion (1957) and Williams' bending eigenfunction expansion(1961) at a crack tip, anti-plane shear crack strip, plane crack strip and bending crack strip are developed, respectively. In which, the cracks are assumed to be perpendicular to the longitudinal axis of strip elements and the stress intensity factors will be directly computed.

Current study incorporates the advantages of both Spline Finite Strip Method and the analytical solution for the area around the crack tip, and provides a new and efficient approach for structural fracture analysis, especially the fracture analysis of bridge structures. Theoretical foundation and some applications in fracture analysis of highway bridges are presented.

1.1 Basic Concepts of Fracture Mechanics

Fracture analysis of structures has been developed in the last 50 years to study the sensitivity of structures to defects, flaws or cracks. In such analysis, an essential work is the evaluation of stresses especially with regard to the high elevation of local stresses around the flaws or cracks, which represents crack propagation mechanisms.

The redistribution of stress in a structure caused by cracks or notches can be worked out by means of linear-elastic stress analysis. Of course, this analysis needs to pay the greatest attention to the high elevation of local stresses around the crack tip which is usually accompanied by some plasticity and other nonlinear effects. Nevertheless, linear-elastic stress analysis properly constructs the basis of most current fracture studies, at least for "small scale yielding" where all substantial nonlinearities are confined within a linear-elastic field around the crack tip. Therefore, the significant characters and parameters of linear-elastic stress field around the crack tip are prime factors in fracture analysis.

1.1.1 Linear Elastic Stress Field around Crack Tip

The surfaces of a crack play a main role in the distribution of stresses around the crack tip, because they are stress-free boundaries of the body. Other remote boundaries and loading forces only affect the intensity of the local stress field at the crack tip.

The stress field around crack tip can be classified into three basic types according to local displacement mode as shown in **Fig. 1.1**. The first mode is defined as opening mode (Mode I),

in which the crack surfaces move directly apart. The second mode is the in-plane shear mode or sliding mode (Mode II), in which the crack surfaces slide over each other perpendicular to the leading edge of the crack. The third mode is the out-of-plane shear mode or tearing mode (Mode III), in which crack surfaces slide with respect to one another parallel to the leading edge. The superposition of these three modes may sufficiently present the most general three-dimensional cases of local deformation and stress field at the crack tip.

To determine the stress and displacement fields related to each mode, the most direct approach follows Irwin's method (1957), which is based on Westergaard's method (1939). Modes I and II can be regarded as two-dimensional elastic problems, which are respectively divided into symmetric and skew-symmetric with respect to the crack plane. Mode III can be regarded as two-dimensional pure shear (or torsion) problem. For a semi-infinite through crack in an infinite plate under proper uniform loading on infinite ends, the resulting stress and displacement fields are given below, referring to the notation in **Fig. 1.2**,

Mode I:

$$\sigma_x = \frac{K_I}{\sqrt{2\pi r}}\cos\frac{\theta}{2}[1-\sin\frac{\theta}{2}\sin\frac{3\theta}{2}]+O(r^{1/2})$$
$$\sigma_y = \frac{K_I}{\sqrt{2\pi r}}\cos\frac{\theta}{2}[1+\sin\frac{\theta}{2}\sin\frac{3\theta}{2}]+O(r^{1/2})$$
$$\tau_{xy} = \frac{K_I}{\sqrt{2\pi r}}\cos\frac{\theta}{2}\sin\frac{\theta}{2}\cos\frac{3\theta}{2}]+O(r^{1/2}) \qquad (1-1)$$

where K_I is called the stress intensity factor in Mode I, which is a measure of stress concentration around the crack tip, and O ($r^{1/2}$) represents higher-order terms. More details about the stress intensity factor will be presented later.

For plane strain(with higher-order terms omitted in the area around the crack tip)

$$\sigma_z = \nu(\sigma_x + \sigma_y), \qquad \tau_{xz} = \tau_{yz} = 0$$

$$u = \frac{K_I}{G}\sqrt{\frac{r}{2\pi}}\cos\frac{\theta}{2}[1 - 2\nu + \sin^2\frac{\theta}{2}]$$

$$v = \frac{K_I}{G}\sqrt{\frac{r}{2\pi}}\sin\frac{\theta}{2}[2 - 2\nu - \cos^2\frac{\theta}{2}]$$

$$w = 0 \qquad (1-2)$$

where G is the shear modulus.

Mode II:

$$\sigma_x = -\frac{K_{II}}{\sqrt{2\pi r}}\sin\frac{\theta}{2}[2 + \cos\frac{\theta}{2}\cos\frac{3\theta}{2}] + O(r^{1/2})$$

$$\sigma_y = \frac{K_{II}}{\sqrt{2\pi r}}\cos\frac{\theta}{2}\sin\frac{\theta}{2}\sin\frac{3\theta}{2} + O(r^{1/2})$$

$$\tau_{xy} = \frac{K_{II}}{\sqrt{2\pi r}}\cos\frac{\theta}{2}[1 - \sin\frac{\theta}{2}\sin\frac{3\theta}{2}] + O(r^{1/2}) \qquad (1-3)$$

in which K_{II} is the stress intensity factor in Mode II.

For plane strain(with higher-order terms omitted in the area around the crack tip)

$$\sigma_z = \nu(\sigma_x + \sigma_y), \qquad \tau_{xz} = \tau_{yz} = 0$$

$$u = \frac{K_{II}}{G}\sqrt{\frac{r}{2\pi}}\sin\frac{\theta}{2}[2 - 2\nu + \cos^2\frac{\theta}{2}]$$

$$v = \frac{K_{II}}{G}\sqrt{\frac{r}{2\pi}}\cos\frac{\theta}{2}[-1 + 2\nu + \sin^2\frac{\theta}{2}]$$

$$w = 0 \qquad (1-4)$$

Mode III:

$$\tau_{xz} = -\frac{K_{III}}{\sqrt{2\pi r}}\sin\frac{\theta}{2} + O(r^{1/2})$$

$$\tau_{yz} = \frac{K_{III}}{\sqrt{2\pi r}}\cos\frac{\theta}{2} + O(r^{1/2})$$

$$\sigma_x = \sigma_y = \sigma_z = \tau_{xy} = 0$$

$$w = \frac{K_{III}}{G}\sqrt{\frac{2r}{\pi}}\sin\frac{\theta}{2}$$

$$u = v = 0 \qquad (1-5)$$

in which K_{III} is the stress intensity factor in Mode III.

Equations (1 – 2) and (1 – 4) are formed for the case of plane strain (i.e., w = 0), but they can be altered to the case of plane stress easily by taking $\sigma_z = 0$ and replacing Poisson's ratio, ν, by $\nu/(1+\nu)$.

Normally, in equations (1 – 1) to (1 – 5), higher-order terms, i.e. O ($r^{1/2}$) are omitted, since these higher-order terms become negligible compared with the leading term $1/\sqrt{r}$ while r becomes smaller and smaller. Therefore, the first term in each expression for stresses or displacements represents the main portion of linear elastic stress or displacement field around the crack tip.

Since parameters, K_I, K_{II}, and K_{III} are independent of coordinates r and θ, they are viewed as the intensity of the stress fields around the crack tip. In other words, they are regarded as the strengths of $1/\sqrt{r}$ stress singularities at the crack tip from mathematical standpoint. Their values depend on other boundaries of the body and the applied loads. Consequently, the formulas of their elevation are obtained by stress analysis for a given configuration and loading.

Similarly, from a physical point of view, K_I, K_{II}, and K_{III} may be considered to represent the intensity of the linear-elastic stress distribution around a crack tip, where small amounts of plasticity or other nonlinearities at the crack tip merged into the linear-elastic field are much less than stress intensity and do not significantly disturb the field. Therefore, a given combination of values for K_I, K_{II}, and K_{III} can represent a unique crack tip stress field in the case of small-scale yielding. Because the fracture process of materials may be affected by the stress field environment around crack tip, the intensity factors K_I, K_{II}, and K_{III} play a great role as fracture correlation parameters in current practice. For this reason, the formulas of K_I, K_{II}, and K_{III} are tabulated for various configurations and loadings in material property table.

Finally, equations (1 – 1) to (1 – 5) show that stress intensity factors have units of

$$(force) \times (length)^{-3/2}$$

It is obvious that stress intensity factors are proportional to the applied loads and they must contain other characteristic lengths on a dimensional basis, such as crack size. This result is a main feature of flaw-size effects in fracture analysis, which indeed are observed and further implies that these size effects can be fully analyzed only if stress analysis includes these effects.

If a structure experiences massive plastic deformation, the above concepts that are based on linear elasticity are not valid. Other approaches based on energy theories are found to be more realistic for predicting the behavior of crack propagation. Among these, J-integration and energy release rate are the most commonly used methods to predict the possibility of structural failure. Those are beyond the scope of the current study. Readers who are interested in these topics may consult some references, e.g. Anderson (1995), Sih (1973) and Tada et al. (2000).

1.1.2 Material Fracture Toughness

The fracture toughness of a material is defined as the capability of the material to resist fracture when a crack exists. Experiments show that the crack will propagate at a progressive rate when the stress intensity factor reaches its critical value i.e., the material toughness K_{c_n} which is a material property and its value can be obtained from material tests (Anderson 1995). The value of K_c also varies under influence of environment. Materials with high K_c at normal temperature may show very low fracture resistance under freezing temperature.

1.1.3 The Fracture Mechanics Approach in Design

Contrasting with the traditional approach for structural design and material selection, the fracture mechanics approach has three important variables, i.e., the applied stress, the fracture toughness and the flaw size rather than two, i.e. the applied stress and the strength as in the traditional approach. Fracture toughness replaces strength as the relevant material property. Fracture mechanics quantifies the critical combinations of these three variables.

There are two alternative approaches for fracture analysis, i.e. the energy criterion and the stress intensity approach. These two approaches are equivalent in certain circumstances. The energy criterion and the energy release rate are discussed in Anderson (1995), Sih (1973) and Tada et al. (2000).

The stress intensity approach states that, if one assumes that the material fails locally at some critical combination of stresses and strains, the fracture must occur at a critical stress intensity, K_c. Namely, failure occurs when $K = K_c$.

1.1.4 Williams' Expansion in Plane Strain/Stress Problem

For the general case of a stationary crack embedded in infinite plane, Williams (1957) developed an eigenfunction expansion for the elastic stress distributions around cracks, based on existing solutions from other researchers. It has been proven that stress functions $\chi(r,\theta)$, i.e. solutions of equilibrium in the absence of body forces, $\nabla^4\chi(r,\theta) = 0$, of the form (**Fig. 1.2**)

$$\chi(r,\theta) = r^{\frac{3}{2}}[a_1(-\cos\frac{\theta}{2} - \frac{1}{3}\cos\frac{3\theta}{2}) + b_1(-\sin\frac{\theta}{2} - \sin\frac{3\theta}{2})] + a_2 r^2[1-\cos 2\theta] + O(r^{5/2}) \qquad (1-6)$$

will satisfy the conditions of stress-free on crack surfaces, in which a_k and b_k represent the polynomial coefficients to be determined by other geometry or loading conditions. From which the associated stresses can be found:

$$\sigma_\theta(r,\theta) = \frac{\partial^2\chi}{\partial r^2} = \frac{1}{4r^{1/2}}[a_1(-3\cos\frac{\theta}{2} - \cos\frac{3\theta}{2}) + b_1(-3\sin\frac{\theta}{2} - 3\sin\frac{3\theta}{2})] + 4a_2\sin^2\theta + O(r^{1/2}) \qquad (1-7)$$

$$\sigma_r(r,\theta) = \nabla^2\chi - \sigma_\theta = \frac{1}{4r^{1/2}}[a_1(-5\cos\frac{\theta}{2} + \cos\frac{3\theta}{2}) + b_1(-5\sin\frac{\theta}{2} + 3\sin\frac{3\theta}{2})] + 4a_2\cos^2\theta + O(r^{1/2}) \qquad (1-8)$$

$$\tau_{r\theta}(r,\theta) = -\frac{\partial}{\partial r}(\frac{1}{r}\frac{\partial\chi}{\partial\theta}) = \frac{1}{4r^{1/2}}[a_1(-\sin\frac{\theta}{2} - \sin\frac{3\theta}{2}) + b_1(\cos\frac{\theta}{2} + 3\cos\frac{3\theta}{2})] - 2a_2\sin 2\theta + O(r^{1/2}) \qquad (1-9)$$

The stress intensity factors, K_I for the opening mode and K_{II} for the sliding mode, which are regarded as the strengths of $1/\sqrt{r}$ stress singularities, can be respectively obtained from the leading terms of the Williams' expansion in the form of

$$K_I = G\sqrt{2\pi}\cdot|a_1|, \qquad K_{II} = G\sqrt{2\pi}\cdot|b_1| \tag{1-10}$$

1.1.5 Williams' Expansion for Bending Stress Distribution

When a plate is subjected to either symmetrical or anti-symmetrical bending, the problem in terms of the usual linear small-deflection theory for plates in bending is formulated by an appropriate differential equation of the deflection $w(r,\theta)$:

$$\nabla^4 w(r,\theta) = q(r,\theta)/D \tag{1-11}$$

where D is known as the flexural rigidity of the plate and

$$D = \frac{Et^3}{12(1-\upsilon^2)} \tag{1-12}$$

t is the thickness of the plate, E and ν are the elastic modulus and Poisson's ratio of the material respectively, while q represents the distributed normal load.

Considering the boundary conditions along crack surfaces ($\theta = \pm\pi$), the characteristic solutions

are of the form

$$
\begin{aligned}
w(r,\theta) = r^{\frac{3}{2}}\{-[\cos\frac{3\theta}{2} - \frac{3(1-\nu)}{7+\nu}\cos\frac{\theta}{2}]a_1 + [\sin\frac{3\theta}{2} - \frac{3(1-\nu)}{5+3\nu}\sin\frac{\theta}{2}]b_1\} \\
+ r^2\{[\cos 2\theta + \frac{1-\nu}{7+\nu}]a_2 + [\sin 2\theta]b_2\} + \cdots \quad \cdots \\
+ r^{\frac{n+2}{2}}\{(-1)^n[\cos\frac{(n+2)\theta}{2} + \frac{(4n-7)(1-\nu)}{7+\nu}\cos\frac{n-2}{2}\theta]a_n \\
+ [\sin\frac{(n+2)\theta}{2} - \frac{(4n-7)(1-\nu)}{5+3\nu}\sin\frac{(n-2)\theta}{2}]b_n\}
\end{aligned}
\tag{1-13}
$$

The stresses σ_r, σ_θ and $\tau_{r\theta}$ are assumed to be linearly distributed through the thickness of the plate and may be expressed in a normalized form as

$$
\begin{aligned}
\frac{2\sigma_r}{3G} = \frac{z}{\sqrt{r}}[(\cos\frac{3\theta}{2} - \frac{3+5\nu}{7+\nu}\cos\frac{\theta}{2})a_1 + (-\sin\frac{3\theta}{2} + \frac{3+5\nu}{5+3\nu}\sin\frac{\theta}{2})b_1] \\
- \frac{8}{3}z[(1+\cos 2\theta)a_2 + (\sin 2\theta)b_2] + O(r^{1/2})
\end{aligned}
\tag{1-14}
$$

$$
\begin{aligned}
\frac{2\sigma_\theta}{3G} = \frac{z}{\sqrt{r}}[(-\cos\frac{3\theta}{2} - \frac{5+3\nu}{7+\nu}\cos\frac{\theta}{2})a_1 + (\sin\frac{3\theta}{2} + \sin\frac{\theta}{2})b_1] \\
- \frac{8}{3}z[(1-\cos 2\theta)a_2 + (\sin 2\theta)b_2] + O(r^{1/2})
\end{aligned}
\tag{1-15}
$$

$$
\begin{aligned}
\frac{2\tau_{r\theta}}{3G} = \frac{z}{\sqrt{r}}[(-\sin\frac{3\theta}{2} + \frac{1-\nu}{7+\nu}\sin\frac{\theta}{2})a_1 + (-\cos\frac{3\theta}{2} + \frac{1-\nu}{5+3\nu}\cos\frac{\theta}{2})b_1] \\
+ \frac{8}{3}z[(\sin 2\theta)a_2 - (\cos 2\theta)b_2] + O(r^{1/2})
\end{aligned}
\tag{1-16}
$$

Then, the stress intensity factors K_I for opening mode and K_{II} for sliding mode can be obtained from the leading terms of the Williams' expansion according to the general form of $K = \sigma\sqrt{\pi a}$.

1.1.6 Tilly Expansion in Anti-Plane Problem

Anti-plane strain deformation is said to occur when there is only one non-zero displacement component which by convention is stipulated to be in the z-direction of an x, y, z Cartesian co-ordinate system. This displacement is a harmonic function of x and y in two dimensions, such as those cylindrical rods subjected to shear, bending or twisting loads (G. C. Sih 1973). The equilibrium equation is written as:

$$\frac{\partial^2 w}{\partial x^2} + \frac{\partial^2 w}{\partial y^2} = 0 \quad or \quad \nabla^2 w = 0 \qquad (1-17)$$

The behavior of $w(x,y)$ near a crack tip may be found by considering a semi-infinite crack in an infinite plate. In terms of polar co-ordinates, r, θ, centered on the crack tip with the crack surfaces at $\theta = \pm\pi$, the deflection w is the function of r, θ, i.e. $w = w(r, \theta)$. Because the shear stress $\tau_{\theta r} = \frac{G}{r}\frac{\partial w}{\partial \theta}$ on the crack surfaces is zero, the following boundary condition holds:

$$\frac{\partial w(r, \pm\pi)}{\partial \theta} = 0 \qquad (1-18)$$

The polar co-ordinate form of equation (1 – 17) is

$$r\frac{\partial^2 w}{\partial r^2} + \frac{\partial w}{\partial r} + \frac{1}{r}\frac{\partial^2 w}{\partial \theta^2} = 0 \qquad (1-19)$$

Tilley (1978) gave the solution for (1 – 19) satisfying the boundary conditions (1 – 18). It is

$$w(r,\theta) = \sum_{n=0}^{\infty} \{A_n r^{(2n+1)/2} \sin[(2n+1)\theta/2] + B_n r^{n+1} \cos[(n+1)\theta]\} \qquad (1-20)$$

where A_n , B_n are coefficients to be determined by other geometry or loading conditions.

If, however, the plate and loading are symmetric along crack edge, an additional boundary condition i.e., $w(r, 0) = 0$ $(r \geq 0)$ applies, resulting in $B_n = 0$ for all n and thus,

$$w(r,\theta) = \sum_{n=0}^{\infty} A_n r^{(2n+1)/2} \sin[(2n+1)\theta/2] \qquad (1-21)$$

In some numerical methods, constants A_n are determined explicitly. However, one is usually only interested in the first of these, namely A_0, which is associated with the mode *III* stress intensity factor, K_{III}, by

$$K_{III} = \sqrt{\frac{\pi}{2}} G A_0 \qquad (1-22)$$

Furthermore, it is often convenient to normalize K_{III} by the value $\sigma_0\sqrt{\pi a}$, where σ_0 is the shear stress applied and ***a*** is the crack length. Thus, the normalized stress intensity factor, K_{III}^N , is obtained as

$$K_{III}^N = \frac{G A_0}{\sigma_0 \sqrt{2a}} \qquad (1-23)$$

1.2 Numerical Fracture Analysis

The numerical fracture analysis by Finite Element Method (FEM) (Luxmoore and Owen 1978, 1984) has been one of the most attractive methods in structural engineering. Unfortunately, traditional FEM does not work well to represent the transition from infinite stresses at the tip of a crack to finite stresses elsewhere and to get stress intensity factor directly. This is the common drawback of traditional FEM in stress analysis. However, some special crack tip elements with the proper singularities were developed. Examples of such method are the special crack tip element with a crack tip eigenfunction expansion (Williams' expansion) as the displacement model (Wilson 1973, Holston 1976, Cai et al. 1983), an element formulation(Byskov 1970) based on classical singularity displacement function by Muskhelishvili (1963), and rectangular element containing a crack (Walsh 1971) using singular displacement fields derived from work by Leicester (1971). Thus, the application of FEM has been extended to fracture analysis. A further problem is that for most actual structures, a full finite element analysis is often both extravagant and unnecessary, and sometimes even impossible.

Boundary elements method (BEM) (Beskos 1989) is a more efficient numerical method in structural engineering, because only the boundary parameters are included in the final matrix equation. With the development of special singular boundary elements, a boundary element has been used in fracture analysis of realistic structures (Mason et al. 1984, Ohtmer 1984). This method, however, requires mathematical analysis of singular integral equations for various problems. This analysis is time consuming and is possible only for simple structures.

Finite strip method was rarely used in numerical fracture analysis until the nineteen nineties. For all the articles I searched, there are only two articles in numerical fracture analysis by finite strip

method or spline finite strip method.

Li (Li et al. 1994) modified the semi-analytical Fourier expansions in the finite strip method for solving the problem of periodically occurring cracks in lay-ups laminates, and the displacement components were assumed to take the form:

$$
\begin{aligned}
U_n &= U_n^h \frac{x}{l} + \sum_{k=1}^{K_n} U_n^k \sin\frac{k\pi x}{l} \\
V_n &= V_n^h \frac{x}{l} + \sum_{k=1}^{K_n} V_n^k \sin\frac{k\pi x}{l} \\
W_n &= W_n^h (\frac{x}{l})^2 + W_n^0 + \sum_{k=1}^{K_n} W_n^k \cos\frac{k\pi x}{l}
\end{aligned}
\qquad (1-24)
$$

where l was the period length of the occurred crack, U_n, V_n and W_n are nodal displacements in x, y, and z directions, and U_n^h, V_n^h, W_n^h, W_n^0, U_n^k, V_n^k and W_n^k are unknown constants to be determined. The approximate model of displacements was formed basing on the conception of stiffness reduction by damage. However, some fracture characteristics such as stress intensity factor and displacement around the crack tips, which play main role in fracture analysis, were not present in this formulation.

Similar to FEM, the spline finite strip takes the nodal displacements as unknown parameters. As a result, it becomes possible to couple with the above mentioned special crack strip elements. In 1996, Cheung and Jiang (1996) developed a cracked strip for plane problems by incorporating the Williams' expansion with the spline finite strip displacement model in polar coordinates:

$$
\begin{aligned}
u_r &= \sum_{i=1}^{n} (\frac{r}{R})^{i/2} [a_i F_{ei}(\theta) + b_i F_{oi}(\theta)] + u_0 \sin\theta + v_0 \cos\theta \\
u_\theta &= \sum_{i=1}^{n} (\frac{r}{R})^{i/2} [a_i G_{oi}(\theta) + b_i G_{ei}(\theta)] + u_0 \cos\theta - v_0 \sin\theta
\end{aligned}
\qquad (1-25)
$$

where R is some characteristic length, u_0 and v_0 represent the rigid-body motion, and a_i, b_i are generalized displacement parameters. In which

$$F'_{ei} = (1-\frac{i}{2})(\frac{i-6}{2}+4\upsilon)\sin(\frac{i}{2}-1)\theta+(\frac{i}{2}+1)[\frac{i}{2}+(-1)^i]\sin(\frac{i}{2}+1)\theta$$

$$G'_{oi} = (\frac{i}{2}-1)(-\frac{i+6}{2}+4\upsilon)\cos(\frac{i}{2}-1)\theta-(\frac{i}{2}+1)[\frac{i}{2}+(-1)^i]\cos(\frac{i}{2}+1)\theta$$

$$F'_{oi} = (\frac{i}{2}-1)(\frac{i-6}{2}+4\upsilon)\cos(\frac{i}{2}-1)\theta-(\frac{i}{2}+1)[\frac{i}{2}-(-1)^i]\cos(\frac{i}{2}+1)\theta$$

$$G'_{ei} = (1-\frac{i}{2})(\frac{i+6}{2}-4\upsilon)\sin(\frac{i}{2}-1)\theta+(\frac{i}{2}+1)[\frac{i}{2}-(-1)^i]\sin(\frac{i}{2}+1)\theta$$

Thus, the stress intensity factor could be directly computed. However, that model is only applicable to longitudinal cracks in plane finite strips. In actual structures, such as bridge structures, the critical cracks are in the transverse direction, while the finite strips are usually deployed along the longitudinal direction of the structure. Therefore, finite strip elements with transverse crack are required for detailed analysis of such problems. This thesis is a step in developing such an element.

1.3 Historic Development of The Finite Strip Method

The finite strip method is a semi-analytical nature and was first proposed by Cheung, Y.K. (1968) for static analysis of simply supported bridge decks. Since then, application of the method has been extended to the modeling and analysis of other more complex structures under various loading conditions such as, buckling and vibration of composite laminated plate (Dawe and Wang 1995), nonlinear analysis of Midlin plates (Azizian and Dawe 1985), doubly curved

laminated shells (Wu et al 2001) and shear- deformable plates (Kong and Cheung 1993). The method has also been used for fracture analysis (Li et al. 1994, Cheung and Jiang 1996).

The semi-analytical finite strip method is very efficient for analysis of prismatic structures under distributed loading, especially for structures with both ends simply supported. It, however, has experienced difficulties in dealing with concentrated forces, multiple spans, discrete supports at strip ends, etc. To overcome these difficulties and to retain the advantages of the finite strip method, a mathematical tool called ' B_3 spline function' was used for the displacement function for the formation of the spline finite strips in analysis of rectangular plates by Cheung et al (1982).

The B_3 spline function can ensure continuity up to the second derivative (the so-called C_2 continuity). In order to get the same continuity condition, the finite element method needs three times as many unknowns at the element nodes. Hence, the use of B_3 splines is computationally more efficient than the finite element method with C_2 continuity. When using the B_3 spline functions, the penalty function approach (Cook et al, 1989) is readily utilized to impose any type of boundary conditions. Thus, the spline finite strip method is more flexible than the original finite strip method.

In the last two decades, the spline finite strip method has been applied to the solution of more complicated problems in the following areas:

- box girder bridges by Cheung and Fan (1983),
- parallelogram plates by Chen et al (1984),
- vibration of irregular plates by Chen and Chong (1984),
- buckling of irregular plates (Chen and Chong 1985, Chong and Chen 1986),
- arbitrary shaped slabs by Li et al (1986),
- arbitrary curved slab bridges by Cheung et al (1986),

- buckling of Thin-Walled Structures by Lau and Hancock (1986).
- vibration and stability analysis of stiffened plates by Cheung et al (1987),
- free vibration and static analysis of general plates by Cheung et al (1988),
- vibration of open cylindrical shells by Mizusawa (1988),
- bending of skew plates by Tham et al (1988),
- postbuckling analysis of shells by Zhu and Cheung (1989),
- continuous haunched bridges (Cheung and Li, 1990, Cheung et al 1992),
- curved reinforced concrete slab bridges (Cheung et al.1993),
- the analysis of shear- deformable plates by Kong and Cheung (1993),
- the buckling and vibration of rectangular composite laminate by Dawe and Wang (1995),
- plane fracture problems by Cheung and Jiang (1996).

Recently, two comprehensive books written about the finite strip method by Cheung, M.S., et al(1996) and by Cheung, Y.K and Tham (1998), summarize the basic theory of the finite strip method and its historic developments.

1.4 Current Study

In this thesis, through the combination of traditional spline finite strips with anti-plane eigenfunction expansion by Tilley (1978), plane eigenfunction expansion by Williams (1957) and bending eigenfunction expansion by Williams (1961) at a crack tip, respectively, three crack strip models are respectively developed for the anti-plane shear (tear) mode, the plane mode and the bending mode of crack problems. The cracks are assumed to be perpendicular to the longitudinal axis of strip elements and the stress intensity factors will be directly computed. Based on plane

crack strips and bending crack strips, the flat shell crack strip is developed for the fracture analysis of box girder bridges. The substructure technique is employed to enhance the efficiency of the analysis. Two types of singular integral method and extra knots are used to ensure the convergence of these models. Several case studies have demonstrated the satisfactory convergence of the proposed method.

The present method, combining the advantage of the spline finite strip method with the analytical solution for the area around the crack tip, provides a new and efficient approach for structural fracture analysis, especially the fracture analysis of bridge structures.

A number of slabs, slabs on girder and box girder bridges under different loads have been successfully analyzed using these crack strips. Their fracture characteristics, such as the effects of crack length on the stress intensity factor, the near field stresses and the near field deflection have been investigated. This investigation will provide important information about bridge safety that is required in bridge design and management.

The fracture analysis of Bryte Bend Bridge located in California, U. S. A. has been performed using the flat shell crack strip method to investigate possible causes of the critical failure in this bridge. The results of analyses agree favorably with the experimental studies conducted by Roberts (1977), and show the accuracy of empirical formulas that he used. The fracture toughness of top flanges in the bridge is studied as well.

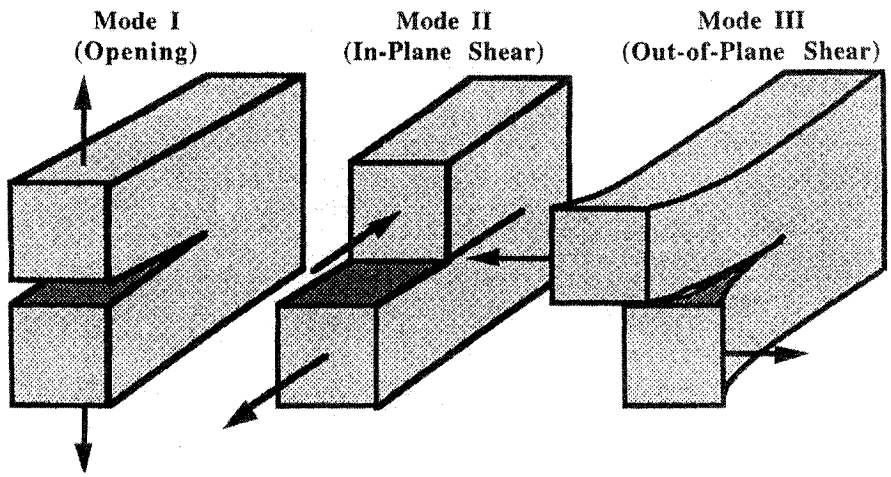

Figure 1.1 Basic modes of crack surface displacements.

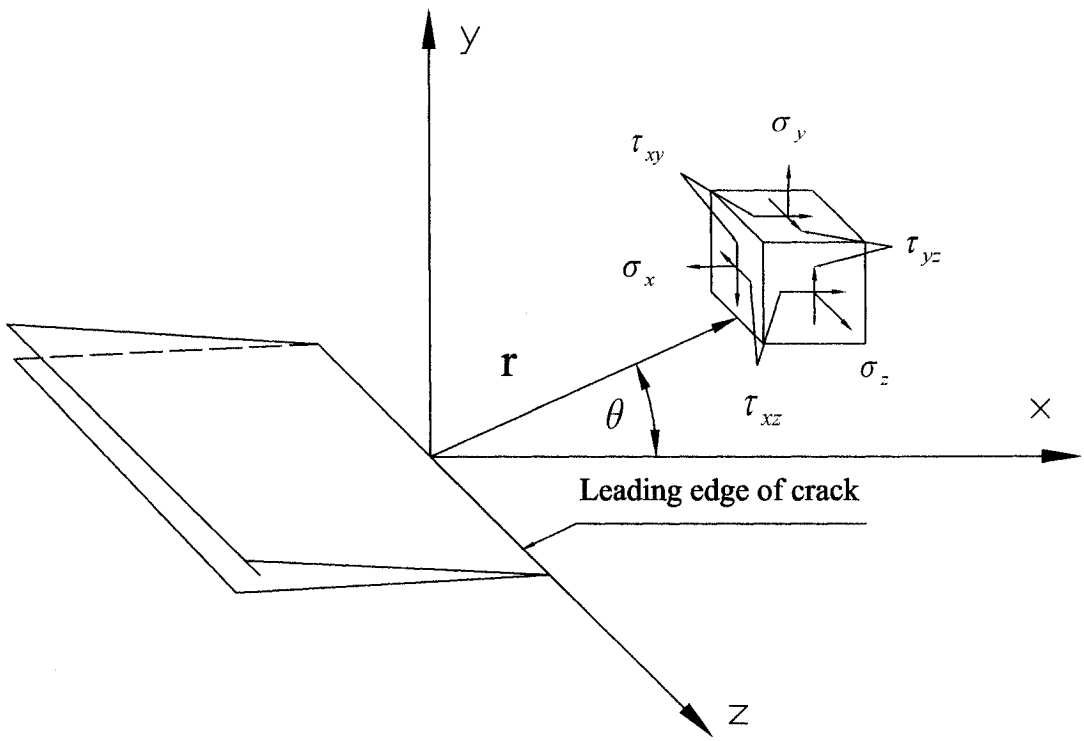

Figure 1.2 Definition of the coordinate axis ahead of a crack tip and stress components

Chapter 2

Spline Finite Strip Method

2.1 Introduction

The finite strip method, first published by Cheung, Y.K. (1968) for the analysis of simply supported bridge deck structures, has been proven to be a powerful, efficient and versatile analysis tool for the structural analysis of bridges of complicated geometric layout and different material properties. In this method, the bridge structure is divided into a number of flat shell (plate) or beam strips in the longitudinal direction. Thus, the finite strip method uses substantially less degrees-of-freedom than the finite element method. As a result the computer time and storage requirement are both reduced drastically. In addition, the finite strip model requires much less effort for input data preparation and output explanation than the finite element method

used for modeling the same bridge structure. Therefore, the efficiency of the analysis is enhanced significantly.

The finite strip method can be considered as a special form of finite element procedure using the displacement approach and is called semi-analytical finite element method. If a structure has constant cross-section, and end boundary conditions do not change transversely; its stress analysis can be easily performed using finite strips instead of finite elements. In each strip, the displacement components at any point are expressed in terms of the displacement parameters of nodal lines by using simple polynomials in the transverse direction and a series of continuously differentiable functions in the longitudinal direction. Those series should satisfy the boundary conditions at both ends of the strip a priori. Using the strain-displacement relationships and following the energy approach, the strain energy of the structure and the potential energy of external loads can also be expressed in terms of the displacement parameters. At equilibrium, the values of the displacement parameters should make the total potential energy of the structure minimum. This results in a set of algebraic equations with the displacement parameters as unknowns. By solving the equations for the displacement parameters, the displacements and as a result stress components at any point in the structure can be obtained.

The above mentioned semi-analytical finite strip method experiences difficulties in dealing with concentrated forces, multiple spans and discrete supports at strip ends, etc. To overcome these difficulties and to retain the advantages of the finite strip method, a mathematical tool called B_3 spline function has been used to provide the longitudinal displacement functions to form the spline finite strips for the analysis of rectangular plates by Cheung, Y.K. et al (1982). In this method, each nodal line is divided into a number of sections by equally or unequally spaced knots. Every knot is then taken as the center of a local B_3 spline, which has non-zero values in only four consecutive sections. All the B_3 splines on a nodal line form a series which is used to simulate the longitudinal variation of displacements.

The B_3 spline function can ensure continuity up to the second derivative (the so-called C_2 continuity). On the other hand, in order to get the same continuity condition, the finite element method needs three times as many unknowns at the element nodes. Hence, the use of B_3 spline is computationally much more efficient than the finite element method when C_2 continuity is required.

The second derivative of B_3 spline varies linearly in each longitudinal section. As a result it can more easily simulate peak values of bending moment at the loaded cross-sections or at intermediate supports. Moreover, similar to the finite element method, a spline finite strip can easily take up any prescribed external and internal boundary conditions by the penalty function approach(Cook et al, 1989). Thus, the spline finite strip method is more flexible than the traditional finite strip method.

2.2 Spline Function Interpolation

Spline functions are well-established mathematical tools. There are many types of spline functions commonly used as interpolation functions for field problems in engineering applications. The advantage of the spline functions is that they can satisfy any required continuity or discontinuity conditions.

The B_3 spline, a piecewise cubic polynomial with continuity up to the second derivative is employed to represent the longitudinal variation of displacement in the finite strip model. Assuming an arbitrary function $f(y)$ over the interval $0 \le y \le l$, the whole length l of the finite strip can be divided into r-1 sections of equal length or un-equal length by r knots. The finite strip with

un-equal length sections is not useful in this thesis. Readers who are interested it may consult, Cheung et al.(1996).

The equally spaced B_3 spline function $\phi_m(y)$ with a knot at $y = y_m$ as the center can be defined by

$$\phi_m(y) = \frac{1}{6h^3}\begin{cases} (y - y_{m-2})^3 & y_{m-2} \le y \le y_{m-1} \\ (h^3 + 3h^2(y - y_{m-1}) + 3h(y - y_{m-1})^2 - 3(y - y_{m-1})^3 & y_{m-1} \le y \le y_m \\ h^3 + 3h^2(y_{m+1} - y) + 3h(y_{m+1} - y)^2 - 3(y_{m+1} - y)^3 & y_m \le y \le y_{m+1} \\ (y_{m+2} - y)^3 & y_{m+1} \le y \le y_{m+2} \\ 0 & otherwise \end{cases} \qquad (2-1)$$

where y_m is the longitudinal coordinate of knot m with $1 \le m \le r$. In particular, $y_1 = 0$, $y_r = l$, $h = l/(r\text{-}1)$ and $y_m = (m-1)h$.

The function is twice differentiable over the interval, and its second derivative is a linear fuction in terms of y. The values of function $\phi_m(y)$ and its first and second derivatives at knots are given in Table 2.1.

Table 2.1 *Values of Spline Function at Knots*

Function	y_{m-2}	y_{m-1}	y_m	y_{m+1}	y_{m+2}
$\phi_m(y)$	0	1/6	2/3	1/6	0
$\phi_m'(y)$	0	$1/(2h)$	0	$-1/(2h)$	0
$\phi_m''(y)$	0	$1/h^2$	$-2/h^2$	$1/h^2$	0

The spline functions centered at all the knots comprise a series $s(y)$ which can be used to interpolate any continuous and differentiable function $f(y)$. In each section, the value of $s(y)$ is related to four splines which are centered at the two ends of this section and the two knots next to those ends, respectively. Therefore, two additional knots y_0 and y_{r+1} are needed to interpolate $f(y)$ in the first and the last sections. Thus the series of spline functions can be expressed as

$$s(y) = \sum_{m=0}^{r+1} d_m \phi_m(y) \qquad (2-2)$$

in which the d_m are coefficient to be determined by interpolation requirements.

Under given boundary conditions, coefficients d_m can be determined in a matrix form:

$$[L]\{d\} = \{f\} \qquad (2-3)$$

in which $\{d\}$ is the vector of interpolation coefficients d_m ,$\{f\}$ is the vector for values of the function at knots, while $[L]$ is the matrix for the values of the spline functions at knots. The entries of $[L]$ depend on the boundary conditions. The next section will give the details of constructing the matrix $[L]$ and the vector $\{f\}$ for two special cases.

Calling the invert matrix of $[L]$ as $[F]$:

$$[F] = [L]^{-1} \qquad (2-4)$$

the interpolation coefficients $\{d\}$ can be calculated from the function values at knots

$$\{d\} = [F]\{f\} \qquad (2-5)$$

2.3 Imposing Boundary Conditions

In this study, special fracture strips are developed for the fracture analysis of structures. In each fracture strip, the area surrounding crack tip is modeled by a special portion, which is derived from analytical solution in fracture mechanics and uses the displacements at knots as degrees of freedom. The rest portion of the strip is simulated by traditional spline finite strips which uses B_3-Spline interpolation and takes interpolation coefficients as degrees of freedom instead of displacements. In order to assemble the stiffness matrix of the entire strip, it is necesary to perform transformation from interpolation coefficient to displacements and vice versa. The mapping between these two sets of degrees of freedom must be one to one determined. To make this mapping possible, one method is to impose necessary displacement and stress boundary conditions at two ends of the strip to eliminate some dependent degrees of freedom and to create a square transformation matrix [L]. For example, the following boundary conditions should be imposed to a beam element:

1. Simple supports at both sides

In addition to zero deflections at both ends, the moments as two extra boundary conditions should also be set to zero at both ends. Thus, the interpolation can be expressed as :

$$
\begin{aligned}
& s''(y_1) = f''(y_1) = 0 \\
& s(y_1) = f(y_1) = 0, \\
& s(y_m) = f(y_m), \quad 2 \le m \le r-1 \\
& s(y_r) = f(y_r) = 0, \\
& s''(y_r) = f''(y_r) = 0
\end{aligned}
\qquad (2-6)
$$

where f(y) represents the deflection, while s(y) denotes the interpolation function, and $f''(y)$ and $s''(y)$ indicate the second derivative of f(y) and s(y) respectively.

In this case, matrix [L] in (2-3) is obtained as the following form

$$[L]=\begin{bmatrix} 1/h^2 & -2/h^2 & 1/h^2 & 0 & 0 & 0 & 0 \\ 1/6 & 2/3 & 1/6 & 0 & 0 & 0 & 0 \\ 0 & 1/6 & 2/3 & 1/6 & 0 & 0 & 0 \\ & & \bullet & \bullet & \bullet & & \\ 0 & 0 & 0 & 0 & 1/6 & 2/3 & 1/6 \\ 0 & 0 & 0 & 0 & 1/h^2 & -2/h^2 & 1/h^2 \end{bmatrix} \qquad (2-7)$$

and

$$\{d\}=\begin{Bmatrix} d_0 \\ d_1 \\ \bullet \\ \bullet \\ \bullet \\ d_{r+1} \end{Bmatrix}, \quad \{f\}=\begin{Bmatrix} f''(y_1) \\ f(y_1) \\ f(y_2) \\ \bullet \\ f(y_r) \\ f''(y_r) \end{Bmatrix} \qquad (2-8)$$

2. One clamped support end and one free end

In addition to zero deflections at the clamped end, the rotation at this end and the bending moment at the free end should be also zero as two extra boundary conditions. Thus, the interpolation expressions can be expressed as :

$$
\begin{aligned}
&s'(y_1) = f'(y_1) = 0 \\
&s(y_1) = f(y_1) = 0, \\
&s(y_m) = f(y_m), \quad 2 \le m \le r \\
&s''(y_r) = f''(y_r) = 0
\end{aligned}
\tag{2 - 9}
$$

where $f'(y)$ and $s'(y)$ indicate the first derivative of f(y) and s(y) respectively.

In this case, matrix $[L]$ in (2-3) is formed as the following form

$$
[L] = \begin{bmatrix}
-1/(2h) & 0 & 1/(2h) & 0 & 0 & 0 & 0 \\
1/6 & 2/3 & 1/6 & 0 & 0 & 0 & 0 \\
0 & 1/6 & 2/3 & 1/6 & 0 & 0 & 0 \\
 & & \bullet & \bullet & \bullet & & \\
0 & 0 & 0 & 0 & 1/6 & 2/3 & 1/6 \\
0 & 0 & 0 & 0 & 1/h^2 & -2/h^2 & 1/h^2
\end{bmatrix}
\tag{2 - 10}
$$

and

$$
\{d\} = \begin{Bmatrix} d_0 \\ d_1 \\ \bullet \\ \bullet \\ \bullet \\ d_{r+1} \end{Bmatrix}, \quad \{f\} = \begin{Bmatrix} f'(y_1) \\ f(y_1) \\ f(y_2) \\ \bullet \\ f(y_r) \\ f''(y_r) \end{Bmatrix}
\tag{2 - 11}
$$

2.4 Spline Finite Strip

The spline finite strip method employs simple polynomials and B_3 spline functions to represent transverse and longitudinal variations of displacement respectively. As mentioned earlier, following the energy approach, the strain energy of the structure and the potential energy of external loads can be expressed in terms of the displacement parameters. At equilibrium, the values of the displacement parameters should make the total potential energy of the structure minimum. This results in a set of algebraic equations with the displacement parameters as unknowns. After solving the equations for the displacement parameters, the displacement and stress components at any point in the structure can be calculated.

B_3 spline functions have been used as the longitudinal displacement functions to form the spline finite strips for the analysis of rectangular plates by Cheung, Y.K. et al (1982). In this method, each nodal line is divided into a number of sections by equally or unequally spaced knots. Every knot is then taken as the center of a local B_3 spline which has non-zero values only in four consecutive sections. All the B_3 splines on a nodal line form a series which is used to simulate the longitudinal variation of displacements.

Taking plane stress analysis of a rectangular plate as an example and assuming that its cross-section is constant and its boundary conditions at both ends are unchnaged transversely; the structure can be divided into S spline strips (**Fig. 2.1**) with $S+1$ nodal lines that have l knots each. The displacement components u and v at any point (x, y) in a strip can be expressed in terms of the displacement parameters u_{im} and v_{im} at the knot m on nodal line i as:

$$u = \sum_{m=0}^{l+1} (C_i \Phi^{u}_{im}(y) u_{im} + C_j \Phi^{u}_{jm}(y) u_{jm})$$
$$v = \sum_{m=0}^{l+1} (C_i \Phi^{v}_{im}(y) v_{im} + C_j \Phi^{v}_{jm}(y) v_{jm}) \qquad (2-12)$$

where $\Phi^{u}_{im}(y)$, $\Phi^{v}_{im}(y)$ are B_3 spline functions centered at y_m for u and v respectively, and C_i is transverse shape function for nodal line ***i*** while C_j is transverse shape function for nodal line ***j***. C_i and C_j are formed by the following,

$$C_i = 1 - X, \qquad C_j = X \qquad (2-13)$$

in which $X = x/b$ and b is the width of the strip.

For prescribed boundary conditions at knot $m = 1$ on the plate boundary, the three local splines centered at y_0, y_1 and y_2 should be modified, while standard splines are used for other knots. If knots $m = 0$ through $m = 4$ are equally spaced, the modified expressions for $\overline{\Phi}_m(y)$ (m = 0 to 2) are summarized in **Table 2.2**:

Table 2.2 Modified Spline Functions around End Knot m = 1

Boundary Condition	Modified Spline Functions		
	$\overline{\Phi}_0$	$\overline{\Phi}_1$	$\overline{\Phi}_2$
Free	Φ_0	Φ_1	Φ_2
Simply supported	0	$\Phi_1 - 4\,\Phi_0$	$\Phi_2 - \Phi_0$
Clamped	0	0	$\Phi_2 - \frac{1}{2}\Phi_1 + \Phi_0$
Sliding clamped	0	Φ_1	$\Phi_2 + \Phi_0$
Continuous	$\Phi_0 - \frac{1}{4}\Phi_1$	0	$\Phi_2 - \frac{1}{4}\Phi_1$

Once the displacement functions for the strip have been chosen, the strip characteristics including stiffness and load matrices can be obtained according to the standard finite strip formulation. Details are described in the following chapters.

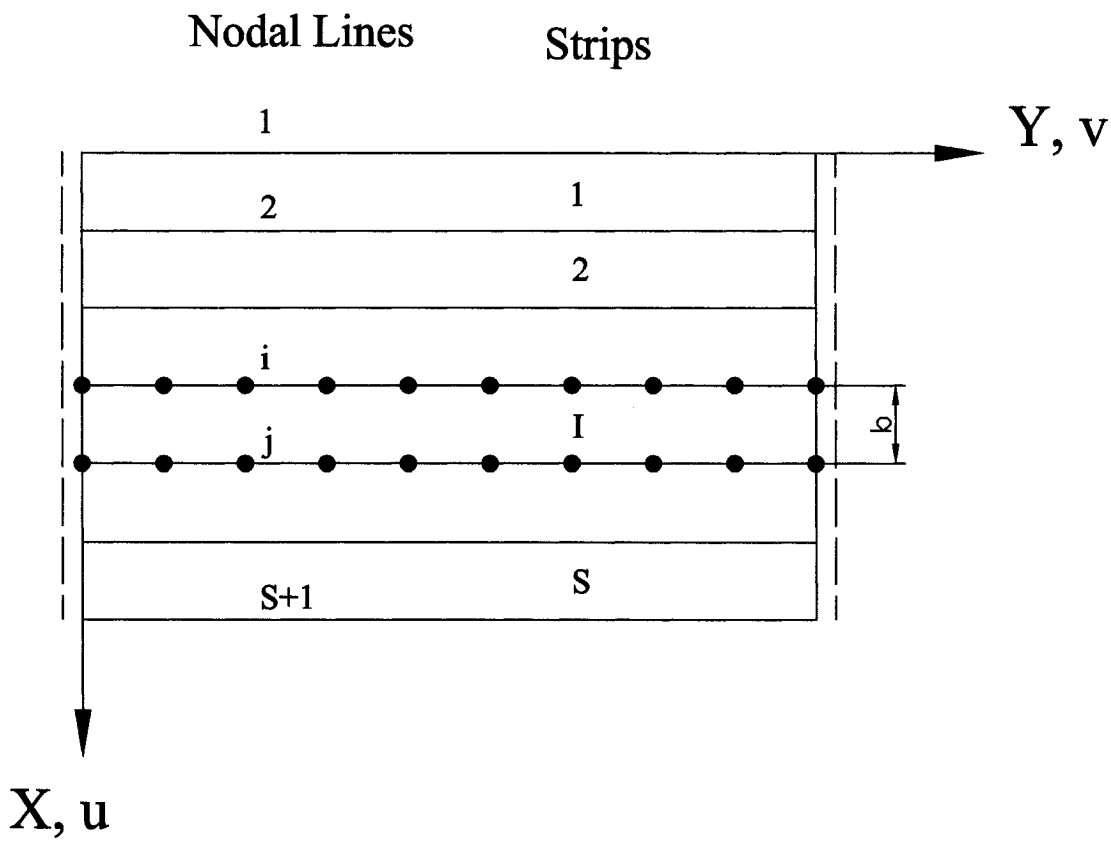

Figure 2.1 Plane Stress Spline Finite Strip

Chapter 3

Crack Strip Model

3.1 Crack Strip Model

In this study, three types of crack strips (**Fig. 3.1 b**) are developed to model structures with transverse cracks (**Fig. 3.1 a**). Each crack strip consists of many parts. A special part, rectangular area (A-C-L-J) surrounding the crack is divided into four identical substructures. To improve accuracy, in each substructure, some extra nodes are added around the crack tip such as nodes 1, 6, 7, 8 and 9 shown in **Fig. 3.2(d)**, in addition to those nodes that are pointed according to spline finite strip. The analytical solution from fracture analysis is used to model the displacement field surrounding the crack tip. The shape functions for remaining parts of the crack strip are identical to those in an ordinary spline finite strip.

As shown in **Fig. 3.2 b**, within the cracked strip, traditional spline strips are connected to the cracked special area on both sides. The left part is connected to the cracked area at nodes A, D, B and E, while the right part is connected at nodes C, I, B, and F. At each common nodes, the traditional part and the cracked area have identical deflection *w*. It should be noticed that the two substructures ①, ② have a common node B on the upper nodal line because of continuous deflection there. Different nodes E and F are located along the lower nodal line at the different edges of the crack.

While the stiffness contribution of the traditional parts can be given by the standard spline finite strip procedure, the contribution of the crack area can be evaluated using the solution of fracture analysis combined with substructure technique, by which the degrees of freedom at the extra nodes and the internal nodes between the four identical parts can be condensed out to those nodes at boundary of these areas. Tilley (1978) presented the anti-plane eigenfunction expansion for the displacement field surrounding the crack tip, and Williams (1957, 1961) gave both the in-plane and the bending eigenfunction expansion for the displacement field surrounding the crack tip.

For the edge crack in a structure, the crack strip can take the form shown in **Fig 3.2**, which has just two substructures in the special area. The procedure to calculate its stiffness contribution remains the same.

3.2 Substructure Technique

The efficiency of analysis can be enhanced significantly by dividing a structure into many substructures. The internal degrees of freedom between substructures can be condensed so that only the external nodes on its boundary are retained in the structural equilibrium

equation. If substructures have the same both geometry and load condition, only one substructure needs to be processed to form the stiffness matrix and load vector, while other identical substructures can obtain their corresponding matrix and vector by a simple coordinate transformation (Cook et al. 1989).

3.2.1 Internal Degrees of Freedom Condensation

Since these internal degrees of freedom are not shared with any other parts of the structure, these degrees of freedom can be represented in terms of the external degrees of freedom and not directly included in the structural matrix equation.

For example, if the stiffness matrix as well as the displacement and load vectors are divided into parts as:

$$\begin{bmatrix} k_{bb} & k_{bi} \\ k_{ib} & k_{ii} \end{bmatrix} \begin{Bmatrix} a_b \\ a_i \end{Bmatrix} = \begin{Bmatrix} p_b \\ p_i \end{Bmatrix} \qquad (3-1)$$

in which subscript 'b' denotes the boundary nodes, while the subscript 'i' indicates the inside nodes, then the structural matrix equation can be condensed as below to include the external degrees of freedom only:

$$\begin{aligned} [k^*_{bb}]\{a_b\} &= \{p^*_b\} \\ k^*_{bb} &= k_{bb} - k_{bi}k_{ii}^{-1}k_{ib} \\ p^*_b &= p_b - k_{bi}k_{ii}^{-1}p_i \end{aligned} \qquad (3-2)$$

3.2.2 Coordinate Transformation

In **Fig 3.1(c)**, substructures ①, ②, ③ and ④ have identical geometries, so that their respective local stiffness matrices should also be identical to $[k_{bb}^{*}]$, which can be derived for substructure ①. However, in order to obtain the stiffness matrix and the equivalent load vectors of each substructure in the global coordinate system, i.e.; $[k_{bb}^{(i)*}]$ and $\{p_b^{(i)*}\}$

$$[k_{bb}^{(i)*}] = [\lambda]^T [k_{bb}^{*}][\lambda]$$
$$\{p_b^{(i)*}\} = [\lambda]^T \{p_b^{*}\} \qquad (i = 1,2,3,4) \qquad (3-3)$$

the following coordinate transformation is required:

$$[\lambda^{(i)}] = \begin{bmatrix} l_{xX} & l_{xY} \\ l_{yX} & l_{yY} \end{bmatrix}$$
$$[\lambda] = \begin{bmatrix} \lambda^{(i)} & & & \\ & \lambda^{(i)} & & \\ & & \cdots & \\ & & & \lambda^{(i)} \end{bmatrix} \qquad (3-4)$$

where l_{xX} and l_{xY} denote the direction cosines of the x axis of local coordinate with respect to the global coordinate system, X, Y, and l_{yX}, l_{yY} denote the direction cosines of the y axis of local coordinate with respect to the global coordinate system, X, Y.

for substructure ①:

$$[\lambda^{(1)}] = \begin{bmatrix} 1 & 0 \\ 0 & 1 \end{bmatrix} \tag{3-5}$$

for substructure ②:

$$[\lambda^{(2)}] = \begin{bmatrix} 1 & 0 \\ 0 & -1 \end{bmatrix} \tag{3-6}$$

for substructure ③:

$$[\lambda^{(3)}] = \begin{bmatrix} -1 & 0 \\ 0 & 1 \end{bmatrix} \tag{3-7}$$

and for substructure ④:

$$[\lambda^{(4)}] = \begin{bmatrix} -1 & 0 \\ 0 & -1 \end{bmatrix} \tag{3-8}$$

After coordinate transformation, the four substructures can be integrated to a larger substructure ACLJ shown in **Fig.3.1(c)**, and the internal degrees of freedom at extra nodes 1,

6, 7, 8 and 9 shown in **Fig. 3.2(d)** can be condensed. Then, this substructure can be connected to other parts of the structure, which are modeled by the traditional spline finite strips.

3.3 Application of Gaussian Quardrature to Singular Integral

It is obvious that r^{-1} singularity appears in the integral of element potential energy, due to the $r^{-1/2}$ singularity of stress at the crack tip, where r represents the distance from the crack tip (**Fig.1.2**).

Since the substructure ① has a rectangular geometry, the Cartesian coordinate system is more convenient than the polar system for calculating the integrations, and the following coordinate transformation is helpful:

$$r = \sqrt{x^2 + y^2}, \quad \theta = \tan^{-1}\left(\frac{y}{x}\right) .$$

However, the following integration becomes singular at crack tip G shown in **Fig. 3.1 (d)**, where $r = 0$:

$$\int_0^h \int_{-a/2}^{(b-a)/2} 1/\sqrt{x^2 + y^2}\, dxdy \qquad (3-9)$$

The integral can be divided into the following two linear integrals to isolate the effect of singularity only

$$\int_{-a/2}^{(b-a)/2} \frac{1}{|x|} dx \qquad \text{(when } y = 0\text{)} \tag{3-10}$$

and

$$\int_{0}^{h} \frac{1}{y} dy \qquad \text{(when } x = 0\text{)} \tag{3-11}$$

This type of singularity is called as r^{-1} singularity.

Because the integration (3 - 10) can also be divided into two parts as:

$$\int_{-a/2}^{(b-a)/2} \frac{1}{|x|} dx = \int_{0}^{(b-a)/2} \frac{1}{x} dx + \int_{0}^{a/2} \frac{1}{x} dx \tag{3-12}$$

all the singular integrations in the above equations have the same form as

$$\int_{0}^{c} \frac{1}{t} dt \tag{3-13}$$

In which c > 0 is the upper bound of the integration.

Based on the Gaussian quadrature for improper integrals (Stroud, 1966), there are two methods to evaluate the result of this singlar integral.

Method I employs the Gaussian quadrature for improper integrals in form $\int_{0}^{\infty} e^{-x} g(x) dx$,

This can be achieved by introducing the following transformation:

$$\frac{1}{t} = x + \frac{1}{c}, \quad dt = \frac{-1}{(x+1/c)^2}dx \tag{3-14}$$

which leads to

$$\int_0^c \frac{1}{t}dt = \int_0^\infty \frac{1}{x+1/c}dx = \int_0^\infty e^{-x}\frac{e^x}{x+1/c}dx \tag{3-15}$$

Because $e^x/(x+1/c)$ is a continuous function over the entire region $[0, \infty)$ of the integration, the above-mentioned Gaussian quadrature can be used:

$$\int_0^c \frac{1}{t}dt \cong \sum_{i=1}^{N} A_i \frac{e^{x_i}}{x_i + 1/c} \tag{3-16}$$

where N is the required number of Gaussian points, A_i is the corresponding Gaussian coefficient for the ith Gaussian point (See Appendix B). when N>19, the absolute error, defined as $\left| \int_0^c \frac{1}{t}dt - \sum_{i=1}^{N} A_i \frac{e^{x_i}}{x_i + 1/c} \right|$, is less than 0.2829×10^{-10}.

Thus, the integration in (3-9) can be evaluated as

$$\int_0^h \int_{-a/2}^{(b-a)/2} 1/\sqrt{x^2+y^2}\,dxdy$$
$$\cong \sum_{i=1}^{N}\sum_{j=1}^{N} A_i A_j \left\{ \frac{e^{\sqrt{y_i^2+x_j^2}}}{\sqrt{(y_i+1/h)^2+[x_j+2/(b-a)]^2}} + \frac{e^{\sqrt{y_i^2+x_j^2}}}{\sqrt{(y_i+1/h)^2+(x_j+2/a)^2}} \right\} \tag{3-17}$$

Method II uses the Gaussian quadrature for improper integrals in form $\int_0^1 \ln(\frac{1}{x}) f(x)dx$

Considering the transformation

$$t = cx, \quad dt = cdx \tag{3 -18}$$

Integral (3 -13) is transformed to

$$\int_0^c \frac{1}{t}dt = \int_0^1 \frac{1}{x}dx = \int_0^1 \ln(\frac{1}{x})\frac{-1}{x\ln x}dx \tag{3 -19}$$

and then Gaussian quadrature can be used:

$$\int_0^c \frac{1}{t}dt \cong \sum_{i=1}^{N} A_i \frac{-1}{x_i \ln x_i} \tag{3 -20}$$

where N is the required number of Gaussian points, A_i is the corresponding Gaussian coefficient for the ith Gaussian point, (Appendix C). When N>8, the approximate error, defined as $\left| \int_0^c \frac{1}{t}dt - \sum_{i=1}^{N} A_i \frac{-1}{x_i \ln x_i} \right|$, is less than 0.1581×10^{-9}.

Thus, the integration in (3 -9) can be evaluated as

$$\int_0^h \int_{-a/2}^{(b-a)/2} 1/\sqrt{x^2 + y^2}\,dxdy \cong -2\sum_{i=1}^{N}\sum_{j=1}^{N} A_i A_j \frac{1}{\sqrt{x_i^2 + y_j^2}\ln\sqrt{x_i^2 + y_j^2}} \tag{3 - 21}$$

Because *ln(1/x)* has lower degree of singularity than that of *1/x* at point $x = 0$, equation (3 - 20) provides a more accurate evaluation of $\int_0^c \frac{1}{t} dt$, even though *1/(xlnx)* is still singular at point $x = 0$

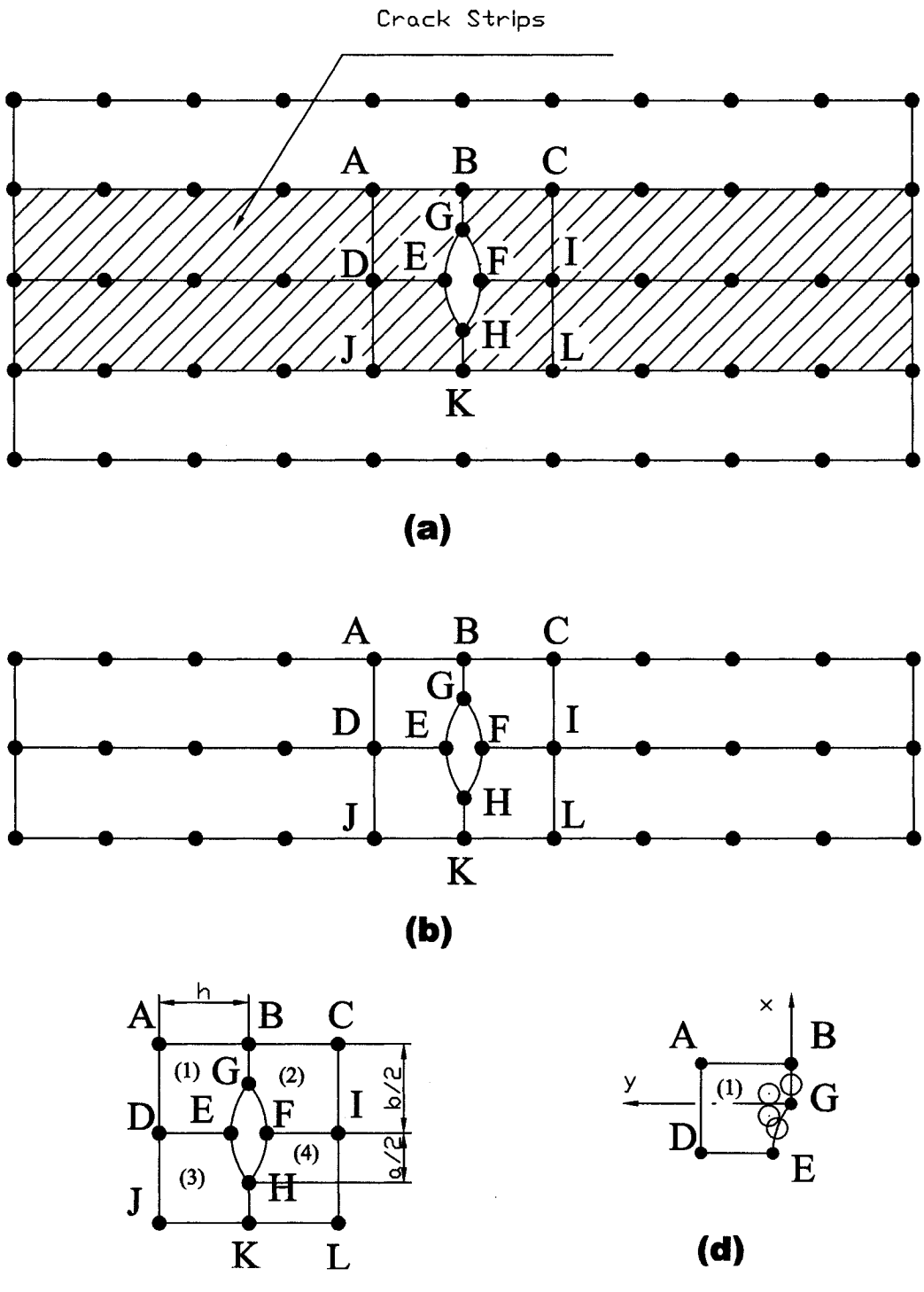

Figure 3.1 Crack Strip Model

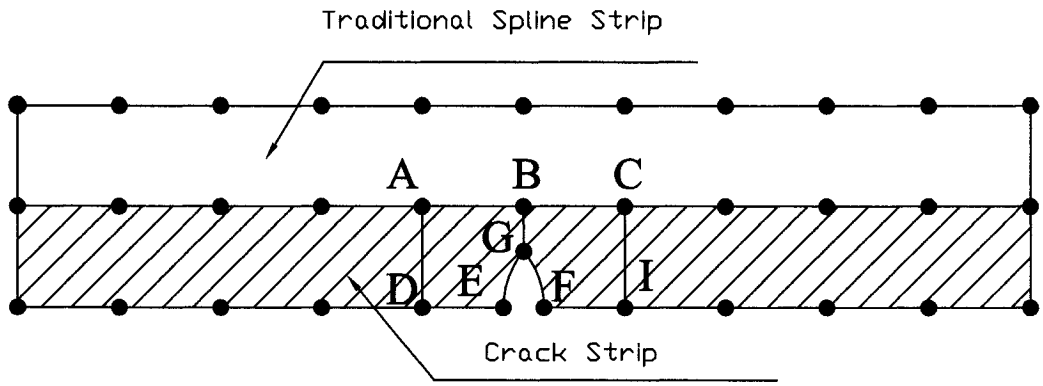

(a)

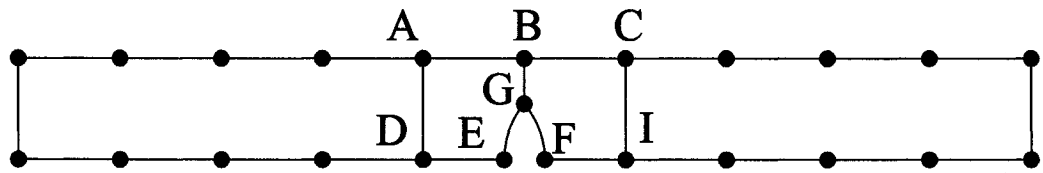

(b)

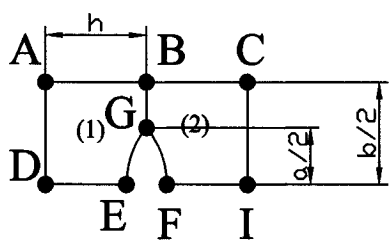

(c)

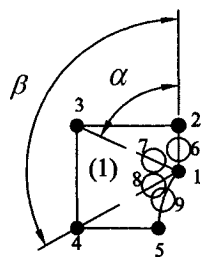

(d)

Figure 3.2 Edge Crack Strip Model

Chapter 4

Anti-plane Shear Crack Strips

4.1 Introduction

As mentioned earlier, there are three types of plane crack mode in fracture analysis, namely, opening mode (Mode I), in-plane shear mode (Mode II) and anti-plane shear mode (Mode III). By incorporating the anti-plane eigenfunction expansion for the displacement field (Tilley, 1978) surrounding the crack tip, Anti-plane Shear Crack Strip is developed corresponding to the Tearing model of plane cracks.

The rod or beam is one of the most commonly used members in engineering structures. The behavior of cracked rods or beams, which are weakened by deep surface flaws or internal cracks

and are subjected to longitudinal shear, torsion or bending loads, is governed by the Laplace equation in two dimensions and is considered as an anti-plane elastic crack propagation. The fracture analysis of a thick plate (Midlin plate) which is deformed under shear force belongs to this mode as well, and the methods of solution are the same as those for anti-plane problems. In those problems, it is common that the stress components around the crack tip are formulated on the basis of equation (1 – 5).

4.2 Traditional Spline Shear Strip

4.2.1 Displacement in Spline Shear Strip

In a cracked plate subjected to anti-plane shear, the portion remote from the crack tip can be modeled by traditional spline shear strip (**Fig. 3.1** and **Fig 3.2**). Each strip has two nodal lines, labeled as i and j, each of which has r equally spaced knots. The deflection w at any point within each strip can be interpolated using the linear function of x transversely and the spline function of y longitudinally as:

$$w = [C][\Phi]\{d\} \qquad (4-1)$$

in which

$$
\begin{aligned}
&[C] = [1 - \bar{x}, \quad \bar{x}] \\
&[\Phi] = \begin{bmatrix} [\phi] & \\ & [\phi] \end{bmatrix} \\
&[\phi] = [\phi_0 \quad \phi_1 \quad \cdot \quad \cdot \quad \cdot \quad \cdot \quad \phi_{r+1}] \\
&\{d\} = [d_i, \quad d_j]^T = [d_{i0}, d_{i1}, \cdot \quad \cdot \quad \cdot, d_{ir+1}, d_{j0}, d_{j1}, \cdot \quad \cdot \quad \cdot, d_{jr+1}]^T
\end{aligned}
\tag{4-2}
$$

where $\bar{x} = x / b$, in which, b denotes the width of the strip, ϕ_i is spline function centered at node i and d_i is the coefficient corresponding to ϕ_i. The shear strains at any point within the strip can be expressed in terms of the displacement parameter based on strain-displacement relationship:

$$
\begin{aligned}
2\varepsilon_{xz} &= \frac{\partial w}{\partial x} \\
2\varepsilon_{yz} &= \frac{\partial w}{\partial y}
\end{aligned}
\tag{4-3}
$$

or

$$
\{\varepsilon\} = [B]\{d\} \tag{4-4}
$$

where

$$
\begin{aligned}
&\{\varepsilon\} = \begin{Bmatrix} 2\varepsilon_{xz} \\ 2\varepsilon_{yz} \end{Bmatrix}, \\
&[B] = \begin{bmatrix} [C'][\Phi] \\ [C][\Phi'] \end{bmatrix} = \begin{bmatrix} [C'] & 0 \\ 0 & [C] \end{bmatrix} \begin{Bmatrix} [\Phi] \\ [\Phi'] \end{Bmatrix}
\end{aligned}
\tag{4-5}
$$

and

$$[C'] = [-1, 1]/b \tag{4-6}$$

The shear stresses at any point within the strip can be expressed in terms of the displacement parameter based on stress-strain relationship:

$$\begin{aligned} \tau_{xz} &= G\varepsilon_{xz} \\ \tau_{yz} &= G\varepsilon_{yz} \end{aligned} \tag{4-7}$$

where G is the shear modulus of elasticity. Thus, The stress vector is formed as:

$$\{\sigma\} = [D]\{\varepsilon\} = [D][B]\{d\} \tag{4-8}$$

where

$$\begin{aligned} \{\sigma\} &= \begin{Bmatrix} \tau_{xz} \\ \tau_{yz} \end{Bmatrix} \\ [D] &= G\begin{bmatrix} 1 & 0 \\ 0 & 1 \end{bmatrix} \end{aligned} \tag{4-9}$$

4.2.2 Stiffness corresponding to {d}

By following the standard procedure in the spline finite strip analysis, the stiffness matrix $[k^e]$ of a traditional spline strip can be formed as:

$$[k^e] = \int [B]^T [D][B] dA \qquad (4-10)$$

where A is the area of the finite strip.

Substituting (4 – 5) and (4 – 9) into the integral in the above equation yields

$$[B^T][D][B] = G[[\Phi]^T \quad [\Phi']^T] \begin{bmatrix} [C']^T[C'] & 0 \\ 0 & [C]^T[C] \end{bmatrix} \begin{Bmatrix} [\Phi] \\ [\Phi'] \end{Bmatrix}$$

Introducing the following notations

$$[C_1] = \int_0^b [C']^T [C'] dx = \int_0^b \begin{bmatrix} 1 & -1 \\ -1 & 1 \end{bmatrix} dx = \frac{1}{b} \begin{bmatrix} 1 & -1 \\ -1 & 1 \end{bmatrix}$$

$$[C_0] = \int_0^b [C]^T [C] dx = b \int_0^1 \begin{bmatrix} (1-\bar{x})^2 & \bar{x}(1-\bar{x}) \\ \bar{x}(1-\bar{x}) & \bar{x}^2 \end{bmatrix} d\bar{x} = \frac{b}{6} \begin{bmatrix} 2 & 1 \\ 1 & 2 \end{bmatrix} \qquad (4-11)$$

Eq. (4 – 10) becomes

$$\begin{aligned} [k^e] &= G \int_0^l [[\Phi]^T \quad [\Phi']^T] \begin{bmatrix} [C_1] & 0 \\ 0 & [C_0] \end{bmatrix} \begin{Bmatrix} [\Phi] \\ [\Phi'] \end{Bmatrix} dy \\ &= G \int_0^l \{[\Phi]^T [C_1][\Phi] + [\Phi']^T [C_0][\Phi']\} dy \\ &= G \left\{ \frac{1}{b} \int_0^l \begin{bmatrix} [\Phi]^T[\Phi] & -[\Phi]^T[\Phi] \\ -[\Phi]^T[\Phi] & [\Phi]^T[\Phi] \end{bmatrix} dy + \frac{b}{6} \int_0^l \begin{bmatrix} 2[\Phi']^T[\Phi'] & [\Phi']^T[\Phi'] \\ [\Phi']^T[\Phi'] & 2[\Phi']^T[\Phi'] \end{bmatrix} dy \right\} \end{aligned} \qquad (4-12)$$

where

$$\int [\Phi]^T [\Phi] dy = \begin{bmatrix} \int [\phi]^T [\phi] dy & 0 \\ 0 & \int [\phi]^T [\phi] dy \end{bmatrix}$$

$$\int [\Phi']^T [\Phi'] dy = \begin{bmatrix} \int [\phi']^T [\phi'] dy & 0 \\ 0 & \int [\phi']^T [\phi'] dy \end{bmatrix} \qquad (4-13)$$

in which

$$\int [\phi]^T [\phi] dy = \begin{bmatrix} \int \phi_0 \phi_0 dy & \int \phi_0 \phi_1 dy & \cdots & \int \phi_0 \phi_{r+1} dy \\ \int \phi_1 \phi_0 dy & \int \phi_1 \phi_1 dy & \cdots & \int \phi_1 \phi_{r+1} dy \\ \cdot & \cdot & \cdots & \cdot \\ \int \phi_{r+1} \phi_0 dy & \int \phi_{r+1} \phi_1 dy & \cdots & \int \phi_{r+1} \phi_{r+1} dy \end{bmatrix} \qquad (4-14)$$

$$\int [\phi']^T [\phi'] dy = \begin{bmatrix} \int \phi'_0 \phi'_0 dy & \int \phi'_0 \phi'_1 dy & \cdots & \int \phi'_0 \phi'_{r+1} dy \\ \int \phi'_1 \phi'_0 dy & \int \phi'_1 \phi'_1 dy & \cdots & \int \phi'_1 \phi'_{r+1} dy \\ \cdot & \cdot & \cdots & \cdot \\ \int \phi'_{r+1} \phi'_0 dy & \int \phi'_{r+1} \phi'_1 dy & \cdots & \int \phi'_{r+1} \phi'_{r+1} dy \end{bmatrix} \qquad (4-15)$$

The items $\int \phi_i \phi_j dy$, $\int \phi'_i \phi'_j dy$ in the above matrices can be evaluated by the following procedures:

$$\int [\phi]^T [\phi] dy = \begin{bmatrix} I_0 & I_1 & I_2 & I_3 & 0 & \cdot & \cdot & 0 \\ I_1 & I_0 & I_1 & I_2 & I_3 & 0 & \cdot & 0 \\ \cdot & \cdot & \cdot & \cdot & \cdot & \cdot & \cdot & \cdot \\ 0 & \cdot & 0 & I_3 & I_2 & I_1 & I_0 & I_1 \\ 0 & \cdot & \cdot & 0 & I_3 & I_2 & I_1 & I_0 \end{bmatrix} \qquad (4-16)$$

$$\int [\phi']^T [\phi'] dy = \begin{bmatrix} I''_0 & I''_1 & I''_2 & I''_3 & 0 & \cdot & \cdot & 0 \\ I''_1 & I''_0 & I''_1 & I''_2 & I''_3 & 0 & \cdot & 0 \\ \cdot & \cdot & \cdot & \cdot & \cdot & \cdot & \cdot & \cdot \\ 0 & \cdot & 0 & I''_3 & I''_2 & I''_1 & I''_0 & I''_1 \\ 0 & \cdot & \cdot & 0 & I''_3 & I''_2 & I''_1 & I''_0 \end{bmatrix} \qquad (4-17)$$

where

$$I_0 = \int_{y_{i-2}}^{y_{i+2}} \phi_i^2 dy, \quad I''_0 = \int_{y_{i-2}}^{y_{i+2}} \phi_i'^2 dy \qquad \text{for } i = j,$$

$$I_1 = \int_{y_{i-1}}^{y_{i+2}} \phi_i \, \phi_j dy, \quad I''_1 = \int_{y_{i-1}}^{y_{i+2}} \phi'_i \, \phi'_j \, dy \qquad \text{for } |i-j| = 1,$$

$$I_2 = \int_{y_i}^{y_{i+2}} \phi_i \, \phi_j dy, \quad I''_2 = \int_{y_i}^{y_{i+2}} \phi'_i \, \phi'_j \, dy \qquad \text{for } |i-j| = 2,$$

$$I_3 = \int_{y_{i+1}}^{y_{i+2}} \phi_i \, \phi_j dy, \quad I''_3 = \int_{y_{i+1}}^{y_{i+2}} \phi'_i \, \phi'_j \, dy \qquad \text{for } |i-j| = 3 \qquad (4-18)$$

and

$$\int \phi_i \phi_j dy = \int \phi'_i \, \phi'_j \, dy \equiv 0 \qquad \text{for } |i-j| \geq 4 \qquad (4-19)$$

4.2.3 Stiffness corresponding to $\{w\}$

It is often required to transform the stiffness matrix with interpolation coefficient vector $\{d\}$ as degrees of freedom to that with the nodal displacement vector $\{w\}$ as degrees of freedom. By means of matrix $[F]$ in equation (2 – 5), which indicates the relationship between the deflections of nodes and the coefficients of spline function interpolation on the nodal line, the stiffness matrix $[k]$ corresponding to $\{w\}$ can be derived from the stiffness matrix $[k^e]$ corresponding to $\{d\}$ as follows

$$[k] = [T]^T [k^e][T] \tag{4 – 20}$$

in which

$$[T] = \begin{bmatrix} [F] & 0 \\ 0 & [F] \end{bmatrix} \tag{4 – 21}$$

4.2.4 Load vector

From equations (4 – 1) and (2 – 5), the displacement w at any point in a traditional spline shear strip can be calculated as below:

$$w = [C][\Phi]\{d\} = [C][\Phi][T]\{w\} = [N]\{w\} \tag{4 – 22}$$

in which, $[N]$ is defined as

$$[N] = [C][\Phi][T] \qquad (4-23)$$

Based on the principle of virtual work, for a load $q(x,y)$ distributed on the strip and acting in the z direction, the vector of nodal forces can be formed as:

$$\{\hat{F}\} = \int_0^b \int_0^l [N]^T q(x,y)dxdy \qquad (4-24)$$

4.3 Special Area Around Crack

4.3.1 Displacement around the crack tip

According to Tilley's expansion (1978) in fracture analysis of mode III, the deflection w at any point around the crack tip in the substructure can be expressed as:

$$\begin{aligned} w(r,\theta) &= A_{-1} + \sum_{i=0}^{n} A_i r^{(2i+1)/2} Sin[(2i+1)\theta/2] \\ &= [H]\{A\} \end{aligned} \qquad (4-25)$$

where

$$[H] = [1 \quad r^{1/2}Sin(\theta/2) \quad r^{3/2}Sin(3\theta/2) \quad \cdot \quad \cdot \quad \cdot \quad r^{(2n+1)/2}Sin[(2n+1)\theta/2]]$$
$$\{A\} = [A_{-1} \quad A_0 \quad \cdot \quad \cdot \quad \cdot \quad A_n \quad]^T \qquad (4-26)$$

in which r and θ are the polar coordinates of the point in the system as shown in **Fig. 1.2**, and A_{-1} denotes the rigid body motion of substructure ①. In theory, the second term ($n=0$) contributes to the major part of stress around the crack tip, while other terms can be neglected. However, in the numerical stress analysis, in order to achieve the desired accuracy, several terms may be required, say up to A_5. Namely, total seven terms are included.

The stiffness derivation has the same procedures as that have been illustrated in section 4.2, and the strain vector $\{\varepsilon\}$ has been defined in equations (4 -3) -(4 -5), the stress vector $\{\sigma\}$ has been defined in equations (4 -7) - (4 -9). However, in this case, the strain matrix [B]is different from the one formed in equation (4 - 5), due to the use of different deflection modes.

Taking into consideration $x = rCos\theta$, $y = rSin\theta$, the strains at any point have the following relationships with the displacement w:

$$\{\varepsilon\} = \begin{Bmatrix} 2\varepsilon_{xz} \\ 2\varepsilon_{yz} \end{Bmatrix} = \begin{bmatrix} \frac{\partial r}{\partial x} & \frac{\partial \theta}{\partial x} \\ \frac{\partial r}{\partial y} & \frac{\partial \theta}{\partial y} \end{bmatrix} \begin{Bmatrix} \frac{\partial w}{\partial r} \\ \frac{\partial w}{\partial \theta} \end{Bmatrix} \qquad (4-27)$$

Thus, the strains at any point can be expressed in terms of the coefficients of Tilley's expansion as

$$\{\varepsilon\} = [B]\{A\} \qquad (4-28)$$

where

$$[B] = \frac{1}{2}\begin{bmatrix} 0 & -r^{-\frac{1}{2}}Sin\frac{\theta}{2} & 3r^{\frac{1}{2}}Sin\frac{\theta}{2} & 5r^{\frac{3}{2}}Sin\frac{3\theta}{2} & . & (2n+1)r^{\frac{(2n-1)}{2}}Sin\frac{(2n-1)\theta}{2} \\ 0 & r^{-\frac{1}{2}}Cos\frac{\theta}{2} & 3r^{\frac{1}{2}}Cos\frac{\theta}{2} & 5r^{\frac{3}{2}}Cos\frac{3\theta}{2} & . & (2n+1)r^{\frac{(2n-1)}{2}}Cos\frac{(2n-1)\theta}{2} \end{bmatrix} \tag{4-29}$$

Stress vector is the same forms as (4 – 8) and (4 – 9), i.e :

$$\{\sigma\} = [D]\{\varepsilon\} = [D][B]\{A\}$$

Then the normalized stress intensity factor K_{III}^{N}, a key parameter in fracture analysis, can be evaluated directly from the second coefficient in Tilley's expansion as

$$K_{III}^{N} = \frac{K_{III}}{\tau_0\sqrt{\pi a/2}} = \frac{A_0 G}{\tau_0\sqrt{a}} \tag{4-30}$$

in which a is the length of the crack, K_{III} is the normal stress intensity factor in mode III, and τ_0 is applied shear stress.

4.3.2 Stiffness corresponding to {A}

By taking $\{ A \}$ as the displacement parameters and following the principle of minimum total potential energy, the stiffness matrix $[\hat{k}]$ of the substructure can be formed as

$$[\hat{k}] = \int [B]^T [D][B] dA = G \int_A [B]^T [B] dA \qquad (4-31)$$

where

$$[B]^T[B] = \begin{bmatrix} 0 & 0 & 0 & 0 & \cdot & 0 \\ & r^{-1} & 3\cos\theta & 5r\cos 2\theta & \cdot & (2n+1)r^{n-1}\cos n\theta \\ & & 9r & 15r^2\cos\theta & \cdot & 3(2n+1)r^n\cos(n-1)\theta \\ & & & 25r^3 & \cdot & 5(2n+1)r^{n+1}\cos(n-2)\theta \\ & & & & \cdot & \cdot \\ & & & & & (2n+1)^2 r^{2n-1} \end{bmatrix} \qquad (4-32)$$

Since the substructure ① has a rectangular geometry, the Cartesian coordinate system is more convenient than the polar system for calculating the integration in equation (4 – 31), and the following coordinate transformation is helpful:

$$r = \sqrt{x^2 + y^2}, \quad \theta = \tan^{-1}\left(\frac{y}{x}\right) \qquad (4-33)$$

With the exception of r^{-1}, all of the integrals in (4 – 34) can be performed using regular Gaussian Quadrature Formulas in Appendix A. The singular integral of r^{-1} can be evaluated by following the procedure in Section 3.3.

4.3.3 Stiffness corresponding to {w}

In the spline finite strip analysis, the nodal deflections are taken as the unknown parameters. Therefore, the stiffness matrix formed in the previous section must be transformed. If the total number of nodes in substructure ① is L, including the interior nodes and the exterior ones, according to (4 – 25), the transformation from the coefficients $\{A\}$ to the L nodal deflections $\{w\}$ can be written as:

$$\{w\} = [U]\{A\} \qquad (4-34)$$

where

$$\{w\} = \begin{bmatrix} w_1 & w_2 & \cdot & \cdot & \cdot & w_L \end{bmatrix}^T \qquad (4-35)$$

and {A} is defined in (4 – 26).

Generally, [U] is not a square matrix, since it has ***L*** rows and ***n*** columns. For example, in **Fig 3.2(d)**, there are five exterior nodes and four extra interior nodes around the crack tip, thus $L = 9$. Consequently, the matrix [U] takes the following form as:

$$[U] = \begin{bmatrix} 1 & 0 & 0 & \cdots & 0 \\ 1 & 0 & 0 & \cdots & 0 \\ 1 & [h^2 + (\frac{b-a}{2})^2]^{1/4} Sin(\frac{\alpha}{2}) & [h^2 + (\frac{b-a}{2})^2]^{3/4} Sin(\frac{3\alpha}{2}) & \cdots & [h^2 + (\frac{b-a}{2})^2]^{(2n+1)/4} Sin[\frac{(2n+1)\alpha}{2}] \\ 1 & [h^2 + (\frac{a}{2})^2]^{1/4} Sin(\frac{\beta}{2}) & [h^2 + (\frac{a}{2})^2]^{3/4} Sin(\frac{3\beta}{2}) & \cdots & [h^2 + (\frac{a}{2})^2]^{(2n+1)/4} Sin[\frac{(2n+1)\beta}{2}] \\ 1 & a^{1/2} & -a^{3/2} & \cdots & (-1)^n a^{(2n+1)/2} \\ 1 & 0 & 0 & \cdots & 0 \\ 1 & (\frac{a}{4})^{1/2} Sin(\frac{\alpha}{2}) & (\frac{a}{4})^{3/2} Sin(\frac{3\alpha}{2}) & \cdots & (\frac{a}{4})^{(2n+1)/2} Sin[\frac{(2n+1)\alpha}{2}] \\ 1 & (\frac{a}{4})^{1/2} Sin(\frac{\beta}{2}) & (\frac{a}{4})^{3/2} Sin(\frac{3\beta}{2}) & \cdots & (\frac{a}{4})^{(2n+1)/2} Sin[\frac{(2n+1)\beta}{2}] \\ 1 & (\frac{a}{4})^{1/2} & -(\frac{a}{4})^{3/2} & \cdots & (-1)^n (\frac{a}{4})^{(2n+1)/2} \end{bmatrix} \tag{4-36}$$

Therefore, it is necessary to use the least squares procedure to invert [U]:

$$[U]^T \{w\} = [U]^T [U] \{A\} \tag{4-37}$$

which leads to

$$\{A\} = [T] \{w\} \tag{4-38}$$

where

$$[T] = [[U]^T [U]]^{-1} [U]^T \tag{4-39}$$

Further, the stiffness matrix corresponding to deflections $\{w\}$ can be obtained as

$$[k] = [T]^T [\hat{k}] [T] \tag{4-40}$$

4.3.4 Load vector

Combining equations (4 – 25) and (4 – 41), the displacement in substructure ① can be written as follows:

$$w(r,\theta) = [H]\{A\} = [H][T]\{w\} = [N]\{w\} \qquad (4-41)$$

where

$$[N] = [H][T] \qquad (4-42)$$

The load vector equivalent to an area load *q(x,y)* in the substructure can be formed as

$$\{\hat{F}\} = \int_0^b \int_0^l [N]^T q(x,y)dxdy \qquad (4-43)$$

4.4 Numerical Example

To demonstrate the efficiency and convergence of the proposed method, a numerical example is presented, and the results are compared with the existing solutions (Westmann and Yang, 1967).

1. Problem Description

As shown in **Fig. 4.1**, a rectangular plate with aspect ratio of 2:1 has a edge crack situated at the midpoint of a longer side in the direction perpendicular to this side. The length of the crack is equal to 30 percent of the plate width. A uniform shear stress, $\sigma_{yz} = \tau_0$, is applied to the shorter edge of the plate.

2. Pre – processing

Obviously, the deformation is anti-symmetric about the crack center line. If the crack center line is assumed to be fixed, then A_{-1}, the parameter related to the rigid body motion, should be equal to zero. There are one traditional spline finite strip, one anti-plane crack strip, (both have the same width *b*), and sixteen nodes in the finite strip mesh in **Fig. 4.1**.

The nodal shear forces can be calculated based on equation (4 – 24). The resulting shear force at any interior node on a short edge is equal to $b\tau_0$, while the force at any corner is equal to $b\tau_0/2$

3. Processing

The stress intensity factor is calculated following the proposed method. In order to investigate convergence of the method, different numbers of extra nodes around the crack tip and various numbers of Gaussian Quadrature points, i.e. 8,19 and 30 points in Method I; 8, 12 and 16 points in Method II (see Section 3.3), are respectively used for the singular integral. However, only five Gaussian Quadrature points are employed for the non-singular integrals.

4. Post – processing

The analytical solution for the normalized stress intensity factor is K_{III}^{N} =1.040, which is obtained by Westmann and Yang (1967) using the method of integral transformation. The numerical results of the current study are given in Table 4.1. It shows that the convergence of the current method is satisfactory, since the numerical error is reduced drastically as the numbers of the extra nodes and Guassian points are increased. When 4 extra nodes and 19 X 19 Gaussian points are employed, the numerical error has reduced to 1.1 percent. It also shows that Method I of singular integral converges faster than Method II .

Table 4.1 K_{III}^{N} value for various numbers of Gaussian Quadrature Points and corresponding Errors

	Method of Integral	8^2		19^2 (I)/12^2 (II)		30^2 (I)/16^2 (II)	
		K_{III}^{N}	error	K_{III}^{N}	error	K_{III}^{N}	error
Four Extra Nodes	I	1.089	4.7%	1.051	1.1%	1.046	0.6%
	II	1.150	10.6%	1.084	4.2%	1.058	1.0%
Three Extra Nodes	I	1.151	10.7%	1.069	2.8%	1.050	1.0%
	II	1.237	18.9%	1.096	5.4%	1.082	4.0%
Two Extra Nodes	I	1.226	17.9%	1.098	5.6%	1.073	3.2%
	II	1.312	26.2%	1.137	9.3%	1.094	5.2%
No Extra Node	I	1.301	25.1%	1.154	11.0%	1.102	6.0%
	II	1.390	33.7%	1.207	16.1%	1.123	8.0%

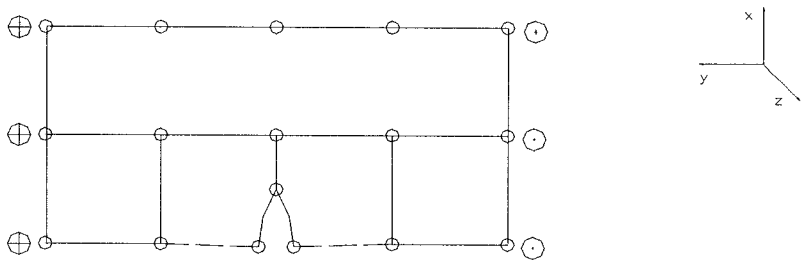

Figure 4.1 Edge Crack under Tearing Shear Stress

Chapter 5

Plane Crack Strips

In this chapter, a plane crack strip is developed for in-plane fracture analysis of structures. Details of strip formulation are presented. This is followed by numerical examples to verify the accuracy and efficiency of the proposed method.

5.1 Traditional Spline Plane Strip

5.1.1 Displacements in spline plane strip

For in-plane fracture analysis of a structure, the portion remote from crack tip can be modeled by traditional spline plane strip (**Fig. 3.1** and **Fig 3.2**). Each strip has two nodal lines,

labeled as i and j, each of which has r equally spaced nodes. The displacement components u and v, in the x and y direction respectively, at any point within each part can be interpolated using the linear functions of x transversely and the spline functions of y longitudinally as:

$$\begin{aligned} u(x,y) &= [C][\Phi]\{d\} \\ v(x,y) &= [C][\Phi]\{e\} \end{aligned} \qquad (5-1)$$

in which

$$\begin{aligned} [C] &= [1-\bar{x},\quad \bar{x}] \\ [\Phi] &= \begin{bmatrix} [\phi] & \\ & [\phi] \end{bmatrix} \\ \{d\} &= [d_i,\quad d_j]^T = [d_{i0}, d_{i1}, \cdots, d_{i(r+1)}, d_{j0}, d_{j1}, \cdots, d_{j(r+1)}]^T \\ \{e\} &= [e_i,\quad e_j]^T = [e_{i0}, e_{i1}, \cdots, e_{i(r+1)}, e_{j0}, e_{j1}, \cdots, e_{j(r+1)}]^T \\ [\phi] &= [\phi_0 \quad \phi_1 \quad \cdots \quad \phi_{r+1}] \end{aligned} \qquad (5-2)$$

where $\bar{x} = x/b$, b denotes the width of the strip, ϕ_i is spline function centered at node i, while d_i and e_i are the coefficients corresponding to ϕ_i for interpolations of u and v respectively. The strain at any point within the strip can be expressed in terms of the displacement parameters based on strain-displacement relationship:

$$\varepsilon_x = \frac{\partial u}{\partial x}$$

$$\varepsilon_y = \frac{\partial v}{\partial y}$$

$$\varepsilon_{xy} = \frac{\partial u}{\partial y} + \frac{\partial v}{\partial x}$$

or

$$\{\varepsilon\} = [B]\{de\} \tag{5-3}$$

where

$$\{\varepsilon\} = [\varepsilon_x \quad \varepsilon_y \quad \tau_{xy}]^T$$
$$[B] = \begin{bmatrix} [C'][\Phi] & 0 \\ 0 & [C][\Phi'] \\ [C][\Phi'] & [C'][\Phi] \end{bmatrix} \tag{5-4}$$
$$\{de\} = [d_{i0}, d_{i1}, \cdots d_{i(r+1)}, d_{j0}, d_{j1}, \cdots d_{j(r+1)}, e_{i0}, e_{i1}, \cdots e_{i(r+1)}, e_{j0}, e_{j1}, \cdots e_{j(r+1)}]^T$$

The stress at any point within the strip can be expressed in terms of the displacement parameter based on stress-strain relationship:

$$\sigma_x = \frac{E}{1-\nu^2}(\varepsilon_x + \nu\varepsilon_y)$$
$$\sigma_y = \frac{E}{1-\nu^2}(\varepsilon_y + \nu\varepsilon_x)$$
$$\tau_{xy} = \frac{E}{2(1+\nu)}\varepsilon_{xy}$$

or

$$\{\sigma\} = [D]\{\varepsilon\} = [D][B]\{de\} \tag{5-5}$$

where

$$\{\sigma\} = [\sigma_x \quad \sigma_y \quad \tau_{xy}]^T$$

$$[D] = \frac{E}{1-\nu^2}\begin{bmatrix} 1 & \nu & 0 \\ \nu & 1 & 0 \\ 0 & 0 & \frac{1-\nu}{2} \end{bmatrix} \qquad \text{(for plane stress analysis)} \qquad (5-6)$$

For plane strain analysis, E and ν should be replaced by $\frac{E}{1-\nu^2}$ and $\frac{\nu}{1-\nu}$, respectively.

5.1.2 Stiffness matrix corresponding to {de}

Stiffness matrix of a finite strip can be formed according to equation (4 – 10). Taking the following notation

$$[C_2] = \int_0^b [C']^T [C] dx = \int_0^b \begin{bmatrix} \bar{x}-1 & -\bar{x} \\ 1-\bar{x} & \bar{x} \end{bmatrix} dx = \frac{b^2}{2}\begin{bmatrix} -1 & -1 \\ 1 & 1 \end{bmatrix} \qquad (5-7)$$

the stiffness matrix $[k^e]$ of traditional spline strip can be expressed as

$$[k^e] = \int_A [B^T][D][B] dA$$

$$= \int_0^l \begin{bmatrix} [\Phi]^T[C_1][\Phi] + \frac{1-\upsilon}{2}[\Phi']^T[C_0][\Phi'] & \upsilon[\Phi]^T[C_2][\Phi'] + \frac{1-\upsilon}{2}[\Phi']^T[C_2]^T[\Phi] \\ \upsilon[\Phi']^T[C_2]^T[\Phi] + \frac{1-\upsilon}{2}[\Phi]^T[C_2][\Phi'] & [\Phi']^T[C_0][\Phi'] + \frac{1-\upsilon}{2}[\Phi]^T[C_1][\Phi] \end{bmatrix} dy$$

$$= \begin{bmatrix} [k_{11}] & [k_{12}] \\ [k_{21}] & [k_{22}] \end{bmatrix} \qquad (5-8)$$

where $[C_0]$ and $[C_1]$ have been introduced in equation (4 – 11), and

$$[k_{11}] = \frac{1}{b}\int_0^l \begin{bmatrix} [\Phi]^T[\Phi] & -[\Phi]^T[\Phi] \\ -[\Phi]^T[\Phi] & [\Phi]^T[\Phi] \end{bmatrix} dy + \frac{(1-\nu)b}{12}\int_0^l \begin{bmatrix} 2[\Phi']^T[\Phi'] & [\Phi']^T[\Phi'] \\ [\Phi']^T[\Phi'] & 2[\Phi']^T[\Phi'] \end{bmatrix} dy$$

$$[k_{12}] = [k_{21}]^T = \frac{\nu b^2}{2}\int_0^l \begin{bmatrix} -[\Phi]^T[\Phi'] & -[\Phi]^T[\Phi'] \\ [\Phi]^T[\Phi'] & [\Phi]^T[\Phi'] \end{bmatrix} dy + \frac{(1-\nu)b^2}{4}\int_0^l \begin{bmatrix} -[\Phi']^T[\Phi] & [\Phi']^T[\Phi] \\ -[\Phi']^T[\Phi] & [\Phi']^T[\Phi] \end{bmatrix} dy$$

$$[k_{22}] = \frac{1-\nu}{2b}\int_0^l \begin{bmatrix} [\Phi]^T[\Phi] & -[\Phi]^T[\Phi] \\ -[\Phi]^T[\Phi] & [\Phi]^T[\Phi] \end{bmatrix} dy + \frac{b}{6}\int_0^l \begin{bmatrix} 2[\Phi']^T[\Phi'] & [\Phi']^T[\Phi'] \\ [\Phi']^T[\Phi'] & 2[\Phi']^T[\Phi'] \end{bmatrix} dy$$

(5 – 9)

Moreover, $\int[\Phi]^T[\Phi]dy$ and $\int[\Phi']^T[\Phi']dy$ can be evaluated using equations (4 – 13) to (4 –19), and

$$\int[\Phi']^T[\Phi]dy = \begin{bmatrix} \int[\phi']^T[\phi]dy & 0 \\ 0 & \int[\phi']^T[\phi]dy \end{bmatrix} \qquad (5-10)$$

where

$$\int[\phi']^T[\phi]dy = \begin{bmatrix} I'_0 & I'_1 & I'_2 & I'_3 & 0 & \cdot & \cdot & 0 \\ I'_1 & I'_0 & I'_1 & I'_2 & I'_3 & 0 & \cdot & 0 \\ \cdot & \cdot & \cdot & \cdot & \cdot & \cdot & \cdot & \cdot \\ 0 & \cdot & 0 & I'_3 & I'_2 & I'_1 & I'_0 & I'_1 \\ 0 & \cdot & \cdot & 0 & I'_3 & I'_2 & I'_1 & I'_0 \end{bmatrix} \qquad (5-11)$$

in which

$$I'_0 = \int_{y_{i-2}}^{y_{i+2}} \phi'_i \phi_i dy \qquad (i = j)$$

$$I'_1 = \int_{y_{i-1}}^{y_{i+2}} \phi'_i \phi_j dy \qquad (|i - j| = 1)$$

$$I'_2 = \int_{y_i}^{y_{i+2}} \phi'_i \phi_j dy \qquad (|i - j| = 2)$$

$$I'_3 = \int_{y_{i+1}}^{y_{i+2}} \phi'_i \phi_j dy \qquad (|i - j| = 3) \qquad (5-12)$$

5.1.3 Stiffness corresponding to {u} and {v}

By means of matrix [F] in equation (2 - 5), which indicates the relationship between the displacements of nodes and the coefficients of spline function interpolation on the nodal line, the stiffness matrix $[k]$ corresponding to $\{u\}$ and $\{v\}$ can be derived from the stiffness matrix $[k^e]$ corresponding to $\{ d \}$ as follows

$$[k] = [T]^T [k^e][T] \qquad (5-13)$$

where

$$[T] = \begin{bmatrix} [F_{ui}] & 0 & 0 & 0 \\ 0 & [F_{uj}] & 0 & 0 \\ 0 & 0 & [F_{vi}] & 0 \\ 0 & 0 & 0 & [F_{vj}] \end{bmatrix} \qquad (5-14)$$

and $[F_{ui}]$, $[F_{uj}]$, $[F_{vi}]$ and $[F_{vj}]$ represent the relationships between the displacements u, v of nodes on nodal line i, j and the coefficients of spline function interpolation, respectively.

5.1.4 Load vector

Based on equations (5 – 1), (2 – 5), (4 – 22) and (4 – 23), the displacements at any point can be written as follows:

$$\begin{aligned}[N_u] &= [C][\Phi][T_u] \\ [N_v] &= [C][\Phi][T_v]\end{aligned} \qquad (5-15)$$

where

$$\begin{aligned}[T_u] &= \begin{bmatrix}[F_{ui}] & 0 \\ 0 & [F_{uj}]\end{bmatrix} \\ [T_v] &= \begin{bmatrix}[F_{vi}] & 0 \\ 0 & [F_{vj}]\end{bmatrix}\end{aligned} \qquad (5-16)$$

The load vectors, equivalent to area loads $p_x(x,y)$, $p_y(x,y)$, acting in the x and y directions respectively, can be formed as

$$\begin{aligned}[P_{ix} \quad P_{jx}]^T &= \int_0^b \int_0^l [N_u]^T p_x(x,y)dxdy \\ [P_{iy} \quad P_{jy}]^T &= \int_0^b \int_0^l [N_v]^T p_y(x,y)dxdy\end{aligned} \qquad (5-17)$$

5.2 Special Area Around Crack

5.2.1 Displacements around the crack tip

The displacements in polar coordinates u_r and u_θ can be expressed by Williams' expansion (1957):

$$u_r = \sum_{i=1}^{n} r^{i/2}[a_i F_{ei}(\theta) + b_i F_{oi}(\theta)] + u_0 \sin\theta + v_0 \cos\theta$$

$$u_\theta = \sum_{i=1}^{n} r^{i/2}[a_i G_{oi}(\theta) + b_i G_{ei}(\theta)] + u_0 \cos\theta - v_0 \sin\theta$$

or in a matrix form:

$$\{u_{r\theta}\} = [H]\{A\} \qquad (5-18)$$

where u_0 and v_0 represent the rigid-body motion, and

$$\{u_{r\theta}\} = [u_r \quad u_\theta]^T$$

$$[H] = \begin{bmatrix} [r^{1/2}F_{e1}(\theta) & rF_{e2}(\theta) & r^{3/2}F_{e3}(\theta) & r^{1/2}F_{o1}(\theta) & rF_{o2}(\theta) & r^{3/2}F_{o3}(\theta) & Sin\theta & Cos\theta] \\ r^{1/2}G_{o1}(\theta) & rG_{o2}(\theta) & r^{3/2}G_{o3}(\theta) & r^{1/2}G_{e1}(\theta) & rG_{e2}(\theta) & r^{3/2}G_{e3}(\theta) & Cos\theta & Sin\theta \end{bmatrix}$$

$$\{A\} = [a_1, a_2, a_3, b_1, b_2, b_3, u_0, v_0]^T \qquad (5-19)$$

and

$$
\begin{aligned}
F_{ei} &= (\frac{i-6}{2}+4\upsilon)\cos(\frac{i}{2}-1)\theta-[\frac{i}{2}+(-1)^i]\cos(\frac{i}{2}+1)\theta \\
G_{oi} &= (-\frac{i+6}{2}+4\upsilon)\sin(\frac{i}{2}-1)\theta-[\frac{i}{2}+(-1)^i]\sin(\frac{i}{2}+1)\theta \\
F_{oi} &= (\frac{i-6}{2}+4\upsilon)\sin(\frac{i}{2}-1)\theta-[\frac{i}{2}-(-1)^i]\sin(\frac{i}{2}+1)\theta \\
G_{ei} &= (\frac{i+6}{2}-4\upsilon)\cos(\frac{i}{2}-1)\theta-[\frac{i}{2}-(-1)^i]\cos(\frac{i}{2}+1)\theta
\end{aligned}
\qquad (5-20)
$$

For the same reason as mentioned in Section 4.3.1, $n = 3$ is taken in the current analysis.

The stiffness derivation procedures have been illustrated in section 5.1, and the strain vector $\{\varepsilon\}$ has been defined in equations (5 -3) -(5 -4), the stress vector $\{\sigma\}$ has been defined in equations (5 -5) - (5 -6). However, in this case, the strain matrix $[B]$ is different from the one defined in equation (5 - 4), due to the use of two different displacement modes.

Strain vector can be obtained using the strain-displacement relationships as:

$$
\{\varepsilon\}=\begin{Bmatrix}\varepsilon_r\\ \varepsilon_\theta\\ \gamma_{r\theta}\end{Bmatrix}=\begin{Bmatrix}\dfrac{\partial u_r}{\partial r}\\ \dfrac{1}{r}\dfrac{\partial u_\theta}{\partial\theta}+\dfrac{u_r}{r}\\ \dfrac{1}{r}\dfrac{\partial u_r}{\partial\theta}+\dfrac{\partial u_\theta}{\partial r}\end{Bmatrix}=[B]\{A\}
$$

where

$$
[B]=\begin{bmatrix}
\frac{1}{2}r^{-\frac{1}{2}}F_{e1}(\theta) & F_{e2}(\theta) & \frac{3}{2}r^{\frac{1}{2}}F_{e3}(\theta) & \frac{1}{2}r^{-\frac{1}{2}}F_{o1}(\theta) & F_{o2}(\theta) & \frac{3}{2}r^{\frac{1}{2}}F_{o3}(\theta) & 0 & 0\\
r^{-\frac{1}{2}}(F_{e1}+G'_{o1}) & F_{e2}+G'_{o2} & r^{\frac{1}{2}}(F_{e3}+G'_{o3}) & r^{-\frac{1}{2}}(F_{o1}+G'_{e1}) & F_{o2}+G'_{e2} & r^{\frac{1}{2}}(F_{o3}+G'_{e3}) & 0 & \frac{2Cos\theta}{r}\\
r^{-\frac{1}{2}}(\frac{G_{o1}}{2}+F'_{e1}) & G_{o2}+F'_{e2} & r^{\frac{1}{2}}(\frac{3G_{o3}}{2}+F'_{e3}) & r^{-\frac{1}{2}}(\frac{G_{e1}}{2}+F'_{o1}) & G_{e2}+F'_{o2} & r^{\frac{1}{2}}(\frac{3G_{e3}}{2}+F'_{o3}) & \frac{Cos\theta}{r} & -\frac{Sin\theta}{r}
\end{bmatrix}
\qquad (5-21)
$$

and

$$
\begin{aligned}
F'_{ei} &= (1-\frac{i}{2})(\frac{i-6}{2}+4\upsilon)\sin(\frac{i}{2}-1)\theta+(\frac{i}{2}+1)[\frac{i}{2}+(-1)^i]\sin(\frac{i}{2}+1)\theta \\
G'_{oi} &= (\frac{i}{2}-1)(-\frac{i+6}{2}+4\upsilon)\cos(\frac{i}{2}-1)\theta-(\frac{i}{2}+1)[\frac{i}{2}+(-1)^i]\cos(\frac{i}{2}+1)\theta \\
F'_{oi} &= (\frac{i}{2}-1)(\frac{i-6}{2}+4\upsilon)\cos(\frac{i}{2}-1)\theta-(\frac{i}{2}+1)[\frac{i}{2}-(-1)^i]\cos(\frac{i}{2}+1)\theta \\
G'_{ei} &= (1-\frac{i}{2})(\frac{i+6}{2}-4\upsilon)\sin(\frac{i}{2}-1)\theta+(\frac{i}{2}+1)[\frac{i}{2}-(-1)^i]\sin(\frac{i}{2}+1)\theta
\end{aligned}
\qquad (5-22)
$$

Then the stress vector can be formed as

$$\{\sigma\} = [D]\{\varepsilon\} = [D][B]\{A\} \qquad (5-23)$$

The stress intensity factors, K_I for the opening mode and K_{II} for the sliding mode can be respectively obtained from the leading terms of the Williams' expansion in the form of

$$K_I = G\sqrt{2\pi}\cdot|a_1|, \qquad K_{II} = G\sqrt{2\pi}\cdot|b_1| \qquad (5-24)$$

where G is the shear modulus.

5.2.2 Stiffness matrix corresponding to $\{A\}$

By taking $\{A\}$ as the displacement parameters and following the principle of minimum total potential energy, the stiffness matrix of the substructure can be formed as

$$[\hat{k}] = \int_A [B]^T [D][B] dA \qquad (5-25)$$

Since the substructure ① has a rectangular geometry, the Cartesian coordinate system is more convenient than the polar system for calculating the integration in Equation (5 -25), and the following coordinate transformation is helpful:

$$r = \sqrt{x^2 + y^2}, \quad \theta = \tan^{-1}\left(\frac{y}{x}\right) \qquad (5-26)$$

With the exception of r^{-1}, all of integrals can be performed by regular Gaussian Quadrature Formulas in Appendix A. The singular integral of r^{-1} can be evaluated using the methods listed in Section 3.3.

5.2.3 Stiffness matrix corresponding to {uv}

If the total number of nodes in substructure ① is L, including the interior nodes and the exterior ones; according to (5 – 18) and (5 – 19), the transformation between the nodal displacements $\{uv\}$ and the coefficients $\{A\}$ can be written as

$$\{u\} = [U]\{A\} \qquad (5-27)$$

where

$$\{u\} = \left[u_{r1}, u_{\theta 1}, u_{r2}, u_{\theta 2}, \cdots, u_{rL}, u_{\theta L}\right]^T \qquad (5-28)$$

and $\{A\}$ is defined in (5 – 19c).

Generally, $[U]$ is not a square matrix, since it has L rows and n columns. For example, in **Fig 3.2(d)**, there are five exterior nodes and four extra interior nodes around the crack tip, thus $L = 9$. Consequently, the matrix $[U]$ takes the form:

$$[U] = \begin{bmatrix}
0 & 0 & 0 & 0 & 0 & 0 & 0 & 1 \\
0 & 0 & 0 & 0 & 0 & 0 & 1 & 0 \\
l_{31} & l_{32} & l_{33} & 0 & 0 & 0 & 0 & 1 \\
0 & 0 & 0 & -l_{31} & -l_{32} & l_{33} & 1 & 0 \\
l_{51} & l_{52} & l_{53} & l_{54} & 0 & l_{56} & \sin\alpha & \cos\alpha \\
l_{61} & l_{62} & l_{63} & l_{64} & l_{65} & l_{66} & \cos\alpha & -\sin\alpha \\
l_{71} & l_{72} & l_{73} & l_{74} & 0 & l_{76} & \sin\beta & \cos\beta \\
l_{81} & l_{82} & l_{83} & l_{84} & l_{85} & l_{86} & \cos\beta & -\sin\beta \\
0 & l_{92} & 0 & l_{92} & 0 & -l_{92} & 0 & -1 \\
l_{92} & 0 & -l_{92} & 0 & l_{92} & 0 & -1 & 0 \\
\lambda_1 l_{31} & \lambda_1^2 l_{32} & \lambda_1^3 l_{33} & 0 & 0 & 0 & 0 & 1 \\
0 & 0 & 0 & -\lambda_1 l_{31} & -\lambda_1^2 l_{32} & -\lambda_1^3 l_{33} & 1 & 0 \\
\lambda_2 l_{51} & \lambda_2^2 l_{52} & \lambda_2^3 l_{53} & \lambda_2 l_{54} & 0 & \lambda_2^3 l_{56} & \sin\alpha & \cos\alpha \\
\lambda_2 l_{61} & \lambda_2^2 l_{62} & \lambda_2^3 l_{63} & \lambda_2 l_{64} & \lambda_2^2 l_{65} & \lambda_2^3 l_{66} & \cos\alpha & -\sin\alpha \\
\lambda_3 l_{71} & \lambda_3^2 l_{72} & \lambda_3^3 l_{73} & \lambda_3 l_{74} & 0 & \lambda_3^3 l_{76} & \sin\beta & \cos\beta \\
\lambda_3 l_{81} & \lambda_3^2 l_{82} & \lambda_3^3 l_{83} & \lambda_3 l_{84} & \lambda_3^2 l_{85} & \lambda_3^3 l_{86} & \cos\beta & -\sin\beta \\
0 & \frac{1}{4} l_{92} & 0 & \frac{1}{2} l_{92} & 0 & \frac{-1}{8} l_{92} & 0 & -1 \\
\frac{1}{2} l_{92} & 0 & \frac{-1}{8} l_{92} & 0 & \frac{1}{4} l_{92} & 0 & -1 & 0
\end{bmatrix} \tag{5-29}$$

in which

$$l_{31} = (2\nu - 1)[2(b-a)]^{1/2} \qquad l_{32} = 2(\nu - 1)(b-a)$$

$$l_{33} = \frac{\sqrt{2}}{2}(2\nu - 1)(b-a)^{3/2}$$

$$l_{51} = r_3^{1/2}[(4\nu - 5/2)\cos(\alpha/2) + \cos(3\alpha/2)/2]$$

$$l_{52} = 2r_3[2\nu - 1 - \cos(2\alpha)]$$

$$l_{53} = r_3^{3/2}[(4\nu - 3/2)\cos(\alpha/2) - \cos(5\alpha/2)/2]$$

$$l_{54} = r_3^{1/2}[(5/2 - 4\nu)\sin(\alpha/2) + 3\sin(3\alpha/2)/2]$$

$$l_{56} = r_3^{3/2}[(4\nu - 3/2)\sin(\alpha/2) - 5\sin(5\alpha/2)/2]$$

$$l_{61} = r_3^{1/2}[(7/2 - 4\nu)\sin(\alpha/2) - \sin(3\alpha/2)/2$$

$$l_{62} = 2r_3\sin(2\alpha)$$

$$l_{63} = r_3^{3/2}[(4\nu - 9/2)\sin(\alpha/2) - \sin(5\alpha/2)/2]$$

$$l_{64} = r_3^{1/2}[(7/2 - 4\nu)\cos(\alpha/2) - 3\cos(3\alpha/2)/2]$$

$$l_{65} = 4r_3(1-\nu)$$

$$l_{66} = r_3^{3/2}[(9/2 - 4\nu)\cos(\alpha/2) - 5\cos(5\alpha/2)/2]$$

$$l_{71} = r_4^{1/2}[(4\nu - 5/2)\cos(\beta/2) + \cos(3\beta/2)/2]$$

$$l_{72} = 2r_4[2\nu - 1 - \cos(2\beta)]$$

$$l_{73} = r_4^{3/2}[(4\nu - 3/2)\cos(\beta/2) - \cos(5\beta/2)/2]$$

$$l_{74} = r_4^{1/2}[(5/2 - 4\nu)\sin(\beta/2) + 3\sin(3\beta/2)/2]$$

$$l_{76} = r_4^{3/2}[(4\nu - 3/2)\sin(\beta/2) - 5\sin(5\beta/2)/2]$$

$$l_{81} = r_4^{1/2}[(7/2 - 4\nu)\sin(\beta/2) - \sin(3\beta/2)/2$$

$$l_{82} = 2r_4\sin(2\beta)$$

$$l_{83} = r_4^{3/2}[(4\nu - 9/2)\sin(\beta/2) - \sin(5\beta/2)/2]$$

$$l_{84} = r_4^{1/2}[(7/2 - 4\nu)\cos(\beta/2) - 3\cos(3\beta/2)/2]$$

$$l_{85} = 4r_4(1-\nu)$$

$$l_{86} = r_4^{3/2}[(9/2 - 4\nu)\cos(\beta/2) - 5\cos(5\beta/2)/2]$$

$$l_{92} = 4(1-\nu) \qquad (5-30)$$

and

$$r_3 = \sqrt{h^2 + (\frac{b-a}{2})^2} \qquad r_4 = \sqrt{h^2 + (\frac{a}{2})^2}$$

$$\lambda_1 = \frac{\sqrt{a}}{2\sqrt{b-a}} \qquad \lambda_2 = \frac{\sqrt{a}}{2\sqrt[4]{4h^2 + (b-a)^2}}$$

$$\lambda_3 = \frac{\sqrt{a}}{2\sqrt[4]{4h^2 + a^2}} \qquad (5-31)$$

Since $[U]$ is not a square matrix, it is necessary to use the least squares procedure to invert $[U]$.

$$[U]^T\{u\} = [U]^T[U]\{A\}$$

which leads to

$$\{A\} = [t]\{u\} \qquad (5-32)$$

where

$$[t] = [[U]^T[U]]^{-1}[U]^T$$

Moreover, the polar coordinate displacement at any node j in substructure ①, i.e. u_r and u_θ can be transformed from u_j and v_j in Cartesian coordinate (see **Fig 5.1**):

$$\begin{Bmatrix} u_{rj} \\ u_{\theta j} \end{Bmatrix} = \begin{bmatrix} \cos\theta_j & \sin\theta_j \\ -\sin\theta_j & \cos\theta_j \end{bmatrix} \begin{Bmatrix} u_j \\ v_j \end{Bmatrix} \qquad (5-33)$$

For the total nine nodes, the transformation can be expressed as

$$\{u\} = [e]\{uv\} \qquad (5-34)$$

where

$$[e] = \begin{bmatrix} [I] & & & & & & & & \\ & [I] & & & & & & & \\ & & [e_1] & & & & & & \\ & & & [e_2] & & & & & \\ & & & & -[I] & & & & \\ & & & & & [I] & & & \\ & & & & & & [e_1] & & \\ & & & & & & & [e_2] & \\ & & & & & & & & -[I] \end{bmatrix} \qquad (5-35)$$

in which

$$[I]=\begin{bmatrix}1 & 0\\ 0 & 1\end{bmatrix} \qquad [e_1]=\begin{bmatrix}\cos\alpha & \sin\alpha\\ -\sin\alpha & \cos\alpha\end{bmatrix}$$

$$[e_2]=\begin{bmatrix}\cos\beta & \sin\beta\\ -\sin\beta & \cos\beta\end{bmatrix} \qquad (5-36)$$

and

$$\{uv\} = \left[u_1, v_1, u_2, v_2, \cdots, u_9, v_9\right]^T \qquad (5-37)$$

Thus, (5–32) can be rewritten as

$$\{A\} = [T]\{uv\} \qquad (5-38)$$

where

$$[T] = [t][e] \qquad (5-39)$$

Therefore, the stiffness matrix corresponding to $\{uv\}$ can be formed as

$$[k] = [T]^T[\hat{k}][T] \qquad (5-40)$$

5.2.4 Load vector

From (5 – 18) and (5– 38), the displacements in substructure ① can be written as the following:

$$\begin{aligned}\{u_{xy}\} &= [E]\{u_{r\theta}\} = [E][H]\{A\} \\ &= [E][H][T]\{uv\} = [N]\{uv\}\end{aligned} \tag{5-41}$$

where

$$\begin{aligned}[N] &= [E][H][T] \\ [E] &= \begin{bmatrix} \cos\theta & \sin\theta \\ -\sin\theta & \cos\theta \end{bmatrix}\end{aligned} \tag{5-42}$$

Thus, the load vector equivalent to loads $p_x(x,y)$, $p_y(x,y)$ in the substructure can be obtained as

$$[P_{ix} \quad P_{jx} \quad P_{iy} \quad P_{jy}]^T = \int_0^b \int_0^l [N]^T [p_x \quad p_y]^T \, dxdy \tag{5-43}$$

5.3 Numerical Examples

Two numerical examples are presented here to verify the proposed method and to show the efficiency and convergence of the plane crack strip model.

5.3.1 Rectangular plate with single edge notch under tension

1. Problem Description

A single edge notched specimen is subjected to uniaxial tension, as shown in Fig 5.2. Dimension, material properties and load are listed below

$$a = 30mm, \quad W = 100mm, \quad l = 150mm, \quad \sigma = 1Mpa,$$
$$\nu = 0.25, \quad E = 200{,}000\,Mpa \qquad (5-44)$$

According to Anderson's (1995) experimental solutions, the stress intensity factor is expressed as:

$$K_I = \sigma\sqrt{W} f(a/W)$$
$$f(a/W) = \frac{\sqrt{2\tan(\pi a/2W)}}{\cos(\pi a/2W)}[0.752 + 2.02(\frac{a}{W}) + 0.37(1 - \sin\frac{\pi a}{2W})^3 \qquad (5-45)$$

Based on the above equations, the following values are obtained for the given specimen:

$$K_I = 4.979$$
$$K_{II} = 0 \qquad (5-46)$$

2. Pre – processing

I. Finite Strip Model

As shown in **Fig 5.3**, the specimen is modeled by one traditional spline strip and one crack strip, each of which is divided into six sections by equally spaced knots. The width of each strip is b = 50 mm, while the knot spacing is h = 25 mm. It should be noticed that nodes 18 and 20 have the same coordinates, but different displacements.

II. Load evaluation

In this model, the stress σ is represented by its equivalent forces acting on the short edges as shown in **Fig. 5.4**, in which $p = \frac{b\sigma}{2}$.

III. Boundary conditions

Because the structure and loading are both symmetrical about the central vertical line, the horizontal displacements at nodes 4, 11 and 19 on this line should be zero

$$v_4 = v_{11} = v_{19} = 0.$$

In addition, in order to eliminate the rigid-body motion, the vertical displacement at node 19 is assumed to be zero $u_{19} = 0$..

3. Processing

The stress intensity factors are calculated following the proposed method. In order to investigate convergence of the method, different numbers of extra nodes around the crack tip and various numbers of Gaussian Quadrature points, i.e. 8,19 and 30 points in Method I; 8, 12 and 16 points in Method II (see Section 3.3), are respectively used for the singular integral. However, only five Gaussian Quadrature points are employed for the non-singular integrals.

4. Post – processing

The resulting stress intensity factors and K_I's errors compared to the value of (5 – 46) are shown in Table 5.1 for plane strain, and in Table 5.2 for plane stress. The convergence of the current method in this example is satisfactory, since the numerical error is drastically reduced to 0.5 percent as the numbers of the extra nodes and Guassian points are increased. They show that Method I of singular integral converges faster than Method II .

Table 5.1 *K* Values of Edge Notch under Tension (Plane Strain)

	Method of Integral	K_I, K_{II} for various numbers of Gaussian Quadrature Points and K_I Errors								
		8^2			19^2 (I)/12^2 (II)			30^2 (I)/16^2 (II)		
		K_I	Error	K_{II}	K_I	Error	K_{II}	K_I	Error	K_{II}
Four Extra Nodes	I	5.243	5.3%	0.010	5.033	1.1%	0.004	5.004	0.5%	0.002
	II	5.487	10.2%	0.021	5.223	4.9%	0.006	5.029	1.0%	0.003
No Extra Node	I	6.184	24.2%	0.045	5.527	11.0%	0.011	5.283	6.1%	0.003
	II	6.547	31.5%	0.071	5.751	15.5%	0.025	5.247	9.0%	0.004

Table 5.2 K Values of Edge Notch under Tension (Plane Stress)

	Method of Integral	K_I, K_{II} for various numbers of Gaussian Quadrature Points and K_I Errors								
		8^2			19^2 (I)/12^2 (II)			30^2 (I)/16^2 (II)		
		K_I	Error	K_{II}	K_I	Error	K_{II}	K_I	Error	K_{II}
Four Extra Nodes	I	5.273	5.9%	0.012	5.074	1.9%	0.006	5.019	0.8%	0.003
	II	5.537	11.2%	0.023	5.238	5.2%	0.008	5.044	1.3%	0.005
No Extra Node	I	6.199	24.5%	0.049	5.547	11.4%	0.015	5.288	6.2%	0.005
	II	6.597	32.5%	0.078	5.766	15.8%	0.026	5.457	9.6%	0.006

5.3.2 Concentrated tangential forces on a crack embedded in infinite plane

1. Problem Description

G. C. Sih (1973) presented analytical solutions for the stress intensity factors of a crack embedded in an infinite plane with two concentrated tangential forces acting on the crack surfaces (**Fig 5.5**). These solutions are shown as:

$$K_I = 0, \quad K_{II} = \frac{q}{\pi\sqrt{a}} \qquad (5-47)$$

In the current analysis, the infinite plane is modeled by a plate with aspect ratio $l/a = 10 >> 5$ (**Fig 5.6**) with the dimensions and material properties listed below

a = 30 mm, l = 300 *mm*, q = 1 Mpa, **v** =0.25, E = 200,000 Mpa

For this model, the analytical solutions can be obtained based on equation (5-47) as

$$K_I = 0, \quad K_{II} = 0.1838 \qquad (5-48)$$

2. Pre – processing

I. Finite strip model

As shown in **Fig 5.7**, the plate is modeled by four traditional spline strips and one crack strip, each of which is divided into six sections by equally spaced knots. The width of each strip and the knot spacing are both equal to 50 mm, i.e $h = b$ = 50 mm. It should be noticed that nodes 25 and 27 have the same coordinates, but different displacements.

II. Boundary conditions

Because of symmetrical geometry and anti-symmetrical loads, the deformation is antisymmetric about central vertical line, for instance, $u_{18} = -u_{35}$, $v_{18} = -v_{35}$ etc..

3. Processing

The procedure is the same as that in example 1.

4. Post – processing

The resulting stress intensity factors and K_{II}'s errors compared to the value of (5 – 48) are listed in Table 5.3 for plane strain, and in Table 5.4 for plane stress. They show that the convergence of the current method is satisfactory, since the numerical error is drastically reduced to 0.7 percent as the numbers of the extra nodes and Guassian points are increased. Method I of singular integral also converges faster than Method II .

Table 5.3 K Values of Crack under Concentrated Tangential Forces on The Crack (Plane Strain)

	Method of Integral	K_I, K_{II} for various numbers of Gaussian Quadrature Points and K_{II} Errors								
		8^2			19^2 (I)/12^2 (II)			30^2 (I)/16^2 (II)		
		K_{II}	Error	K_I	K_{II}	Error	K_I	K_{II}	Error	K_I
Four Extra Nodes	I	0.191	3.9%	0.006	0.189	2.8%	0.003	0.185	0.7%	0.001
	II	0.202	9.9%	0.008	0.191	3.9%	0.005	0.186	1.1%	0.001
No Extra Node	I	0.241	31.1%	0.021	0.195	6.1%	0.009	0.190	3.4%	0.002
	II	0.249	35.5%	0.035	0.220	19.7%	0.010	0.200	8.8%	0.002

Table 5.4 K Values of Crack under Concentrated Tangential Forces on The Crack (Plane Stress)

	Method of Integral	K_I, K_{II} for various numbers of Gaussian Quadrature Points and K_{II} Errors								
		8^2			19^2 (I)/12^2 (II)			30^2 (I)/16^2 (II)		
		K_{II}	Error	K_I	K_{II}	Error	K_I	K_{II}	Error	K_I
Four Extra Nodes	I	0.190	3.4%	0.009	0.188	2.3%	0.004	0.185	0.7%	0.002
	II	0.210	14.3%	0.011	0.191	3.9%	0.006	0.187	1.8%	0.002
No Extra Node	I	0.239	30.0%	0.022	0.199	8.3%	0.010	0.191	3.9%	0.002
	II	0.249	35.5%	0.036	0.220	19.7%	0.011	0.200	8.8%	0.003

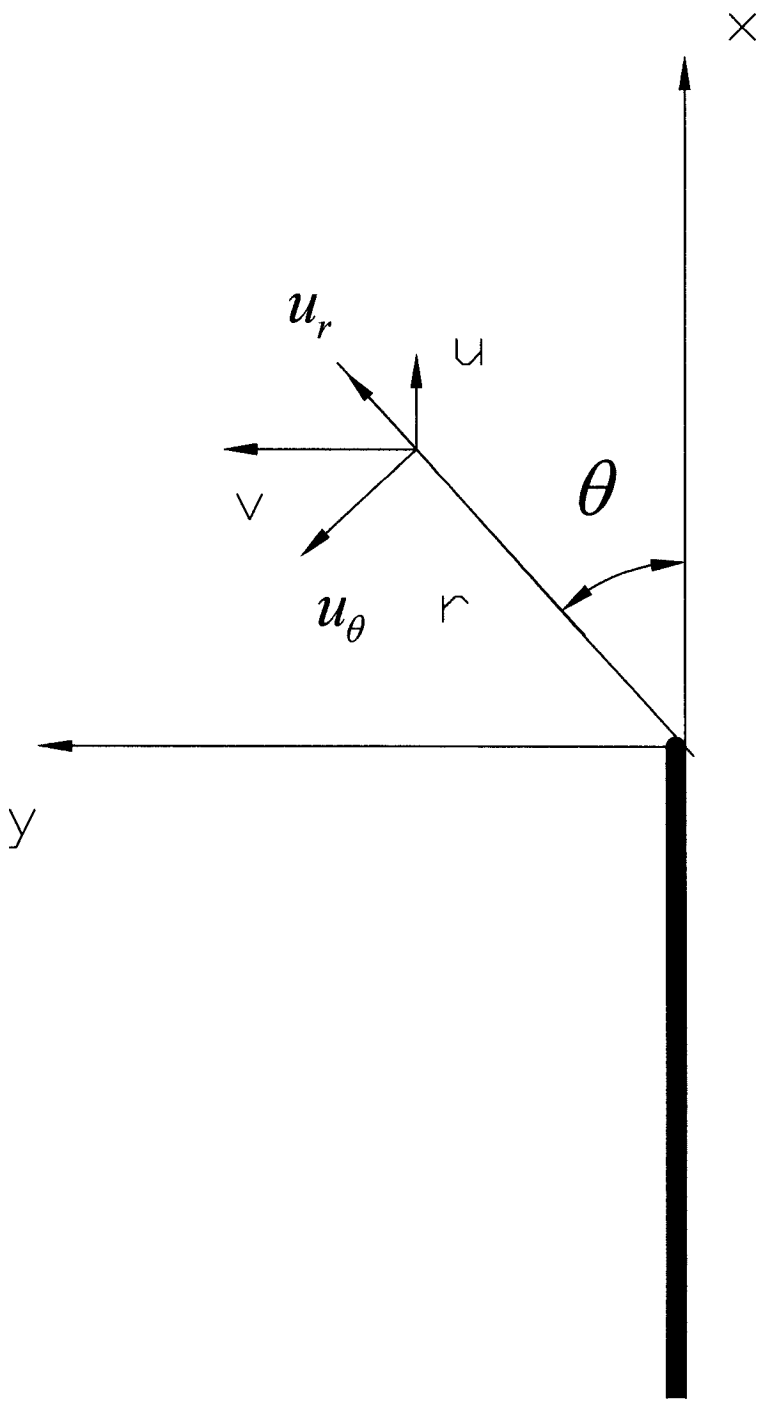

Figure 5.1 Cartesian coordinate and polar coordinate

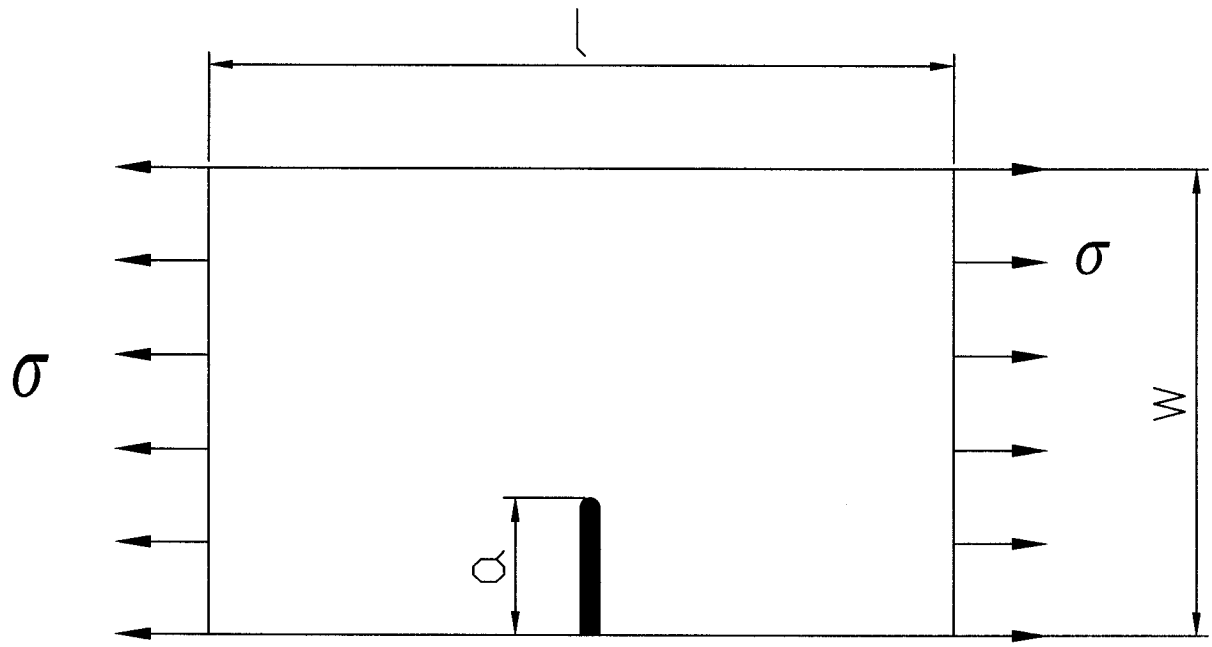

Figure 5.2 Single Edge Notch under Tension

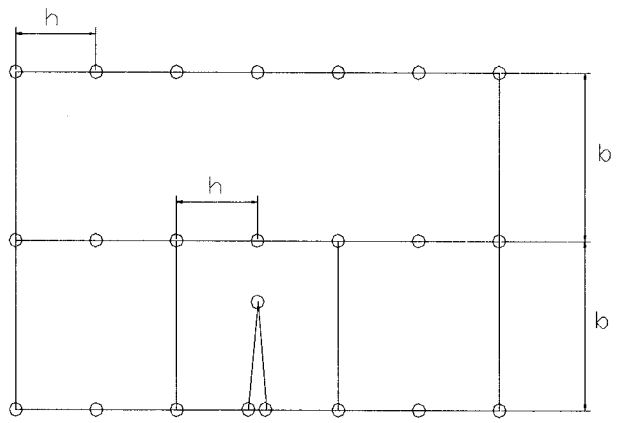

Figure 5.3 Finite Strip Mesh of Example 1

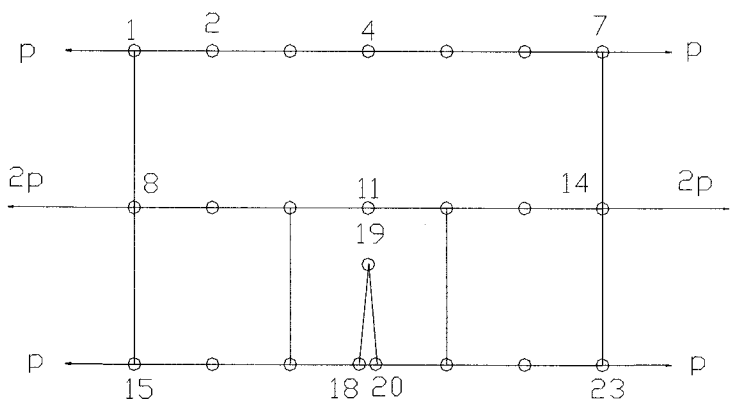

Figure 5.4 Load vector

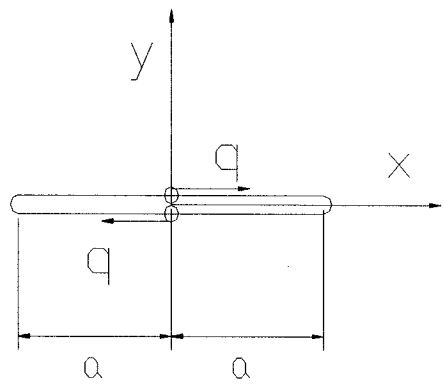

Figure 5.5 Concentrated Tangential Forces on The Crack Embedded in Infinite Plane

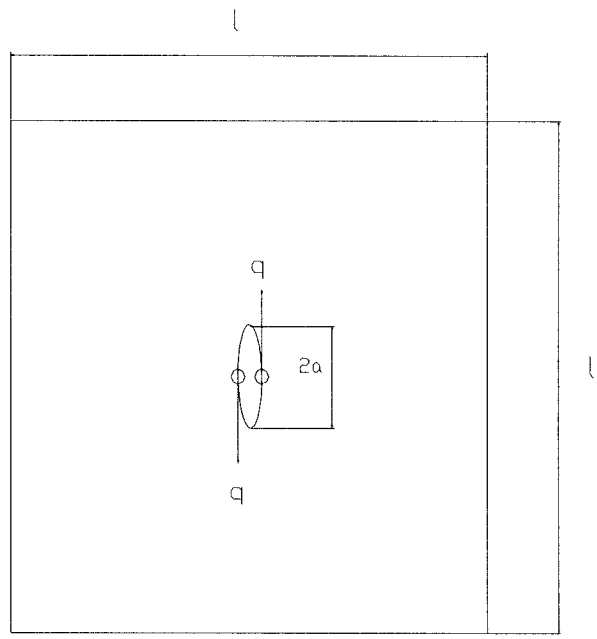

Figure 5.6 Example 2: Concentrated Tangential Forces on The Crack

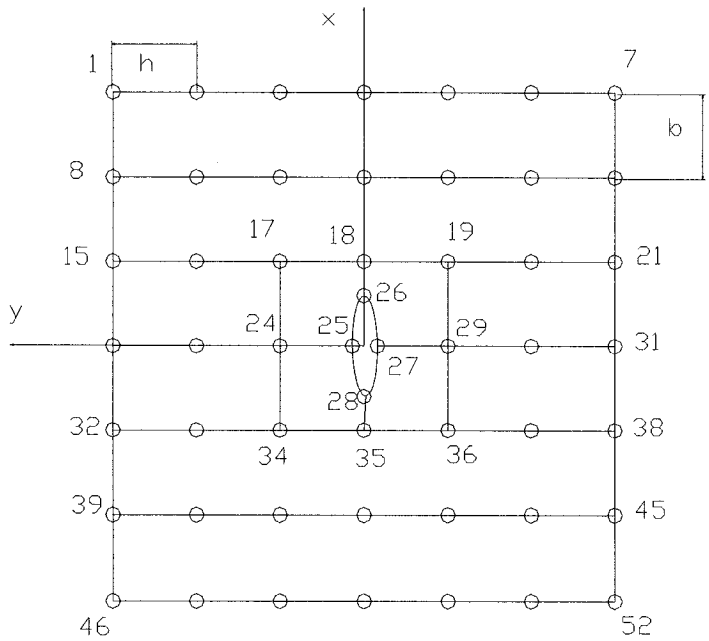

Figure 5.7 Finite Strip Mesh of Example 2

Chapter 6

Bending Crack Strips

6.1 Instruction

In this chapter, a bending crack strip is developed to evaluate the stress intensity factor in plates subjected to bending. Problems of cracked plates are, strictly speaking, three-dimensional in nature and their solution should satisfy the equations of the three-dimensional theory of elasticity in conjunction with the appropriate boundary conditions. However, in order to make the problem manageable, assumptions are made to relax some of the differential equations and boundary conditions. Along these lines several theories of bending plates have been developed and

used to study problems of cracked plates. A solution of cracked plates based on the classical Kirchhoff theory is briefly presented below.

6.1.1 Kirchhoff Theory of Bending Plate

If the deflection of a thin plate is small in comparison with the plate thickness, then the following assumptions can be made:

(1) The middle plane of the plate remain un-stretched after bending.

(2) The normals to the middle plane remain normal to the middle surface in the deflected position.

(3) The stress component σ_z is small compared to the other stress components and may be neglected in the stress-strain relations.

A cracked plate of thickness t in a system of Cartesian coordinates $Oxyz$ with the Oxy-plane coinciding with the plane that bisects the plate thickness, and the plate containing a through crack placed along the Oxz-plane and subjected to bending (**Fig 6.1**) is considered for the following development. The above assumptions lead to the following expressions for moment intensity:

$$M_x(x,y) = \int_{-t/2}^{t/2} \sigma_x(x,y,z) z dz = -D\left(\frac{\partial^2 w}{\partial x^2} + \nu \frac{\partial^2 w}{\partial y^2}\right)$$

$$M_y(x,y) = \int_{-t/2}^{t/2} \sigma_y(x,y,z) z dz = -D\left(\frac{\partial^2 w}{\partial y^2} + \nu \frac{\partial^2 w}{\partial x^2}\right)$$

$$M_{xy}(x,y) = \int_{-t/2}^{t/2} \tau_{xy}(x,y,z) z dz = -D(1-\nu)\frac{\partial^2 w}{\partial x \partial y} \qquad (6-1)$$

where D denotes $Et^3 / 12(1-\nu^2)$ and is known as the flexural rigidity of the plate. The shear forces per unit length parallel to the x and y axes, respectively, are given by

$$Q_x(x,y) = \int_{-t/2}^{t/2} \tau_{xz}(x,y,z) dz = D\frac{\partial}{\partial x}(\nabla^2 w)$$

$$Q_y(x,y) = \int_{-t/2}^{t/2} \tau_{yz}(x,y,z) dz = D\frac{\partial}{\partial y}(\nabla^2 w) \qquad (6-2)$$

where

$$\nabla^2 w = \frac{\partial^2 w}{\partial x^2} + \frac{\partial^2 w}{\partial y^2} \qquad (6-3)$$

The equilibrium equation of the plate in terms of the normal displacement w takes the following form:

$$\nabla^4 w = \frac{q}{D} \tag{6-4}$$

where

$$\nabla^4 w = \nabla^2 \nabla^2 w = \frac{\partial^4 w}{\partial x^4} + 2\frac{\partial^4 w}{\partial x^2 \partial y^2} + \frac{\partial^4 w}{\partial x^4} \tag{6-5}$$

and $q(x, y)$ is the normal load applied to the surface of the plate.

The in-plane stresses σ_x, σ_y and τ_{xy} at any point (x,y,z) vary linearly with z, i.e.

$$\sigma_x = \frac{12z}{t^3} M_x, \quad \sigma_y = \frac{12z}{t^3} M_y, \quad \tau_{xy} = \frac{12z}{t^3} M_{xy} \tag{6-6}$$

while the shear stresses τ_{xz} and τ_{yz} vary parabolically with z, i.e.

$$\tau_{xz} = \frac{3}{2t}\left[1 - \left(\frac{2z}{t}\right)^2\right] Q_x, \quad \tau_{yz} = \frac{3}{2t}\left[1 - \left(\frac{2z}{t}\right)^2\right] Q_y \tag{6-7}$$

The in-plane stress components near a crack tip are found (Sih, 1977)

$$\sigma_x = -\frac{K_I}{\sqrt{2r}}\kappa\left(3\cos\frac{\theta}{2} + \cos\frac{5\theta}{2}\right) + \frac{K_{II}}{\sqrt{2r}}\kappa\left(\frac{9+7\nu}{\nu-1}\sin\frac{\theta}{2} + \sin\frac{5\theta}{2}\right) + O(r^0)$$

$$\sigma_y = \frac{K_I}{\sqrt{2r}}\kappa\left(\frac{11+5\nu}{1-\nu}\cos\frac{\theta}{2} + \cos\frac{5\theta}{2}\right) + \frac{K_{II}}{\sqrt{2r}}\kappa\left(\sin\frac{\theta}{2} + \sin\frac{5\theta}{2}\right) + O(r^0)$$

$$\tau_{xy} = -\frac{K_I}{\sqrt{2r}}\kappa\left(\sin\frac{\theta}{2} + \frac{7+\nu}{1+\nu}\sin\frac{5\theta}{2}\right) + \frac{K_{II}}{\sqrt{2r}}\kappa\left(\frac{3\nu+5}{1-\nu}\cos\frac{\theta}{2} - \cos\frac{5\theta}{2}\right) + O(r^0)$$

(6 – 8)

in which

$$\kappa = \frac{1-\nu}{4(3+\nu)} \qquad (6-9)$$

The bending stress intensity factors K_I and K_{II} in equations (6 – 8) are defined such that they are consistent with the plane extension problem of the Griffith crack in which $K_I = \sigma\sqrt{\pi a}$, σ being the applied uniform stress and *a* being the half crack length. Thus, in the case of uniform bending of a plate with a crack length *2a*, K_I and K_{II} are given by

$$K_I = \frac{12z}{t^3} M\sqrt{\pi a}$$
$$K_{II} = \frac{12z}{t^3} M_{xy}\sqrt{\pi a} \qquad (6-10a)$$

where $12zM/t^3$ is the stress in a given layer of the plate in a state of uniform bending, and $12zM_{xy}/t^3$ is the shear in a given layer of the plate in a state of uniform torsion. The maximum value of K_I and K_{II} occur at the surface layer of the plate, i.e.

$$K_I = 6M\sqrt{\pi a}/t^2, \quad K_{II} = 6M_{xy}\sqrt{\pi a}/t^2 \qquad (6-10b)$$

For the special case of vanishingly thin plate the stress intensity factor is

$$K_I = \frac{(1+\nu)}{(3+\nu)} M_0 \sqrt{\pi a}, \qquad K_{II} = 0 \tag{6-11}$$

The boundary conditions along the crack plane are

$$M_y(x,0) = M_{xy}(x,0) = Q_y(x,0) = 0 \tag{6-12}$$

The Kirchhoof theory of plate bending neglects the effect of transverse shear deformation and thus replaces the last two boundary condition on M_{xy} and Q_y by a single one on $Q_y + \partial M_{xy} / \partial x$. Thus the tree boundary conditions of Equation (6 – 12) are replaced by the following two:

$$M_y(x,0) = Q_y(x,0) + \frac{\partial M_{xy}(x,0)}{\partial x} = 0 \tag{6-13}$$

6.1.2 Williams' Eigenfunction Expansion

Based on Kirchhoof theory, and using the method of eigenfunction expansion, Williams (1961) gave the asymptotic behavior of the bending stresses in the vicinity of the crack in a polar coordinate system.

The governing differential equation for deflection $w(r,\theta)$ in a polar coordinate system in (6 – 4)

is

$$\nabla^4 w(r,\theta) = \frac{q(r,\theta)}{D} \tag{6-14}$$

Taking the usual Kirchhoff conditions for a free edge as the boundary conditions along the edges $\theta_0 = \pm\pi$:

$$M_\theta(r,\theta_0) = -D(\frac{1}{r}\frac{\partial w}{\partial r} + \frac{1}{r^2}\frac{\partial^2 w}{\partial \theta^2} + \nu\frac{\partial^2 w}{\partial r^2}) = 0$$

$$V_\theta(r,\theta_0) = -D[\frac{1}{r}\frac{\partial \nabla^2 w}{\partial \theta} + (1-\nu)\frac{\partial}{\partial r}(\frac{1}{r}\frac{\partial^2 w}{\partial r \partial \theta} - \frac{1}{r^2}\frac{\partial w}{\partial \theta})] = 0 \tag{6-15}$$

the eigenfunction solution which satisfies (6 – 14) and (6 – 15) is:

$$\begin{aligned} w(r,\theta) = r^{\frac{3}{2}}\{-[\cos\frac{3\theta}{2} - \frac{3(1-\nu)}{7+\nu}\cos\frac{\theta}{2}]a_1 + [\sin\frac{3\theta}{2} - \frac{3(1-\nu)}{5+3\nu}\sin\frac{\theta}{2}]b_1\} \\ + r^2\{[\cos 2\theta + \frac{1-\nu}{7+\nu}]a_2 + [\sin 2\theta]b_2\} + \cdots \quad \cdots \\ + r^{\frac{n+2}{2}}\{(-1)^n[\cos\frac{(n+2)\theta}{2} + \frac{(4n-7)(1-\nu)}{7+\nu}\cos\frac{n-2}{2}\theta]a_n \\ + [\sin\frac{(n+2)\theta}{2} - \frac{(4n-7)(1-\nu)}{5+3\nu}\sin\frac{(n-2)\theta}{2}]b_n\} \end{aligned} \tag{6-16}$$

in which a_k and b_k are the polynomial coefficients.

Then, the stress intensity factors K_I for opening mode and K_{II} for sliding mode can be obtained from the leading terms of the Williams' expansion combined with (6 – 10).

6.2 Traditional Spline Plate Strip

The spline plate strip presented here is a lower order strip. If desired, higher order strips can also be formulated without any difficulty.

6.2.1 Displacement Formation in The Strip

In the lower order spline finite strip, each node requires two degrees of freedom (deflection w and normal rotation θ , as shown in Fig 6.2) to satisfy the continuity requirements. If there are r nodes on each side of the spline strip, the displacement and rotation on the two sides, i.e. side i and side j, are:

$$
\begin{aligned}
w_i &= \sum_{m=0}^{r+1} c_m \phi_m = [\phi]\{c\} \\
\theta_i &= \sum_{m=0}^{r+1} d_m \phi_m = [\phi]\{d\} \\
w_j &= \sum_{m=0}^{r+1} e_m \phi_m = [\phi]\{e\} \\
\theta_j &= \sum_{m=0}^{r+1} f_m \phi_m = [\phi]\{f\}
\end{aligned}
\qquad (6-17)
$$

where

$$
\begin{aligned}
[\phi] &= [\phi_0 \quad \phi_1 \quad \cdots \quad \phi_r \quad \phi_{r+1}] \\
\{c\} &= [c_0 \quad c_1 \quad \cdots \quad c_r \quad c_{r+1}]^T \\
\{d\} &= [d_0 \quad d_1 \quad \cdots \quad d_r \quad d_{r+1}]^T \\
\{e\} &= [e_0 \quad e_1 \quad \cdots \quad e_r \quad e_{r+1}]^T \\
\{f\} &= [f_0 \quad f_1 \quad \cdots \quad f_r \quad f_{r+1}]^T
\end{aligned} \tag{6-18}
$$

in which Φ_k is the B_3 spline function, while c_k, d_k, e_k and f_k represent the interpolation coefficients.

The deflection field in the strip can be interpolated as

$$w = [C][\Phi]\{\delta\} \tag{6-19}$$

where

$$
\begin{aligned}
[C] &= [1 - 3\bar{x}^2 + 2\bar{x}^3, \quad x(1 - 2\bar{x} + \bar{x}^2), \quad 3\bar{x}^2 - 2\bar{x}^3, \quad x(\bar{x}^2 - \bar{x})] \\
[\Phi] &= \begin{bmatrix} [\phi] & & & \\ & [\phi] & & \\ & & [\phi] & \\ & & & [\phi] \end{bmatrix} \\
\{\delta\} &= [\{c\}^T \quad \{d\}^T \quad \{e\}^T \quad \{f\}^T]^T
\end{aligned} \tag{6-20}
$$

and $\bar{x} = x / b$.

Based on strain-displacement relationships, the strain(curvature) vector can be expressed in terms of the displacement parameters as

$$\{\varepsilon\} = \begin{Bmatrix} \kappa_x \\ \kappa_y \\ 2\kappa_{xy} \end{Bmatrix} = \begin{Bmatrix} -\dfrac{\partial^2 w}{\partial x^2} \\ -\dfrac{\partial^2 w}{\partial y^2} \\ 2\dfrac{\partial^2 w}{\partial x \partial y} \end{Bmatrix} = \begin{bmatrix} -[C^{''}][\Phi] \\ -[C][\Phi^{''}] \\ 2[C^{'}][\Phi^{'}] \end{bmatrix} \{\delta\} = [B]\{\delta\} \qquad (6-21)$$

in which

$$[B] = \begin{bmatrix} -[C^{''}][\Phi] \\ -[C][\Phi^{''}] \\ 2[C^{'}][\Phi^{'}] \end{bmatrix} = \begin{bmatrix} -[C^{''}] & 0 & 0 \\ 0 & -[C] & 0 \\ 0 & 0 & 2[C^{'}] \end{bmatrix} \begin{Bmatrix} [\Phi] \\ [\Phi^{''}] \\ [\Phi^{'}] \end{Bmatrix} \qquad (6-22)$$

Then, the stress(moment) vector can be obtained as

$$\{\sigma\} = \begin{Bmatrix} M_x \\ M_y \\ M_{xy} \end{Bmatrix} = [D]\{\varepsilon\} = [D][B]\{\delta\} \qquad (6-23)$$

in which, the rigidity matrix [D] is defined respectively for isotropic plates and orthotropic plates as:

(i) for isotropic plates

$$[D] = \frac{Et^3}{12(1-\upsilon^2)}\begin{bmatrix} 1 & \upsilon & 0 \\ \upsilon & 1 & 0 \\ 0 & 0 & \dfrac{1-\upsilon}{2} \end{bmatrix} \qquad (6-24)$$

(ii) for orthotropic plates

$$[D] = \begin{bmatrix} D_x & D_1 & 0 \\ D_1 & D_y & 0 \\ 0 & 0 & D_{xy} \end{bmatrix} \qquad (6-25)$$

where

$$D_x = \frac{E_x t^3}{12(1-\upsilon_x\upsilon_y)}; \quad D_y = \frac{E_y t^3}{12(1-\upsilon_x\upsilon_y)};$$
$$D_1 = \frac{\upsilon_y E_x t^3}{12(1-\upsilon_x\upsilon_y)} = \frac{\upsilon_x E_y t^3}{12(1-\upsilon_x\upsilon_y)}; \quad D_{xy} = \frac{Gt^3}{12} \qquad (6-26)$$

6.2.2 Stiffness Matrix Corresponding to $\{\delta\}$

The stiffness matrix of a traditional spline plate strip can be formed as:

$$[k^e] = \int_v [B^T][D][B]dv = \int \{[\Phi]^T[L_1][\Phi] + [\Phi]^T[L_2][\Phi''] + [\Phi'']^T[L_3][\Phi] + [\Phi'']^T[L_4][\Phi''] + 4[\Phi']^T[L_5][\Phi']\}dy \qquad (6-27)$$

in which

$$[L_1] = \int_0^b [C'']^T D_x [C'']dx; \quad [L_2] = \int_0^b [C]^T D_1 [C'']dx;$$

$$[L_3] = \int_0^b [C'']^T D_1 [C]dx; \quad [L_4] = \int_0^b [C]^T D_y [C]dx;$$

$$[L_5] = \int_0^b [C']^T D_{xy} [C']dx; \qquad (6-28)$$

All above integrations can be performed analytically. The integrations in the direction y can be simplified for the strips with equally spaced nodes if the following expressions are employed:

$$I^{(1)} = \int [\Phi]^T [\Phi]dy = \begin{bmatrix} I_0^{(1)} & I_1^{(1)} & I_2^{(1)} & I_3^{(1)} & 0 & \cdot & \cdot & 0 \\ I_1^{(1)} & I_0^{(1)} & I_1^{(1)} & I_2^{(1)} & I_3^{(1)} & 0 & \cdot & 0 \\ \cdot & \cdot & \cdot & \cdot & \cdot & \cdot & \cdot & \cdot \\ 0 & \cdot & 0 & I_3^{(1)} & I_2^{(1)} & I_1^{(1)} & I_0^{(1)} & I_1^{(1)} \\ 0 & \cdot & \cdot & 0 & I_3^{(1)} & I_2^{(1)} & I_1^{(1)} & I_0^{(1)} \end{bmatrix}$$

$$I^{(2)} = \int [\Phi'']^T [\Phi] dy = \begin{bmatrix} I_0^{(2)} & I_1^{(2)} & I_2^{(2)} & I_3^{(2)} & 0 & \cdot & \cdot & 0 \\ I_1^{(2)} & I_0^{(2)} & I_1^{(2)} & I_2^{(2)} & I_3^{(2)} & 0 & \cdot & 0 \\ \cdot & \cdot & \cdot & \cdot & \cdot & \cdot & \cdot & \cdot \\ 0 & \cdot & 0 & I_3^{(2)} & I_2^{(2)} & I_1^{(2)} & I_0^{(2)} & I_1^{(2)} \\ 0 & \cdot & \cdot & 0 & I_3^{(2)} & I_2^{(2)} & I_1^{(2)} & I_0^{(2)} \end{bmatrix}$$

$$I^{(3)} = \int [\Phi]^T [\Phi''] dy = \begin{bmatrix} I_0^{(3)} & I_1^{(3)} & I_2^{(3)} & I_3^{(3)} & 0 & \cdot & \cdot & 0 \\ I_1^{(3)} & I_0^{(3)} & I_1^{(3)} & I_2^{(3)} & I_3^{(3)} & 0 & \cdot & 0 \\ \cdot & \cdot & \cdot & \cdot & \cdot & \cdot & \cdot & \cdot \\ 0 & \cdot & 0 & I_3^{(3)} & I_2^{(3)} & I_1^{(3)} & I_0^{(3)} & I_1^{(3)} \\ 0 & \cdot & \cdot & 0 & I_3^{(3)} & I_2^{(3)} & I_1^{(3)} & I_0^{(3)} \end{bmatrix}$$

$$I^{(4)} = \int [\Phi'']^T [\Phi''] dy = \begin{bmatrix} I_0^{(4)} & I_1^{(4)} & I_2^{(4)} & I_3^{(4)} & 0 & \cdot & \cdot & 0 \\ I_1^{(4)} & I_0^{(4)} & I_1^{(4)} & I_2^{(4)} & I_3^{(4)} & 0 & \cdot & 0 \\ \cdot & \cdot & \cdot & \cdot & \cdot & \cdot & \cdot & \cdot \\ 0 & \cdot & 0 & I_3^{(4)} & I_2^{(4)} & I_1^{(4)} & I_0^{(4)} & I_1^{(4)} \\ 0 & \cdot & \cdot & 0 & I_3^{(4)} & I_2^{(4)} & I_1^{(4)} & I_0^{(4)} \end{bmatrix}$$

$$I^{(5)} = \int [\Phi']^T [\Phi'] dy = \begin{bmatrix} I_0^{(5)} & I_1^{(5)} & I_2^{(5)} & I_3^{(5)} & 0 & \cdot & \cdot & 0 \\ I_1^{(5)} & I_0^{(5)} & I_1^{(5)} & I_2^{(5)} & I_3^{(5)} & 0 & \cdot & 0 \\ \cdot & \cdot & \cdot & \cdot & \cdot & \cdot & \cdot & \cdot \\ 0 & \cdot & 0 & I_3^{(5)} & I_2^{(5)} & I_1^{(5)} & I_0^{(5)} & I_1^{(5)} \\ 0 & \cdot & \cdot & 0 & I_3^{(5)} & I_2^{(5)} & I_1^{(5)} & I_0^{(5)} \end{bmatrix}$$

(6 – 29)

in which

$$\begin{cases} I_0^{(1)} = \int_{y_{i-2}}^{y_{i+2}} \phi_i^{\,2} dy; \quad I_0^{(2)} = I_0^{(3)} = \int_{y_{i-2}}^{y_{i+2}} \phi_i \phi_i^{"} dy; \\ I_0^{(4)} = \int_{y_{i-2}}^{y_{i+2}} \phi_i^{"2} dy; \quad I_0^{(5)} = \int_{y_{i-2}}^{y_{i+2}} \phi_i^{'2} dy; \end{cases} \quad (i = j)$$

$$\begin{cases} I_1^{(1)} = \int_{y_{i-1}}^{y_{i+2}} \phi_i \phi_j dy; \quad I_1^{(2)} = I_1^{(3)} = \int_{y_{i-1}}^{y_{i+2}} \phi_i \phi_j^{"} dy; \\ I_1^{(4)} = \int_{y_{i-1}}^{y_{i+2}} \phi_i^{"} \phi_j^{"} dy; \quad I_1^{(5)} = \int_{y_{i-1}}^{y_{i+2}} \phi_i^{'} \phi_j^{'} dy; \end{cases} \quad (|i-j| = 1)$$

$$\begin{cases} I_2^{(1)} = \int_{y_i}^{y_{i+2}} \phi_i \phi_j dy; \quad I_2^{(2)} = I_2^{(3)} = \int_{y_i}^{y_{i+2}} \phi_i \phi_j^{"} dy; \\ I_2^{(4)} = \int_{y_i}^{y_{i+2}} \phi_i^{"} \phi_j^{"} dy; \quad I_2^{(5)} = \int_{y_i}^{y_{i+2}} \phi_i^{'} \phi_j^{'} dy; \end{cases} \quad (|i-j| = 2)$$

$$\begin{cases} I_3^{(1)} = \int_{y_{i+1}}^{y_{i+2}} \phi_i \phi_j dy; \quad I_3^{(2)} = I_3^{(3)} = \int_{y_{i+1}}^{y_{i+2}} \phi_i \phi_j^{"} dy; \\ I_3^{(4)} = \int_{y_{i+1}}^{y_{i+2}} \phi_i^{"} \phi_j^{"} dy; \quad I_3^{(5)} = \int_{y_{i+1}}^{y_{i+2}} \phi_i^{'} \phi_j^{'} dy; \end{cases} \quad (|i-j| = 3)$$

(6 – 30)

Thus, the stiffness matrix is formed as:

$$[k^e]=\frac{1}{420b^3}\begin{bmatrix}
5040D_x[I^{(1)}] & 2520bD_x[I^{(1)}] & -5040D_x[I^{(1)}] & 2520bD_x[I^{(1)}] \\
-504b^2D_1[I^{(2)}] & -462b^3D_1[I^{(2)}] & 504b^2D_1[I^{(2)}] & -42b^3D_1[I^{(2)}] \\
-504b^2D_1[I^{(3)}] & -42b^3D_1[I^{(3)}] & 504b^2D_1[I^{(3)}] & -42b^3D_1[I^{(3)}] \\
156b^4D_y[I^{(4)}] & 22b^5D_y[I^{(4)}] & 54b^4D_y[I^{(4)}] & -13b^5D_y[I^{(4)}] \\
2016b^2D_{xy}[I^{(5)}] & 168b^3D_{xy}[I^{(5)}] & -2016b^2D_{xy}[I^{(5)}] & 168b^3D_{xy}[I^{(5)}] \\
 & 5040D_x[I^{(1)}] & -2520bD_x[I^{(1)}] & 840b^2D_x[I^{(1)}] \\
 & -504b^2D_1[I^{(2)}] & 42b^3D_1[I^{(2)}] & 14b^3D_1[I^{(2)}] \\
 & -504b^2D_1[I^{(3)}] & 42b^3D_1[I^{(3)}] & 14b^4D_1[I^{(3)}] \\
 & 156b^4D_y[I^{(4)}] & 13b^5D_y[I^{(4)}] & -3b^6D_y[I^{(4)}] \\
 & 2016b^2D_{xy}[I^{(5)}] & -168b^3D_{xy}[I^{(5)}] & -56b^4D_{xy}[I^{(5)}] \\
 & & 5040D_x[I^{(1)}] & -2520bD_x[I^{(1)}] \\
 & & -504b^2D_1[I^{(2)}] & 462b^3D_1[I^{(2)}] \\
 & SYM & -504b^2D_1[I^{(3)}] & 42b^3D_1[I^{(3)}] \\
 & & 156b^4D_y[I^{(4)}] & -22b^5D_y[I^{(4)}] \\
 & & 2016b^2D_{xy}[I^{(5)}] & -168b^3D_{xy}[I^{(5)}] \\
 & & & 5040D_x[I^{(1)}] \\
 & & & -504b^2D_1[I^{(2)}] \\
 & & & -504b^2D_1[I^{(3)}] \\
 & & & 156b^4D_y[I^{(4)}] \\
 & & & 2016b^2D_{xy}[I^{(5)}]
\end{bmatrix} \qquad (6-31)$$

6.2.3 Stiffness Matrix Corresponding to $\{w\}$

It is often required to transform the stiffness matrix with interpolation coefficient vector $\{\delta\}$ as degrees of freedom to that with the nodal displacement vector $\{ w \}$ as degrees of freedom. By means of matrix $[F]$ in (2 - 5), which indicates the relationship between the displacements of nodes, $\{w\}$, and the coefficients of spline function interpolation, $\{\delta\}$, in the nodal line,

$$\{\delta\} = [T]\{w\} \tag{6-32}$$

in which

$$\{w\} = [w_{i0} \quad w_{i1} \quad \cdot \quad w_{i(r+1)} \quad \theta_{i0} \quad \theta_{i1} \quad \cdot \quad \theta_{i(r+1)} \quad w_{j0} \quad w_{j1} \quad \cdot \quad w_{j(r+1)} \quad \theta_{j0} \quad \theta_{j1} \quad \cdot \quad \theta_{j(r+1)}]^T$$

$$[T] = \begin{bmatrix} [F_i] & & & \\ & [F_{\theta i}] & & \\ & & [F_j] & \\ & & & [F_{\theta j}] \end{bmatrix} \tag{6-33}$$

and $[F_i]$, $[F_{\theta i}]$, $[F_j]$ and $[F_{\theta j}]$ represent the relationships between the displacements of nodes on nodal line ***i, j*** and the coefficients of spline function interpolation, respectively.

Then the stiffness matrix corresponding to $\{w\}$ can be obtained via;

$$[k] = [T]^T[k^e][T] \tag{6-34}$$

6.2.4 Load Vector

Combining (6 – 17) and (2 – 5), the deflection of middle plane in a spline plate strip can be expressed in terms of $\{w\}$:

$$w = [C][\Phi]\{\delta\} = [C][\Phi][T]\{w\} = [N]\{w\}$$
$$[N] = [C][\Phi][T] \qquad (6-35)$$

Then, the load vector equivalent to a distributed transverse load $q(x,y)$ acting on the strip can be formed as

$$[Q_i \quad M_i \quad Q_j \quad M_j]^T = \int_0^b \int_0^l [N]^T q(x,y) dxdy \qquad (6-36)$$

6.3 Special Area Around Crack

6.3.1 Displacement Field Around The Crack

The deflection $w(r,\theta)$, which is expressed in equation (6 – 16) by Williams' expansion,

can be written in a matrix form

$$w(r,\theta) = [H]\{A\} \tag{6-37}$$

in which

$$\begin{aligned}[H] = [1 \quad & -r^{\frac{3}{2}}[\cos\frac{3\theta}{2} - \frac{3(1-\nu)}{7+\nu}\cos\frac{\theta}{2}] \quad r^2[\cos 2\theta + \frac{1-\nu}{7+\nu}] \quad \cdots \\ & (-1)^n r^{\frac{n+2}{2}}[\cos\frac{(n+2)\theta}{2} + \frac{(4n-7)(1-\nu)}{7+\nu}\cos\frac{n-2}{2}\theta] \\ & r^{\frac{3}{2}}[\sin\frac{3\theta}{2} - \frac{3(1-\nu)}{5+3\nu}\sin\frac{\theta}{2}] \quad r^2[\sin 2\theta] \quad \cdots \\ & r^{\frac{n+2}{2}}[\sin\frac{(n+2)\theta}{2} - \frac{(4n-7)(1-\nu)}{5+3\nu}\sin\frac{(n-2)\theta}{2}]] \end{aligned} \tag{6-38}$$

$$\{A\} = \begin{bmatrix} w_0 & a_1 & a_2 & \cdots & a_n & b_1 & b_2 & \cdots & b_n \end{bmatrix}^T$$

where w_0 is the displacement around the crack tip in the local coordinate of the substructure ①, and represents the rigid body motion of substructure ①.

The stiffness derivation procedures have been shown in section 6.2, and the strain (curvature) vector $\{\varepsilon\}$ has been defined in equations (6 -21) -(6 -22), the stress (moment) vector $\{\sigma\}$ has been defined in equations (6 -23) - (6 -26). However, in this case, the strain matrix $[B]$ is different from the one as shown in equation (6 -22), due to the use of two different deflection modes.

The strain(curvature) vector in polar coordinates takes the following form:

$$\{\varepsilon\} = \begin{Bmatrix} \kappa_x \\ \kappa_y \\ 2\kappa_{xy} \end{Bmatrix} = \begin{Bmatrix} -\dfrac{\partial^2 w}{\partial x^2} \\ -\dfrac{\partial^2 w}{\partial y^2} \\ 2\dfrac{\partial^2 w}{\partial x \partial y} \end{Bmatrix} = [J_2]\{\Delta\} \tag{6-39}$$

where

$$[J_2]=\begin{bmatrix} -\cos^2\theta & \frac{2\sin\theta\cos\theta}{r} & -\frac{\sin^2\theta}{r} & -\frac{2\sin\theta\cos\theta}{r^2} & -\frac{\sin^2\theta}{r^2} \\ -\sin^2\theta & -\frac{2\sin\theta\cos\theta}{r} & -\frac{\cos^2\theta}{r} & \frac{2\sin\theta\cos\theta}{r^2} & -\frac{\cos^2\theta}{r^2} \\ 2\sin\theta\cos\theta & 2\frac{\cos^2\theta-\sin^2\theta}{r} & -\frac{2\sin\theta\cos\theta}{r} & 2\frac{\sin^2\theta-\cos^2\theta}{r} & -\frac{2\sin\theta\cos\theta}{r^2} \end{bmatrix}$$

$$\{\Delta\}=[\frac{\partial^2 w}{\partial r^2} \quad \frac{\partial^2 w}{\partial r\partial\theta} \quad \frac{\partial w}{\partial r} \quad \frac{\partial w}{\partial\theta} \quad \frac{\partial^2 w}{\partial\theta^2}]^T \qquad (6-40)$$

Moreover,

$$\{\Delta\}=[N']\{A\}$$

$$[N']=\begin{bmatrix} 0 & N_{11} & N_{12} & \cdots & N_{1n} & N_{1(n+1)} & N_{1(n+2)} & \cdots & N_{1(2n)} \\ 0 & N_{21} & N_{22} & \cdots & N_{2n} & N_{2(n+1)} & N_{2(n+2)} & \cdots & N_{2(2n)} \\ 0 & N_{31} & N_{32} & \cdots & N_{3n} & N_{3(n+1)} & N_{3(n+2)} & \cdots & N_{3(2n)} \\ 0 & N_{41} & N_{42} & \cdots & N_{4n} & N_{4(n+1)} & N_{4(n+2)} & \cdots & N_{4(2n)} \\ 0 & N_{51} & N_{52} & \cdots & N_{5n} & N_{5(n+1)} & N_{5(n+2)} & \cdots & N_{5(2n)} \end{bmatrix} \qquad (6-41)$$

The items in the above matrix are expressed as

$$N_{1i}=(-1)^i\frac{(i+2)i}{4}r^{\frac{i-2}{2}}[\cos\frac{(i+2)\theta}{2}+\frac{(4i-7)(1-\nu)}{7+\nu}\cos\frac{i-2}{2}\theta]$$

$$N_{1(n+i)} = \frac{(i+2)i}{4} r^{\frac{i-2}{2}} [\sin\frac{(i+2)\theta}{2} - \frac{(4i-7)(1-\nu)}{5+3\nu}\sin\frac{(i-2)\theta}{2}]$$

$$N_{2i} = (-1)^{i-1}(\frac{i+2}{2})^2 r^{\frac{i}{2}} [\sin\frac{(i+2)\theta}{2} + \frac{(4i-7)(1-\nu)(i-2)}{(7+\nu)(i+2)}\sin\frac{i-2}{2}\theta]$$

$$N_{2(n+i)} = (\frac{i+2}{2})^2 r^{\frac{i}{2}} [\cos\frac{(i+2)\theta}{2} - \frac{(4i-7)(1-\nu)(i-2)}{(5+3\nu)(i+2)}\cos\frac{(i-2)\theta}{2}]$$

$$N_{3i} = (-1)^i \frac{i+2}{2} r^{\frac{i}{2}} [\cos\frac{(i+2)\theta}{2} + \frac{(4i-7)(1-\nu)}{7+\nu}\cos\frac{i-2}{2}\theta]$$

$$N_{3(n+i)} = \frac{i+2}{2} r^{\frac{i}{2}} [\sin\frac{(i+2)\theta}{2} - \frac{(4i-7)(1-\nu)}{5+3\nu}\sin\frac{(i-2)\theta}{2}]$$

$$N_{4i} = (-1)^{i-1} \frac{i+2}{2} r^{\frac{i+2}{2}} [\sin\frac{(i+2)\theta}{2} + \frac{(4i-7)(1-\nu)(i-2)}{(7+\nu)(i+2)}\sin\frac{i-2}{2}\theta]$$

$$N_{4(n+i)} = \frac{i+2}{2} r^{\frac{i+2}{2}} [\cos\frac{(i+2)\theta}{2} - \frac{(4i-7)(1-\nu)(i-2)}{(5+3\nu)(i+2)}\cos\frac{(i-2)\theta}{2}]$$

$$N_{5i} = (-1)^{i-1}(\frac{i+2}{2})^2 r^{\frac{i+2}{2}} [\cos\frac{(i+2)\theta}{2} + \frac{(4i-7)(1-\nu)(i-2)^2}{(7+\nu)(i+2)^2}\cos\frac{i-2}{2}\theta]$$

$$N_{5(n+i)} = (\frac{i+2}{2})^2 r^{\frac{i+2}{2}} [-\sin\frac{(i+2)\theta}{2} + \frac{(4i-7)(1-\nu)(i-2)^2}{(5+3\nu)(i+2)^2}\sin\frac{(i-2)\theta}{2}]$$

(6 – 42)

Thus, equation (6 – 39) can be rewritten in a concise form:

$$\{\varepsilon\} = [B]\{A\} \qquad (6-43)$$

where

$$[B] = [J_2][N'] \qquad (6-44)$$

Then, the stress(moment) vector can be obtained as the following:

$$\{\sigma\} = \begin{Bmatrix} M_x \\ M_y \\ M_{xy} \end{Bmatrix} = [D]\{\varepsilon\} = [D][B]\{A\} \qquad (6-45)$$

The rigidity matrix $[D]$ is already given in equations (6 – 24) or (6 – 25).

6.3.2 Stiffness Matrix Corresponding to $\{A\}$

In this section, the stiffness matrix is formed by taking the coefficients $\{A\}$ in William's Expansion as degrees of freedom. Following the principle of minimum total potential energy, the stiffness matrix corresponding to $\{A\}$ can be written as:

$$[\hat{k}] = \int_0^b \int_0^l [B^T][D][B]dxdy \qquad (6-46)$$

The items in this matrix are usually calculated numerically due to the complexity involved in the integration procedure. Since the integration region is a rectangle, the Cartesian Coordinate system is more convenience to use, and a coordinate transformation based on $r = \sqrt{x^2 + y^2}$ and $\theta = \tan^{-1}(y/x)$ is required. Except the terms with r^{-1}, all of integrals can be computed by regular Gaussian Quadrature in Appendix A. The singular integration of the terms with r^{-1} can be conducted according the procedure developed in section 3.3.

6.3.3 Stiffness Matrix Corresponding to $\{w\}$

In the spline finite strip analysis of plates, the nodal deflections are taken as the unknown parameters (Cheung M.S. et al., 1996). Therefore, the stiffness matrix formed in the previous section must be transformed. If nine nodes are included in substructure ①, including the interior nodes and the exterior ones, and assuming $n = 2$ from (6 – 38) to (6 – 42), the transformation from the coefficients {A} (see equation 6-38C) to the nine nodal deflections {w} can be written as

$$\{w\} = [U]\{A\} \qquad (6-47)$$

where

$$\{w\} = \left[w_1, \alpha_1, w_2, \alpha_2, \cdots, w_9, \alpha_9\right]^T \qquad (6-48)$$

and α denotes the normal rotation.

The normal rotation α can be expressed using the polar coordinates as

$$\alpha = \frac{\partial w}{\partial x} = \frac{\partial w}{\partial r}\frac{\partial r}{\partial x} + \frac{\partial w}{\partial \theta}\frac{\partial \theta}{\partial x} \qquad (6-49)$$

Considering the following relationships

$$\frac{\partial r}{\partial x} = \cos\theta, \qquad \frac{\partial \theta}{\partial x} = \frac{\sin\theta}{r} \qquad (6-50)$$

and substituting William's Expansion in equation (6-37) into (6-49), the normal rotation can be expressed in terms of the William's coefficients a_k and b_k as

$$\alpha = \sum_{i=1}^{2} r^{\frac{i}{2}} \left\{ \begin{array}{c} (-1)^i \{\frac{i+2}{2}\cos\frac{i+4}{2}\theta - \frac{(4i-7)(1-\nu)}{7+\nu}[i\cos\frac{i\theta}{2} + 2\cos\frac{i-4}{2}\theta]\}a_i \\ + \{\frac{i+2}{2}\sin\frac{i+4}{2}\theta - \frac{(4i-7)(1-\nu)}{5+3\nu}[i\sin\frac{i\theta}{2} + 2\sin\frac{i-4}{2}\theta]\}b_i \end{array} \right\} \qquad (6-51)$$

Thus, the transformation matrix [U] is formed as

$$
[U] = \begin{bmatrix}
1 & 0 & 0 & 0 & 0 \\
0 & 0 & 0 & 0 & 0 \\
1 & l_{32} & l_{33} & 0 & 0 \\
0 & l_{42} & l_{43} & 0 & 0 \\
1 & l_{52} & l_{53} & l_{54} & l_{55} \\
0 & l_{62} & l_{63} & l_{64} & l_{65} \\
1 & l_{72} & l_{73} & l_{74} & l_{75} \\
0 & l_{82} & l_{83} & l_{84} & l_{85} \\
1 & 0 & l_{93} & l_{94} & 0 \\
0 & 0 & l_{13} & l_{14} & 0 \\
1 & \lambda_1^3 l_{32} & \lambda_1^4 l_{33} & 0 & 0 \\
0 & \lambda_1 l_{42} & \lambda_1^2 l_{43} & 0 & 0 \\
1 & \lambda_2^3 l_{52} & \lambda_2^4 l_{53} & \lambda_2^3 l_{54} & \lambda_2^4 l_{55} \\
0 & \lambda_2 l_{62} & \lambda_2^2 l_{63} & \lambda_2 l_{64} & \lambda_2^2 l_{65} \\
1 & \lambda_3^3 l_{72} & \lambda_3^4 l_{73} & \lambda_3^3 l_{74} & \lambda_3^4 l_{75} \\
0 & \lambda_3 l_{82} & \lambda_3^2 l_{83} & \lambda_3 l_{84} & \lambda_3^2 l_{85} \\
1 & 0 & \frac{l_{93}}{16} & \frac{l_{94}}{8} & 0 \\
0 & 0 & \frac{l_{13}}{4} & \frac{l_{13}}{2} & 0
\end{bmatrix} \qquad (6-52)
$$

where

$$l_{32} = -4(1+\nu)(b-a)^{3/2}/(7+\nu)$$

$$l_{33} = 8(b-a)^{2}/(7+\nu)$$

$$l_{42} = -(39+\nu)(b-a)^{1/2}/[2(7+\nu)]$$

$$l_{43} = (10+6\nu)(b-a)/(7+\nu)$$

$$l_{52} = r_3^{3/2}[-\cos(3\alpha/2)+3(1-\nu)\cos(\alpha/2)/(7+\nu)]$$

$$l_{53} = r_3^{2}[\cos(2\alpha)+(1-\nu)/(7+\nu)]$$

$$l_{54} = r_3^{3/2}[\sin(3\alpha/2)-3(1-\nu)\sin(\alpha/2)/(5+3\nu)]$$

$$l_{55} = r_3^{2}\sin(2\alpha)$$

$$l_{62} = -r_3^{1/2}\{3\cos(5\alpha/2)/2+3(1-\nu)[\cos(\alpha/2)+2\cos(3\alpha/2)]/(7+\nu)\}$$

$$l_{63} = 2r_3[\cos(3\alpha)-2(1-\nu)\cos\alpha/(7+\nu)]$$

$$l_{64} = r_3^{1/2}\{3\sin(5\alpha/2)/2+3(1-\nu)[\sin(\alpha/2)-2\sin(3\alpha/2)]/(5+3\nu)\}$$

$$l_{65} = 2r_3\sin(3\alpha)$$

$$l_{72} = r_4^{3/2}[-\cos(3\beta/2)+3(1-\nu)\cos(\beta/2)/(7+\nu)]$$

$$l_{73} = r_4^{2}[\cos(2\beta)+(1-\nu)/(7+\nu)]$$

$$l_{74} = r_4^{3/2}[\sin(3\beta/2)-3(1-\nu)\sin(\beta/2)/(5+3\nu)]$$

$$l_{75} = r_4^{2}\sin(2\beta)$$

$$l_{82} = -r_4^{1/2}\{3\cos(5\beta/2)/2+3(1-\nu)[\cos(\beta/2)+2\cos(3\beta/2)]/(7+\nu)\}$$

$$l_{83} = 2r_4[\cos(3\beta)-2(1-\nu)\cos\beta/(7+\nu)]$$

$$l_{84} = r_4^{1/2}\{3\sin(5\beta/2)/2+3(1-\nu)[\sin(\beta/2)-2\sin(3\beta/2)]/(5+3\nu)\}$$

$$l_{85} = 2r_4\sin(3\beta)$$

$$l_{93} = 8a/(7+\nu)$$

$$l_{94} = 8a^{3/2}/(5+3\nu)$$

$$l_{13} = -2a(5+3\nu)/(7+\nu)$$

$$l_{14} = 3a^{1/2}(11-3\nu)/[2(5+3\nu)] \qquad (6-53)$$

in which

$$r_3 = \sqrt{h^2 + (\frac{b-a}{2})^2} \qquad r_4 = \sqrt{h^2 + (\frac{a}{2})^2}$$

$$\lambda_1 = \frac{\sqrt{a}}{2\sqrt{b-a}} \qquad \lambda_2 = \frac{\sqrt{a}}{2\sqrt[4]{4h^2 + (b-a)^2}}$$

$$\lambda_3 = \frac{\sqrt{a}}{2\sqrt[4]{4h^2 + a^2}} \qquad (6-54)$$

It is necessary to use the least squares procedure to invert [U], because [U] is not a square matrix.

$$[U]^T\{w\} = [U]^T[U]\{A\}$$

From which

$$\{A\} = [T]\{w\}$$
$$[T] = [[U]^T[U]]^{-1}[U]^T \qquad (6-55)$$

and the stiffness matrix corresponding to $\{w\}$ is

$$[k] = [T]^T[\hat{k}][T] \qquad (6-56)$$

6.3.4 Load Vector

Based on equations (6 – 38) and (6 – 55), the deflection at any point in substructure ① can be written as follows:

$$w(r,\theta) = [H]\{A\} = [H][T]\{w\} = [N]\{w\}$$
$$[N] = [H][T] \qquad (6-57)$$

The load vector equivalent to distributed load $q(x,y)$ in the substructure can be obtained as

$$[Q_i \quad M_i \quad Q_j \quad M_j]^T = \int_0^b \int_0^l [N]^T q(x,y)dxdy \qquad (6-58)$$

6.4 Numerical Example

1. Problem Description

The stress intensity factors of a through crack with length $2a$ embedded in a thin plate, which is subjected to uniform moments of intensity M_0 at infinity (**Fig. 6.3**), was derived by Sih(1973) for the special case of vanishingly thin plate as:

$$K_I = \frac{(1+\nu)}{(3+\nu)} M_0 \sqrt{a}$$

$$K_{II} = 0 \qquad (6-59)$$

where ν is the Poisson's ratio.

To demonstrate the efficiency and convergence of the bending crack strip model, a numerical example is presented and the results are compared to the Sih's solution (6 – 59). The configuration selected for this purpose is also shown in **Fig 6.3**, in which infinite plate is modeled by $l/a = 10 >> 5$, $t/a = 0.01$. The plate is simply supported around four edges and has the following characteristics

$$a = 3 \text{ m}, \quad l = 30 \text{ m}, \quad t = 0.03 \text{ m}, \quad M_0 = 1 \text{ m·kg} \qquad (6-60)$$

The materials properties are $\nu = 0.25$, $E = 20{,}000$ Mpa and the stress intensity factors can be calculated according to (6 – 59) as:

$$K_I = 0.666, \quad K_{II} = 0 \qquad (6-61)$$

2. Pre – processing

I. Finite strip mesh

The plate is modeled by 4 traditional spline finite strips and 2 crack strips with total 52 nodes, as shown in **Fig 6.4.** Nodes 25 and 27 have the same coordinates but different deflections. The width

of the strip and the node spacing are both equal to 5 m

$$h = b = 5 \text{ m} \tag{6-62}$$

II. Load evaluation

In this case, loads are applied to the nodes located on edges only. The nodal forces equivalent to the uniform moment applied on plate edges can be calculated based on the principle of virtual work. For the top traditional spline strip, moment M_0 performs a virtual work during the rotation θ of edge *1 – 7*, also performs a virtual work during the rotation $\partial w / \partial y$ on edge *7 – 14*, as shown in **Fig 6.5**. Based on (6 – 17), the work done by moment M_0 on edge *1 – 7* can be evaluated as

$$W = \int M_0 \theta_j dy = M_0 \int_l [\phi]\{d\} dy = M_0 [\int_l \phi_0 dy \quad \int_l \phi_1 dy \quad \cdots \quad \int_l \phi_8 dy]\{d\}$$

$$= M_0 h [\frac{1}{24} \quad \frac{1}{2} \quad 1 \quad 1 \quad 1 \quad 1 \quad 1 \quad \frac{1}{2} \quad \frac{1}{24}]\{d\} \tag{6-63}$$

or

$$W = M_0 h [\frac{1}{24} \quad \frac{1}{2} \quad 1 \quad 1 \quad 1 \quad 1 \quad 1 \quad \frac{1}{2} \quad \frac{1}{24}][F_{\theta j}]\{f\} \tag{6-64}$$

where

$$\{f\} = \begin{bmatrix} \theta_0 & \theta_1 & \theta_2 & \cdots & \theta_6 & \theta_7 & \theta_8 \end{bmatrix}^T \tag{6-65}$$

and $[F_{\theta j}]$ indicates the relationship between the nodal rotations and the coefficients of spline function interpolation along the nodal line. It depends on the boundary conditions at both ends, referring to (2 – 5) , (6 – 33) and next section. Therefore, the load vector can be formed as

$$\{q\} = M_0 h[\frac{1}{24} \quad \frac{1}{2} \quad 1 \quad 1 \quad 1 \quad 1 \quad 1 \quad \frac{1}{2} \quad \frac{1}{24}][F_{\theta j}] \qquad (6-66)$$

On edge ***7 – 14*** or ***21 – 31*** in the crack strip, as illustrated in **Fig 6.5**(c) or (d), the work done by moment M_0 can be calculated as

$$W = \int_0^b M_0 \left.\frac{\partial w}{\partial y}\right|_{y=l} dx \qquad (6-67)$$

Based on equation (6 – 19), the edge rotation can be expressed in terms of interpolation coefficients as

$$\left.\frac{\partial w}{\partial y}\right|_{y=l} = [C][\Phi'']\{\delta\} \qquad (6-68)$$

where

$$[\Phi''] = \begin{bmatrix} [\phi''] & & & \\ & [\phi''] & & \\ & & [\phi''] & \\ & & & [\phi''] \end{bmatrix}$$

$$[\phi''] = [0 \quad 0 \quad 0 \quad 0 \quad 0 \quad 0 \quad \frac{h}{2} \quad 0 \quad -\frac{h}{2}] \qquad (6-69)$$

Thus, equation (6 – 67) can be rewritten as

$$W = M_0 \int_0^b [C]dx \cdot [\Phi'][\delta] = M_0[R][\Phi'][T]\{w\} \qquad (6-70)$$

where

$$[R] = [\frac{b}{2} \quad \frac{7b^2}{12} \quad \frac{b}{2} \quad -\frac{b^2}{12}] \qquad (6-71)$$

$[T]$ and $\{w\}$ are the transformation matrix and nodal deflection vector respectively, as defined in equation (6 – 33). Further, the load vector takes the following form:

$$\{q\} = M_0[R][\Phi'][T] \qquad (6-72)$$

III. Boundary conditions

Because the four edges are simply supported, the deflection of nodes on four edges are zero

$$w_k = 0, \quad (k = \text{the number of nodes on the four edges.}) \qquad (6-73)$$

The rotations around y -axis on both edges 1 – 7 and 46 – 52 are also zero

$$\frac{\partial w}{\partial y} = 0, \quad \text{(On edges } \boldsymbol{1-7} \text{ and } \boldsymbol{46-52}\text{)} \qquad (6-74)$$

while the rotation around x-axis on both edges 1 – 46 and 7 – 52 are zero,

$$\frac{\partial w}{\partial x} = 0, \quad \text{(On edges } \boldsymbol{1-46} \text{ and } \boldsymbol{7-52}\text{)} \tag{6-75}$$

Followings are obtained respectively on edges $\boldsymbol{1-7}$ and $\boldsymbol{46}-52$

$$\frac{\partial w_i}{\partial y} = [\phi']\{c\} = 0 \quad \text{(on edge } \boldsymbol{1-7}\text{)}$$

$$\frac{\partial w_j}{\partial y} = [\phi']\{e\} = 0 \qquad \text{(on edge } \boldsymbol{46-52}\text{)} \tag{6-76}$$

thus, there are two additional boundary conditions needed to determine the coefficients $\{c\}$ and $\{e\}$:

$$c_0 = c_2, \qquad c_{r-1} = c_{r+1} \qquad \text{(on edge } \boldsymbol{1-7}\text{)} \tag{6-77}$$

and

$$e_0 = e_2, \qquad e_{r-1} = e_{r+1} \qquad \text{(on edge } \boldsymbol{46-52}\text{)} \tag{6-78}$$

Substitute $[C'] = [0 \quad 1-4\bar{x}+3\bar{x}^2 \quad 0 \quad 3\bar{x}^2-2\bar{x}]$ into equation (6 – 76) on edges $\boldsymbol{1-46}$ and $\boldsymbol{7-52}$ respectively, and the followings are obtained in each strip

$$\theta_i(1-4\bar{x}+3\bar{x}^2)+\theta_j(3\bar{x}^2-2\bar{x}) = 0 \quad (y = 0 \text{ and } y = l) \tag{6-79}$$

For any x, there must be $\theta_i|_{y=0,y=l} = 0, \quad \theta_j|_{y=0,y=l} = 0$. Therefore, the two additional

conditions needed to determine the coefficient $\{d\}$ and $\{f\}$ are obtained respectively

$$d_0 + 4d_1 + d_2 = 0 \ , \quad d_{r-1} + 4d_r + d_{r+1} = 0 \qquad (6-80)$$

and

$$f_0 + 4f_1 + f_2 = 0 \ , \quad f_{r-1} + 4f_r + f_{r+1} = 0 \qquad (6-81)$$

3. Processing

The stress analysis is performed with four extra nodes or without any extra node in the substructure. Various numbers of Gaussian points in both method 1 and method 2 (described in section 3.3) are employed in singular integrals, while only five Gaussian points are uesd in the non-singular integrals.

4. Post – processing

The resulting stress intensity factors and K_I's errors compared to the value of (6 – 61) are shown in Table 6.1. It shows that the convergence of the current method is satisfactory, since the numerical error is reduced drastically as the numbers of the extra nodes and Guassian points are increased. When 4 extra nodes and 31 X 31 Gaussian points are employed, the numerical error was reduced to 1.1 percent. It also shows that Method I of singular integral converges faster than Method II .

Table 6.1 *K* Values of The Cracked Plate under Pure Bending

	Method of Integral	K_I, K_{II} for various numbers of Gaussian Quadrature Points and K_I Errors								
		8^2			19^2 (I)/12^2 (II)			30^2 (I)/16^2 (II)		
		K_I	Error	K_{II}	K_I	Error	K_{II}	K_I	Error	K_{II}
Four Extra Nodes	I	0.723	8.6%	0.000	0.710	6.6%	0.000	0.670	1.1%	0.000
	II	0.730	9.6%	0.000	0.722	8.4%	0.000	0.710	6.6%	0.000
No Extra Node	I	0.739	10.9%	0.100	0.723	8.6%	0.100	0.680	1.8.%	0.100
	II	0.750	12.6%	0.100	0.735	10.4%	0.100	0.700	5.1%	0.100

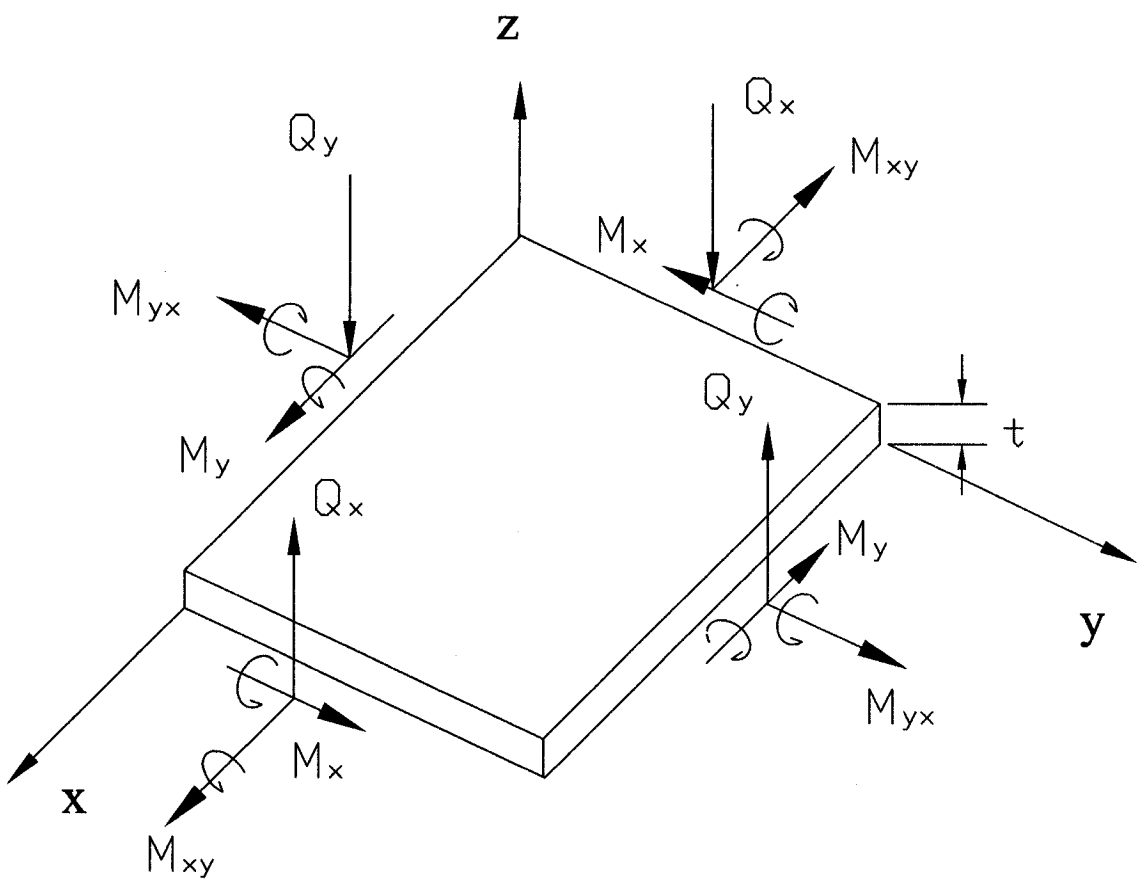

Figure 6.1 Notations for moments and shear resultant

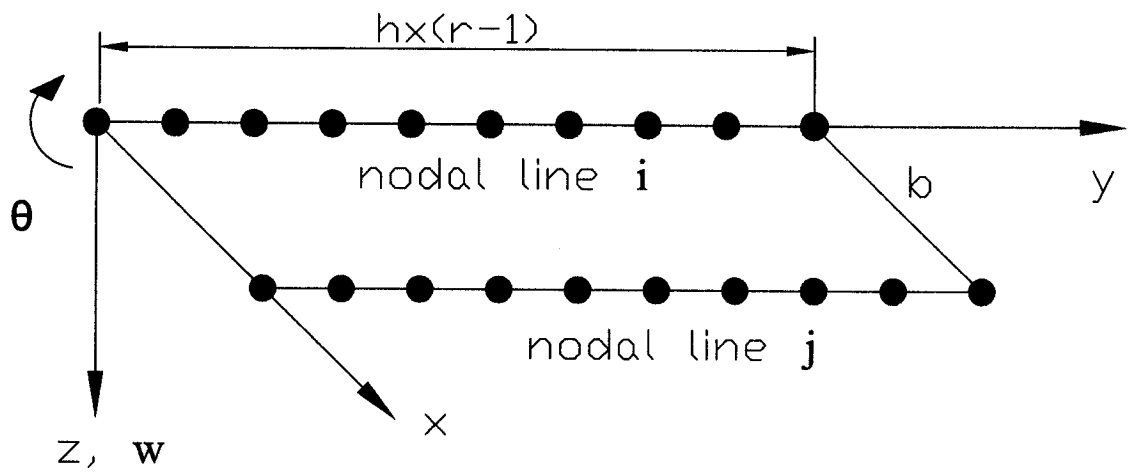

Figure 6.2 Spline Plate Strip

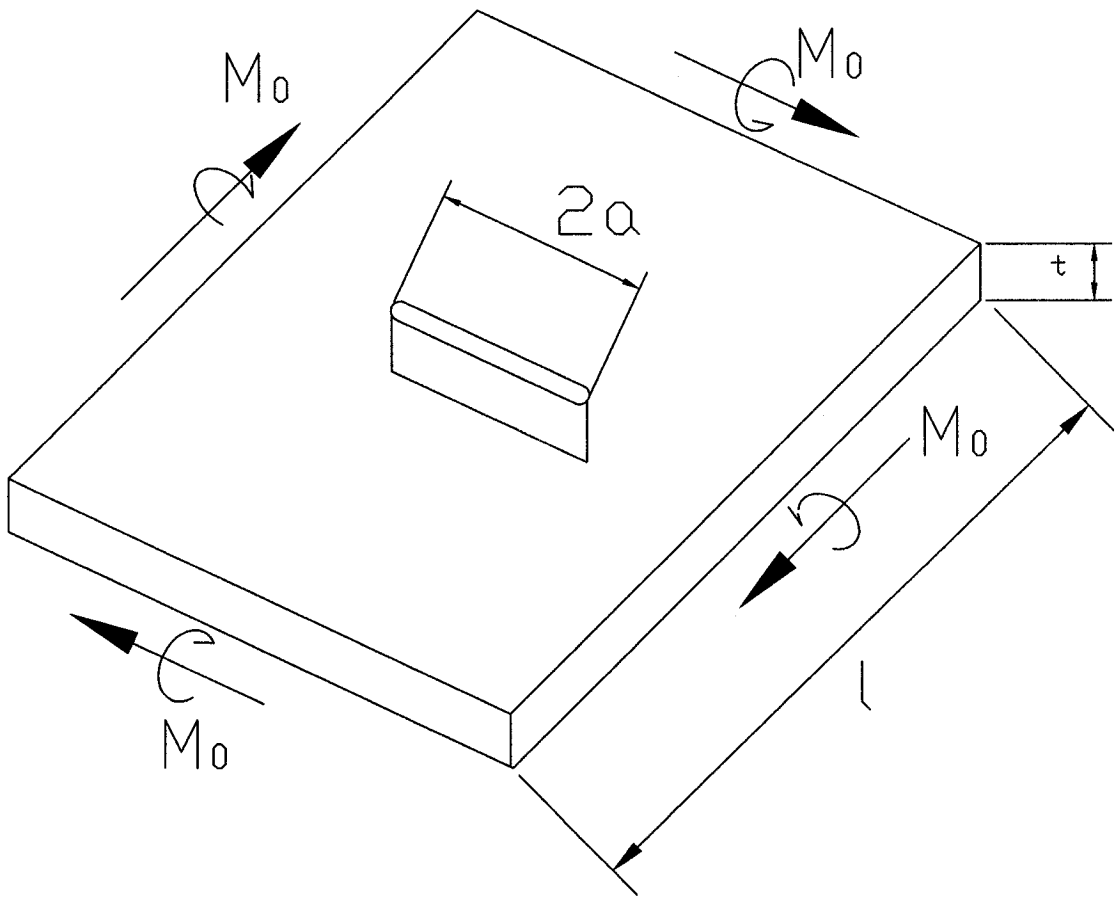

Figure 6.3 Example: Cracked thin plate under pure bending

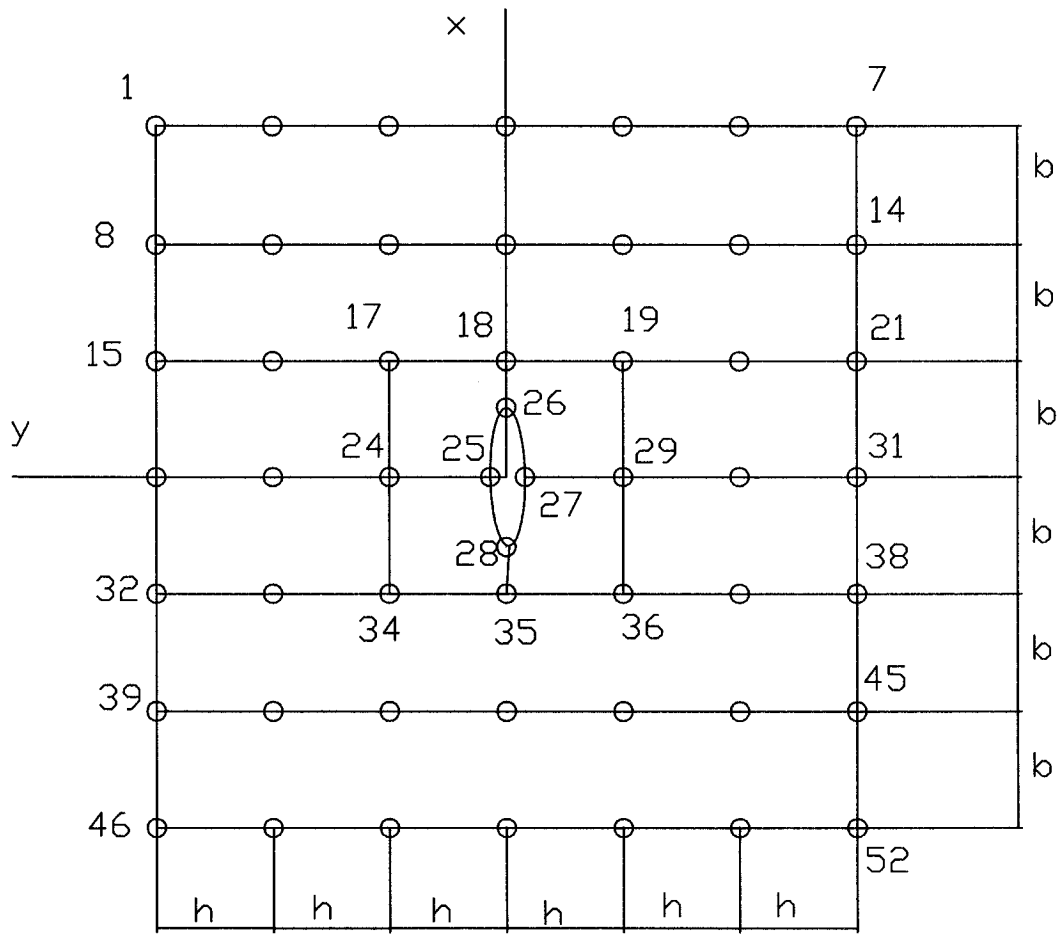

Figure 6.4 Mesh of the plate

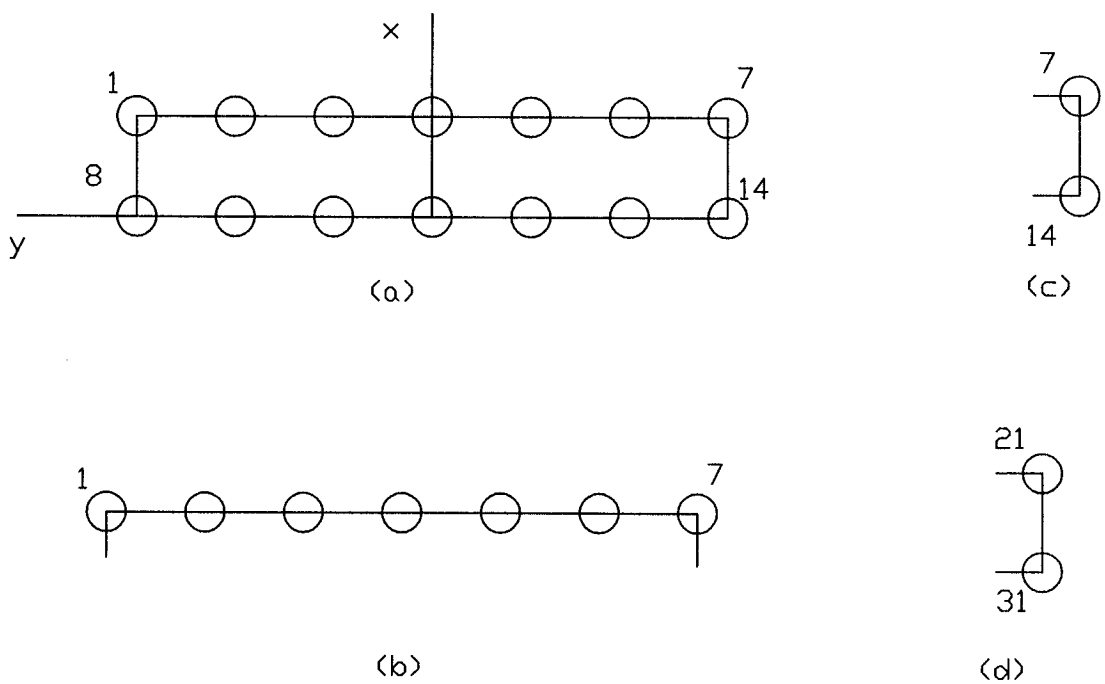

Figure 6.5 Edge nodes with loads

Chapter 7

Applications to Bridge Structures

7.1 Introduction

In previous chapters, the performance and convergence of the proposed methods were tested through simple case studies with positive results. In this chapter the applicability of these methods to fracture analysis of some bridge structures is studied. A number of slab, slab on girder and box girder bridges under different loads are analyzed in order to investigate their fracture characteristics, such as the effects of crack length on the stress intensity factor, the near field stresses and the near field deflections. This investigation will provide important information for

bridge design, management and safety.

7.2 Slab Bridges

Many short or medium span highway bridges are slab bridges. If a straight bridge has a constant cross-section longitudinally and the boundary conditions at both ends do not change transversely, Kirchhoff bending plate strip and the bending crack strip are very efficient tools for numerical fracture analysis of the bridges, especially for simply supported rectangular bridges under distributed loads.

Some bridge decks are voided or stiffened slabs. For understanding the overall behavior of such bridges, the deck can be idealized as an orthotropic plate with equivalent elasticity properties, analyzed using the plate strips.

If a bridge is continuous over intermediate supports, which may have gone through settlements, each term of the leading diagonal in global stiffness matrix is replaced by a large number, while the corresponding terms in load vector are changed to the product of the settlement by the same number. In this way, the resulting deflections of the bridge at the supports will be equal to the given settlements with sufficient accuracy.

The most critical cracks in bridge fracture analysis are those located in the area with high moment, such as those at the middle of spans and at intermediate supports.

7.2.1 Simply Supported Slab Bridge

The simply supported slab bridge with a crack at the center and subjected to a truck loading as shown in **Fig 7.1** is analyzed using the bending crack strip and spline plate strips. The numerical model is shown in **Fig 7.2.** The slab is discretized into 6 spline plate strips and 2 bending crack strips. On each nodal line 11 nodes are included for spline plate strip, while 12 nodes are used on the nodal line crossing the crack. In addition, four extra nodes are employed around the tip of the crack. The material properties are $E = 190{,}000$ Mpa, $\nu = 0.25$, while the slab thickness is 0.1m.

The resulting stress intensity factors are listed in Table 7.1 for $2a$ = 0.1m, 0.3m and 0.5m, respectively. The deflection and bending moment for $2a$ = 0.5m are depicted in **Fig 7.3** and **Fig 7.4** respectively.

Table 7.1 Stress intensity factor for a simply supported slab bridge (Mpa $\sqrt{m}$)

$2a$ (m)	K_I	K_{II}
0.1	13.69	0.02
0.3	23.09	0.03
0.5	30.23	0.03

It is reasonablely shown in **Fig 7.3** and **Fig 7.4** that the deflection and the moment in a cracked bridge are larger than those in an uncracked bridge, due to the reduction of global stiffness resulting from the presence of crack. The stress intensity factors shown in **Table 7.1** are almost in direct proportion to $\sqrt{a}$, which is in excellent agreement with (6 – 10b).

7.2.2 Continuous Slab Bridge

The bending crack strip and spline plate strips are used to analyze a two-span slab bridge subjected to a truck loading, as shown in **Fig 7.5** . The numerical model is shown in **Fig 7.6.** The slab is discretized into 14 spline plate strips and 2 bending crack strips. On each nodal line 17 nodes are included for spline plate strip, while 18 nodes are used on the nodal line crossing the crack. In addition, four extra nodes are employed around the tip of the crack. The material properties are given by E = 25,000 Mpa, ν = 0.15, while the slab thickness is 0.2m.

The resulting stress intensity factors are listed in **Table 7.2** for $2a$ = 0.1m, 0.3m and 0.5m, respectively. It can be seen that the results are also in direct proportion to $\sqrt{a}$. The near field deflection and near field bending moment on cross-section A-A for $2a$ = 0.5m are respectively depicted in Figures 7.7 and 7.8. The results obtained for the uncracked two-span slab in the same situation are also shown in these figures for comparison.

Table 7.2 Stress intensity factor for a two-span slab bridge (MPa $\sqrt{m}$)

$2a$ (m)	K_I	K_{II}
0.1	4.58	0.01
0.3	7.99	0.01
0.5	10.97	0.02

7.3 Box Girder Bridge

Box girder bridges are very popular for highways because of their high torsional rigidity and good appearance. However, the structural analysis of box girder bridges is a very difficult undertaking because of their complex deformation pattern and stress distribution, especially when the structure contains cracks. In this section, in order to take advantage of spline finite strip method, the implementation of the crack strip model is presented as an economical solution for the fracture analysis of box girder bridges.

In the analysis of the bridges, the flat shell strips are employed to model the box girders, and each end support of the bridge is assumed to be a diaphragm which is infinitely stiff in its own plane but infinitely flexible out of plane. Consequently, an idealized simply supported boundary condition is achieved for both in-plane and out-of-plane behaviors.

7.3.1 Flat Shell Strip

A prismatic folded plate structure or box girder bridge is an assembly of rectangular plates that can offer resistance to both bending and in-plane loadings. This type of structure can be analyzed using the flat shell strip which is formed by combining the plate strip and the plane stress strip so that it is capable of simulating both the bending and in-plane deformations. Moreover, the fracture characteristics of the structures, such as stress intensity factors, can also be a linear combination of the one for plate bending and the one for plane stress, due to the nature of linear fracture mechanics. That is,

$$\begin{aligned} K_I &= (K_I)_{MaxOfBending} + (K_I)_{in-plane} \\ K_{II} &= (K_{II})_{MaxOfBending} + (K_{II})_{in-plane} \end{aligned} \qquad (7-1)$$

A flat shell strip subjected simultaneously to in-plane and bending forces is considered. For the in-plane action, the nodal line displacement parameters are related to the nodal line force vectors by

$$\{F^p\} = [k^p]\{\delta^p\} \qquad (7-2)$$

where

$$\{\delta^p\} = [u_i \quad v_i \quad u_j \quad v_j]^T \qquad (7-3)$$

and

$$\{F^p\} = [P_{ix} \quad P_{iy} \quad P_{jx} \quad P_{jy}]^T \qquad (7-4)$$

They were defined in Chapter 5

Similarly, for the bending action, the nodal line displacement parameters are related to the nodal line force vectors by

$$\{F^b\} = [k^b]\{\delta^b\} \qquad (7-5)$$

where

$$\{\delta^b\} = [w_i \quad \theta_i \quad w_j \quad \theta_j]^T \qquad (7-6)$$

and

$$\{F^p\} = [Q_i \quad M_i \quad Q_j \quad M_j]^T \qquad (7-7)$$

The details were mentioned in Chapter 6.

Combining the nodal line displacement parameters and forces for both action, there is

$$\{F\} = [k]\{\delta\} \qquad (7-8)$$

where

$$\{\delta\} = [u_i \quad v_i \quad w_i \quad \theta_i \quad u_j \quad v_j \quad w_j \quad \theta_j]^T \qquad (7-9)$$

$$\{F\} = [P_{ix} \quad P_{iy} \quad Q_i \quad M_i \quad P_{jx} \quad P_{jy} \quad Q_j \quad M_j]^T \tag{7-10}$$

and

$$[k] = \begin{bmatrix} [k_{ii}^p] & 0 & [k_{ij}^p] & 0 \\ 0 & [k_{ii}^b] & 0 & [k_{ij}^b] \\ [k_{ij}^p] & 0 & [k_{jj}^p] & 0 \\ 0 & [k_{ij}^b] & 0 & [k_{jj}^b] \end{bmatrix} \tag{7-11}$$

All of the above derivations are carried out in a local coordinate system whose x and y axes coincide with the mid-surface of a strip. Since box girder bridges have strips that may in general meet at an angle, it is necessary to carry out the assembly procedure of the system matrices and vectors of non-coplanar strips in a global coordinate system that is common to all strips. This is done by transforming displacement and force vectors from local coordinates to global coordinates.

Transformation of displacement and force vectors from local coordinates x, y, z to the global coordinates x', y', z' is performed as follows:

$$\{\delta\} = [T]\{\delta_G\} \tag{7-12}$$

in which $[T]$ is a transformation matrix and the subscript G refers to global coordinates

$$[T] = \begin{bmatrix} [t] & 0 \\ 0 & [t] \end{bmatrix} \tag{7-13}$$

where

$$[t] = \begin{bmatrix} \cos\alpha & 0 & \sin\alpha & 0 \\ 0 & 1 & 0 & 0 \\ -\sin\alpha & 0 & \cos\alpha & 0 \\ 0 & 0 & 0 & 1 \end{bmatrix} \qquad (7-14)$$

with α being the angle between the x and x' axes, and between the z and z' axes.

Thus, the stiffness matrix and the load vector of the strip in the global system are obtained as follows:

$$[k_G] = [T]^T[k][T]$$
$$\{F_G\} = [T]^T\{F\} \qquad (7-15)$$

7.3.2 Example 1: Single - cell box girder

A concrete single-cell box girder bridge as shown in **Fig 7.9**, is 9 m long, 3 m wide and 1.5 m deep, and it is subjected to a uniformly distributed vertical load 15 kN/m^2 applied on the top slab. The top and bottom slabs of the box are 0.25 m thick, while the two webs are 0.35m thick. A crack is located at the center of the bottom slab at midspan. The material properties of the bridge are given by:

$$E = 25 \times 10^3 \text{ MPa}$$
$$\nu = 0.15$$

Fig 7.10 shows the finite strip model of the bridge. Each web and the top slab are respectively discretized into 4 and 6 spline flat shell strips, while the bottom slab is divided into 4 spline flat shell strips and 2 crack flat shell strips. 19 nodes are included on each nodal line in the spline flat shell strips, while 20 nodes are used for the nodal line crossing the crack. In addition, four extra nodes are employed around the tip of the crack. The width of the crack flat shell strip should be larger than the crack length. For comparison purpose, the analysis is also performed for the same structure without any crack. In this case, the top and bottom slabs are each divided into 6 equally wide spline flat shell strips.

The resulting stress intensity factors are listed in **Table 7.3** for $2a$ = 0.1m, 0.3m and 0.5m, respectively. It can be seen that the results are also in direct proportion to $\sqrt{a}$. The near field deflection and near field bending moment on cross-section A-A for $2a$ = 0.3m are respectively depicted in Figures 7.11 and 7.12. Comparisons are made with the results for the structure without any crack.

Table 7.3 Stress intensity factor for a single-cell box girder bridge (MPa $\sqrt{m}$)

$2a$ (m)	K_I	K_{II}
0.1	9.53	0.01
0.2	16.67	0.01
0.3	21.58	0.00

7.3.3 Example 2: Top opened box girder

7.3.3.1 The background of the Bryte Bend Bridge

The Bryte Bend Bridge located in California, U. S. A., as shown in **Fig 7.13,** is a box girder bridge with the top opened superstructure, which consists of twin parallel structures **(Fig 7.14)**. Each bridge carries three lanes of traffic plus shoulder. The main river section consists of four continuous spans of 281 - 370 - 370 - 281 ft. (85.6 - 112.8 - 112.8 - 85.6 m) spans **(Fig 7.15).**

The superstructure is a trapezoidal steel box supported on reinforced concrete piers as shown in **Fig 7.14**. The exterior webs of the box were sloped 1:2 **(Fig 7.16)** to reduce the width of the compression flanges in the continuous spans and to improve overall appearance. The boxes were designed with the top open. Conventional girder flanges were welded to the tops of the box sides and to a single longitudinal web plate stiffening the center of the box. The bridge was fabricated from plates of A36, A441 and an A517 type steel. The A36 steel was used in all areas of low stress. The A441 steel was used for the maximum positive moment section and the A517 type steel was used for the top flanges at maximum negative moment section at each river pier. Each top flange is 30 inch (762mm) wide and 2-1/4 inch(57mm) thick. All fabrication was done by welding.

While the composite concrete deck was being placed in June, 1970, a brittle fracture occurred across one of the outer flanges at pier 12, as shown in **Fig 7.17**. It was initiated at the intersection of a 1/2 inch (12.5 mm) thick lateral attachment welded to the 2-1/4 inch (57 mm) thick flange, as shown in **Fig 7.18.** The fracture propagated across the entire 30 inch (762 mm) wide flange and 4 inch (101 mm) down into the web where it was arrested **(Fig 7.19).** The fracture surface was a classic herringbone type brittle fracture, with the herringbone patterns pointing back toward the

crack origin and very small shear lips.

According to information provided by Roberts in 1977, the nominal yield strength of this material (A517) was 100 *ksi* (690 MPa) while the design stress was 45 *ksi* (310 MPa). At the time the crack propagated, the dead load stress was about 28 *ksi* (193 MPa) and the ambient temperature was about 60F (15.5 C).

7.3.3.2 Fracture analysis of the Bryte Bend Bridge by Roberts

The fracture analysis of the Bryte Bend Bridge was performed by Roberts (1977). The observation of the fracture surface indicated that a weld crack about 0.2 inch (5 mm) deep (**Fig 7.20**) was present in a residual stress field, and initiated sometime during the fabrication or erection. As the initial weld crack propagated out of the residual stress field, it arrested at a distance of about 1.3 inch (33 mm) from the edge of the plate. During pouring of the concrete deck, as the dead load stress was increased to about 28 *ksi*(193 MPa), complete fracture of the top flange occurred.

The K_{IC} (fracture toughness) tests of material from the cracked flange plate using Standard Compact Specimen (ASTM Standard E-399) showed that the K_{IC} value at the service temperature of 60F (15.5 C) and slow loading rate was $55 ksi\sqrt{in}$ $(60.5 MPa\sqrt{m})$. Roberts said that this value was considerably lower than the expected K_{IC} value of A514 - 517 steels. He also said that the K_{IC} value of $150 ksi\sqrt{in}$ $(165 MPa\sqrt{m})$ is more representative of these steels, but there was no evidence to prove this in this fracture analysis.

Using $K_I = 1.12\sigma\sqrt{\pi a}$, the empirical equation for a simple edge-crack; the stress-flaw size

relations for both $K_{IC}=55ksi\sqrt{in}$ $(60.5MPa\sqrt{m})$ and $K_{IC}=150ksi\sqrt{in}$ $(165MPa\sqrt{m})$ are shown in **Fig 7.21**. For a K_{IC} of $55ksi\sqrt{in}$ $(60.5MPa\sqrt{m})$, the combination of an applied stress of 28 *ksi*(193 MPa) and the 1.3 inch (33 mm) deep crack caused the stress intensity K_I to reach the critical value K_{IC} of $55ksi\sqrt{in}$ $(60.5MPa\sqrt{m})$. In contrast to value of $55ksi\sqrt{in}$ $(60.5MPa\sqrt{m})$, even at the maximum design stress of 45 *ksi* (310 MPa), the critical crack size is about 3 inch (76 mm) for the K_{IC} of $150ksi\sqrt{in}$ $(165MPa\sqrt{m})$. If the flange material of A514-517 steel had the level of fracture toughness normally found, failure should not have occurred. Thus, Roberts concluded that even though the engineer should be able to expect certain minimum mechanical properties for a particular grade of steel, fracture toughness values should be specified where desired because of their greater sensitivity to thermo-mechanical history.

7.3.3.3 Fracture analysis of the Bryte Bend bridge based on beam theory and empirical approach

The objective of this example is to use a numerical method to verify the empirical equation $K_I = 1.12\sigma\sqrt{\pi a}$ for a single edge-crack specimen, (Anderson 1995, Tada 2000), and to investigate possible causes of the critical failure in this bridge.

In the current study, the fracture analysis is carried out using a two-span bridge model shown in **Fig 7.22(a)**. At the intermediate support, the bottom flange is laid on the top of pier 12, while the

two ends of the bridge is clamped to model the continuity with the adjacent spans. As mentioned earlier, the top flanges around the intermediate support are made of Steel A517 with E = 200,000 MPa and ν = 0.3.

Generally, the maximum negative longitudinal moment occurs at intermediate support, while the maximum positive one occurs at midspan. The reaction "*R*" from intermediate support can be estimated based on preliminary theory of structural analysis. The result is obtained as

$$R = \frac{l^3}{8ab} W \qquad (7-24)$$

where, W is the vertical load per unit length of the bridge, a and b are respectively the lengths of the first and second spans, while l is the total length of the bridge. For this bridge a = 85.6 m, b = 112.8 m and l = 198.4 m.

The longitudinal bending moment at the intermediate support, $x = a$, is the maximum negative moment, which is equal to

$$M_a = \frac{1}{4}(ab - \frac{l^2}{3})(W_s + W_c) \qquad (7-25)$$

in which W_s and W_c are the weights of steel girder and concrete deck respectively, and $W = W_s + W_c$

The specific weight of top-open box girder is

$$\rho_s = 490lb/ft^3 = 76981.2N/m^3 \qquad (7-26)$$

Further, for the section shown in **Fig 7.23(a)**, the weight per unit length of the bridge is calculated as:

$$\begin{aligned} W_s &= 76981.2 \times [2 \times 0.762 \times 0.057 + (2 \times 5.367 + 7.39) \times 0.05] \\ &= 76447.57N/m \end{aligned} \qquad (7-27)$$

Substituting (7-27) into (7 – 25) leads to the maximum negative moment as

$$M_a = -(66226014.51 + 866.29W_c)N \cdot m \qquad (7-28)$$

The location of the neutral axis of the cross-section of top-open box girder, shown in **Fig 7.23(b),** is determined as

$$y_c = \frac{2 \times 762 \times 57 \times 4.8 + 2 \times 5367 \times 50 \times 2.4}{2 \times 762 \times 57 + (2 \times 5367 + 7390) \times 50} = 1.72m \qquad (7-29)$$

The moments of inertia of top flange I_{1c}, webs I_{2c} and bottom flange I_{3c} are obtained as

follows,

$$I_{1c} = 2 \times 762 \times 57 \times 10^{-6} \times 3.083^2 = 0.82567m^4$$

$$I_{2c} = [\frac{\sqrt{5} \times 50}{12 \times 2} \times 4.8^3 + \frac{\sqrt{5}}{2} \times 50 \times 4.8 \times (2.4 - 1.717)^2] \times 10^{-3}$$
$$= 0.64036m^4$$

$$I_{3c} = 7.39 \times 50 \times 10^{-6} \times 1.717^2 = 1.08932m^4$$

Then, the total moment of inertia of the cross-section of top-open box girder is

$$I_c = I_{1c} + I_{2c} + I_{3c} = 2.55535m^4 \qquad (7-30)$$

Thus, the tensile stress at the top flange can be determined as

$$\sigma = \frac{|M_a|y}{I_c} = (79.9 + 1045.1728W_c \times 10^{-6})\,MPa \qquad (7-31)$$

where y = 3.083 m. Therefore, the tensile stress varies linearly with concrete dead load.

If the concrete deck is 280 mm thick, as shown in **Fig 7.23(a)**, and the specific weight of concrete

is

$$\rho_c = 150lb/ft^3 = 23565.6N/m^3 \qquad (7-32)$$

the weight per unit length of the concrete deck W_c is

$$\begin{aligned} W_c &= 23565.6 \times 0.28 \times 15.65 \\ &= 103264.46N/m \end{aligned} \qquad (7-33)$$

Substituting (7-33) into (7 – 31) yields the following result:

$$\sigma = 186.9\,MPa \qquad (7-34)$$

which is close to the critical dead load stress 28 *ksi*(193 MPa).

A crack is initiated from the interior edge of top flange shown in **Fig 7.24** and propagates while the concrete deck is poured and the dead load Q per unit area is increased accordingly. The contact force between concrete deck and the top flange of the girder is idealized as a uniform area load ***q*** shown in **Fig 7.25.** Thus, $q = 10.2\,Q$. If the concrete deck is 280 mm thick, for example, shown in **Fig 7.23(a)**, and the specific weight of concrete is as of that in (7 – 32), the weight of the concrete deck per unit area is calculated as

$$Q = 23565.6 \times 0.28 = 6598.368N/m^2 \qquad (7-36)$$

Then, the weight per unit length of the concrete deck is determined as

$$W_c = 15.65Q \qquad (7-37)$$

By substituting (7-36) and (7-37) into (7 – 31), the tensile stress at the middle plane of top flange induced by the weight of deck Q is obtained as

$$\sigma = (79.9 + 16497.8043Q \times 10^{-6})\, MPa \qquad (7-38)$$

Thus, the stress intensity factor K_I can be evaluated according to aforementioned empirical equation

$$K_I = 1.12\sigma\sqrt{\pi a} \qquad (7-39)$$

Results for different crack lengths and deck thickness are obtained and summarized in Tables 7.4 and 7.5.

7.3.3.4 Fracture analysis of the bridge using crack flat shell strips

The two-span top-open box girder bridge with a crack shown in **Fig 7.24** is analyzed using crack flat shell strips. As shown in **Fig 7.26**, the continuous box girder bridge is discretized into 8 spline flat shell strips and 1 crack flat shell strip. 116 nodes are included on each nodal line, except for the nodal line crossing the crack, on which 117 nodes are located. 33 extra nodes are

employed to gather more data around the tip of the crack.

Under given dead load $Q = 6855.46$ N/m^2 of the concrete deck, the stress intensity factor K_I is calculated using crack flat shell strips for the crack length ranging from 10 mm to 33 mm. The results are shown in **Table 7.4**. The values obtained from both beam theory and empirical solution (7 – 39) are also given in this table for comparison.

Table 7.4 Stress intensity factor at $\sigma = 193\,MPa$ (Mpa $\sqrt{m}$) for various crack length

a (mm)	K_I	$K_I(7-39)$	Difference (%)
10	39.40	38.31	2.88
18	53.07	51.40	3.24
25	63.71	60.58	5.17
33	76.77	69.60	10.30

It can be seen that for crack length of $a = 10$ mm, 18 mm and 25 mm, the results obtained from the finite strip analysis are in a close agreement with the empirical solutions based on (7 – 39). For the crack longer than 25 mm, the resulting stress intensity factors based on both solutions have exceeded the critical measured value $K_{Ic} = 60.5\ \sqrt{m}$ Mpa, and failure is expected. On the

another hand, the resulting stress intensity factors based on both solutions are much lower than 165.0 MPa $\sqrt{m}$ which is the expected K_{IC} value of A514 - 517 steels. This means that the critical stress intensity factor K_{Ic} is unlikely equal to 165.0 MPa $\sqrt{m}$. Otherwise, failure would not have occurred at the crack length a = 1.3 inch (33 mm).

Under given crack length a = 1.3 inch (33mm) in the top flange, the stress intensity factor K_I is also calculated using crack flat shell strips for the dead load Q of the deck varying from 3000 N/m^2 to 6598.36 N/m^2 . The results are shown in **Table 7.5**. The values obtained from empirical solution (7 – 39) are also given in this table for comparison.

Table 7.5 Stress intensity factor at a = 33 mm(1.3 in) for various dead load (Mpa $\sqrt{m}$)

Q (N/m^2)	σ (MPa)	K_I	K_I (7 – 39)	Difference(%)
3000.00	129.39	48.32	46.66	3.55
4000.00	145.89	54.74	52.61	4.05
5326.16	167.77	63.45	60.47	4.94
6598.36	186.90	74.01	67.40	9.81

The results not only verify the empirical solution of (7 – 39), but also show that for the dead

load Q of the deck greater than 5326.16N/, the resulting stress intensity factors from both FSM and empirical solution (7 – 39) have exceeded the critical measured value = 60.5 MPa, and failure was expected.

Thus, the following conclusions can be drawn:

- Based on the beam theory, the empirical solution for the single edge-crack specimen, , represents adequately the relationship between the stress intensity factor and both stress level and crack length in the top flange.

- The combination of an applied stress of 28 *ksi*(193 MPa) and the 1.3 inch(33 mm) deep crack caused the stress intensity to reach the critical value of , which is much lower than the critical value of , which is expected from the original material.

- As concluded by Roberts, fracture toughness values should be specified considering the thermo-mechanical history of the material.

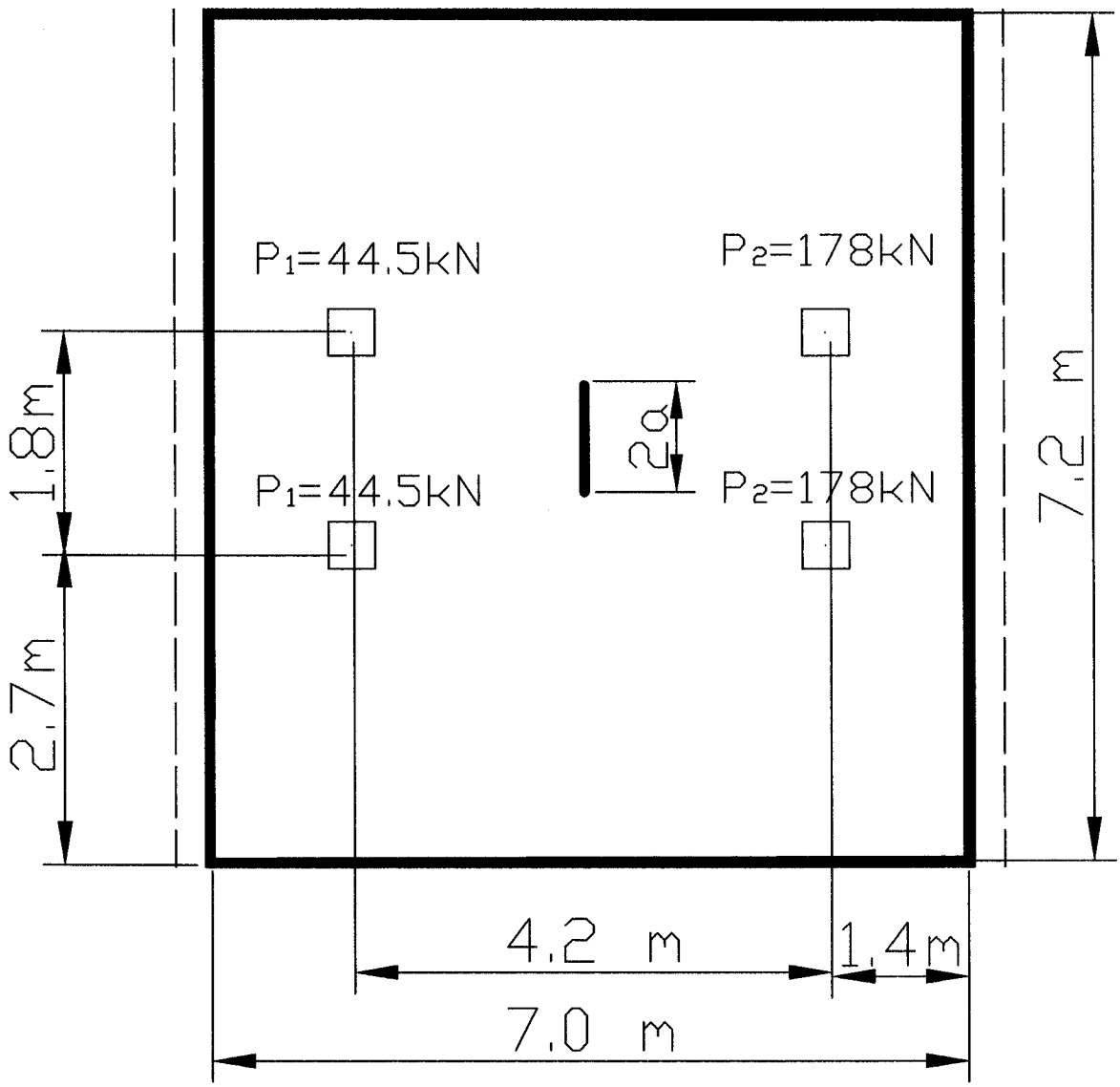

Figure 7.1 Simply supported slab bridge

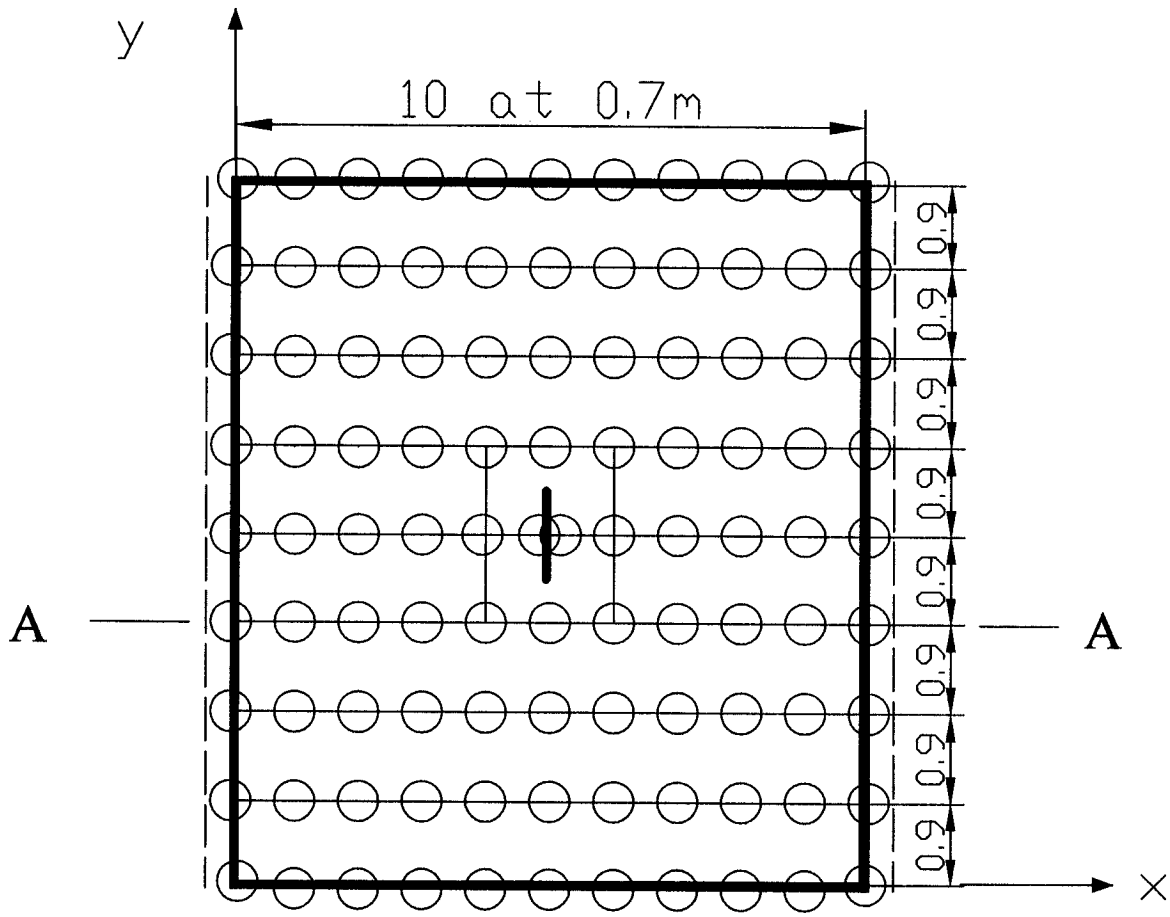

Figure 7.2 Finite strip mesh of the slab bridge

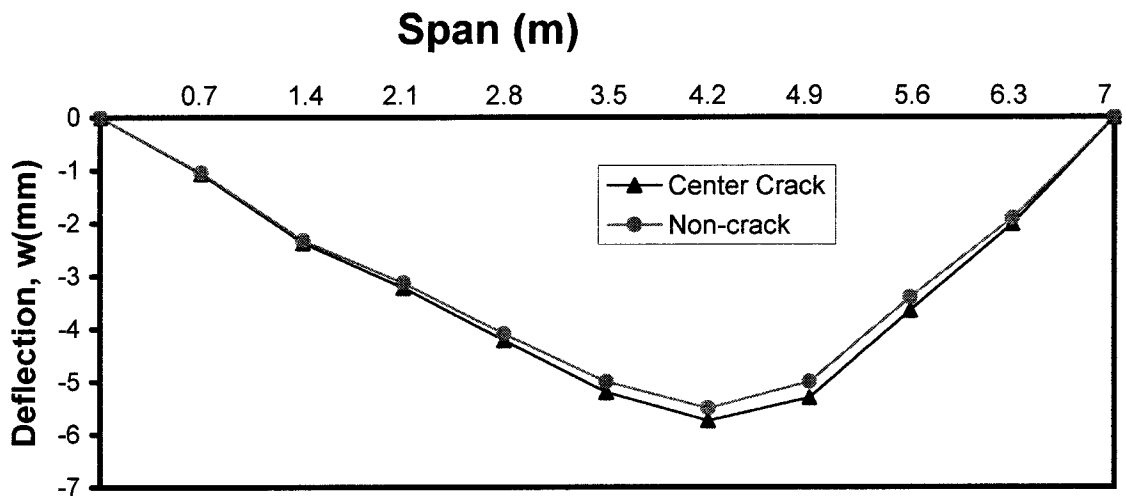

Figure 7.3 Deflection along A-A, in slab bridge

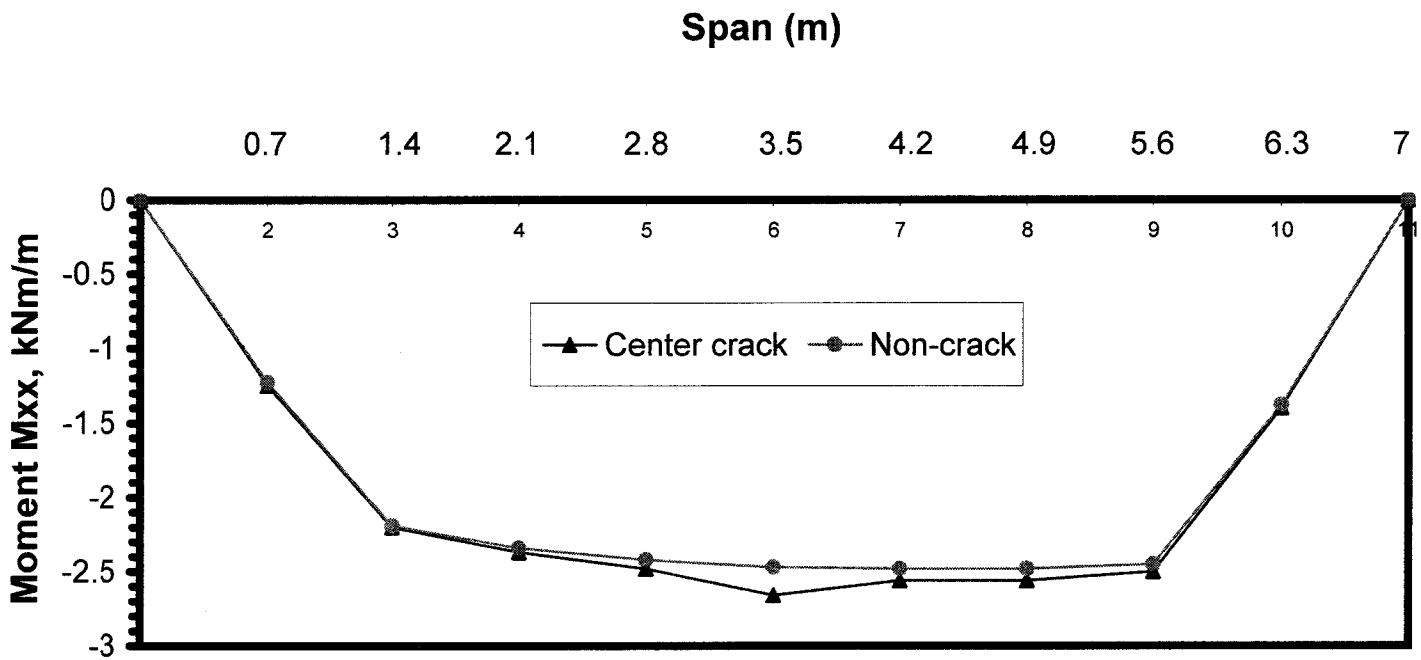

Figure 7.4 Longitudinal moment along A-A, in slab bridge

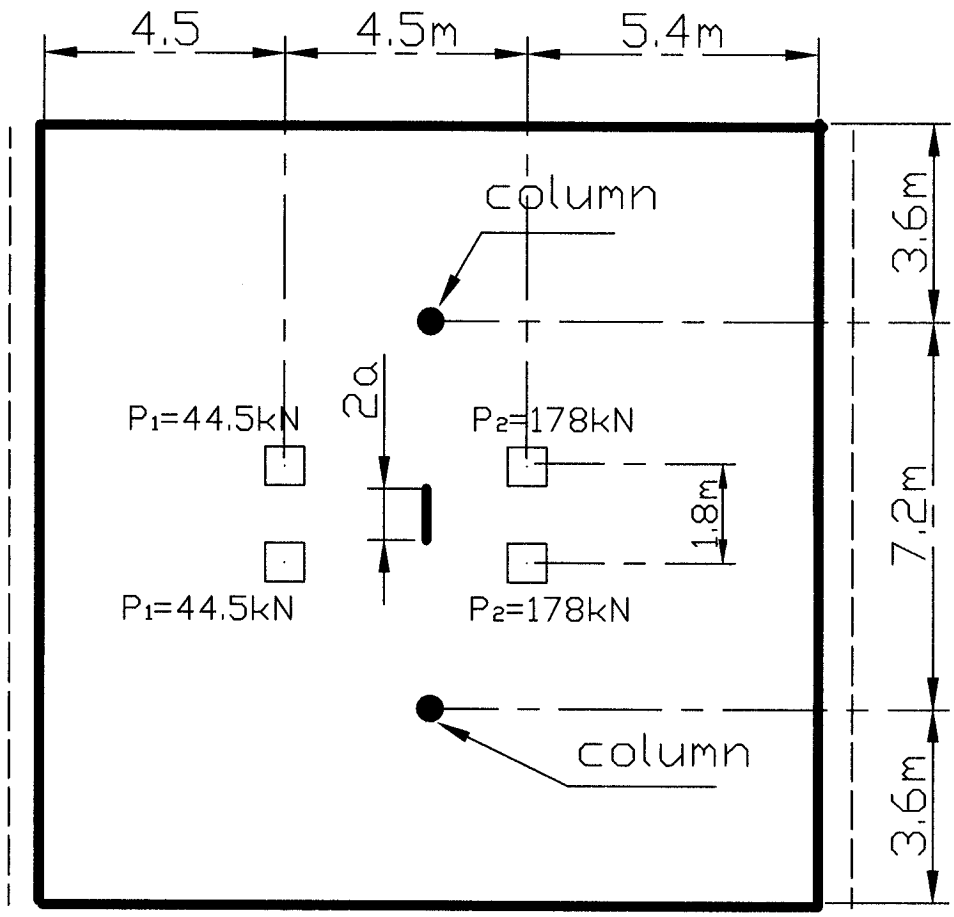

Figure 7.5 Two-span slab bridge

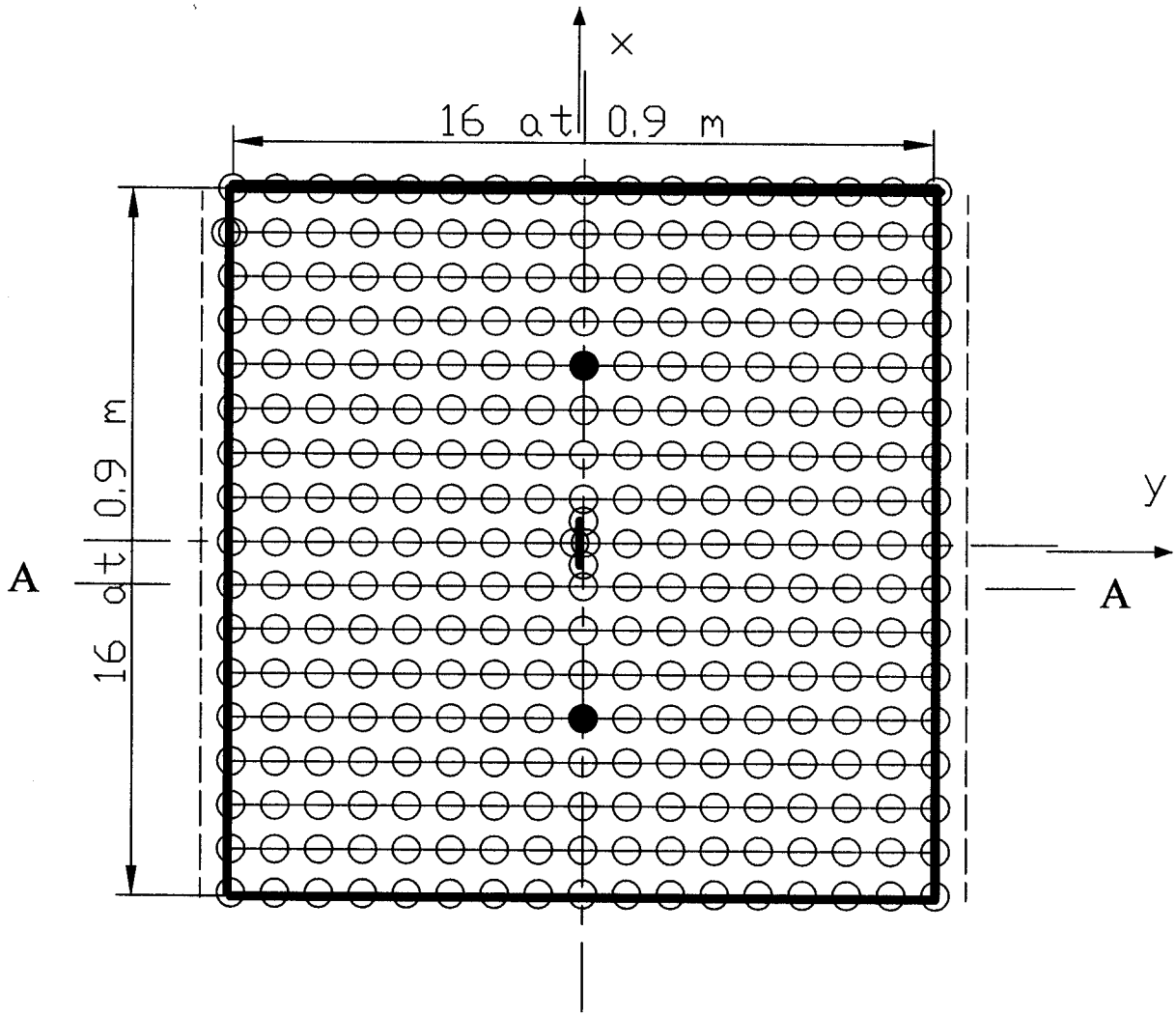

Figure 7.6 Finite strip mesh of two-span bridge

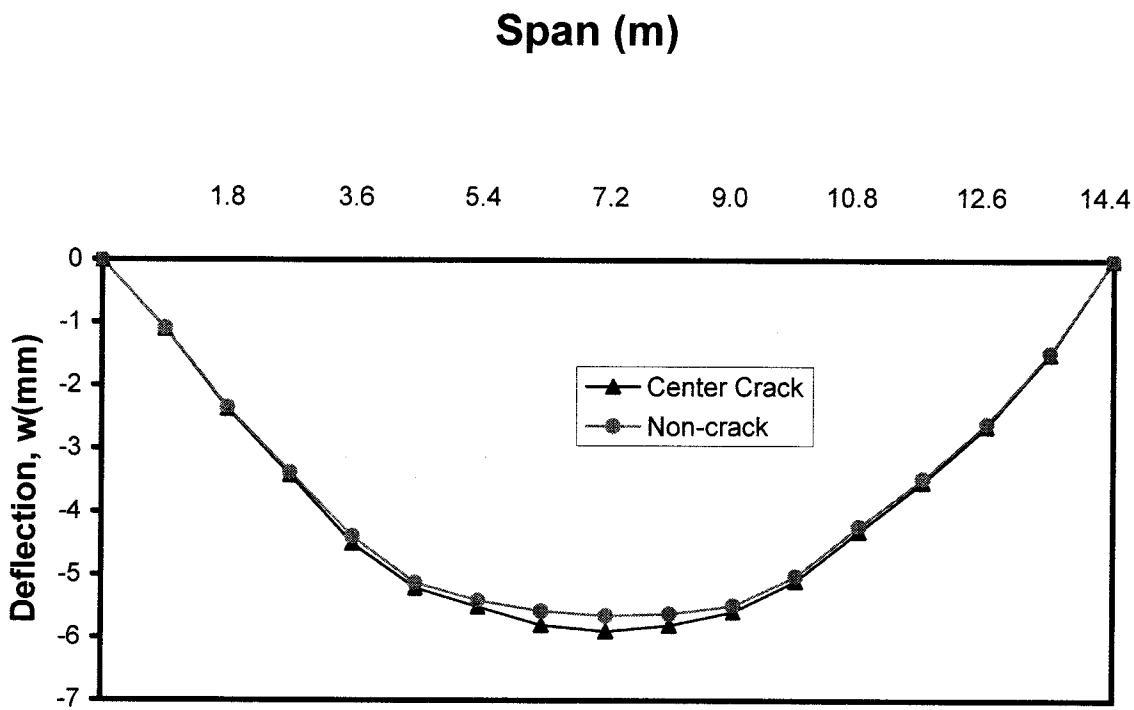

Figure 7.7 Deflection along A-A, in two-span slab bridge

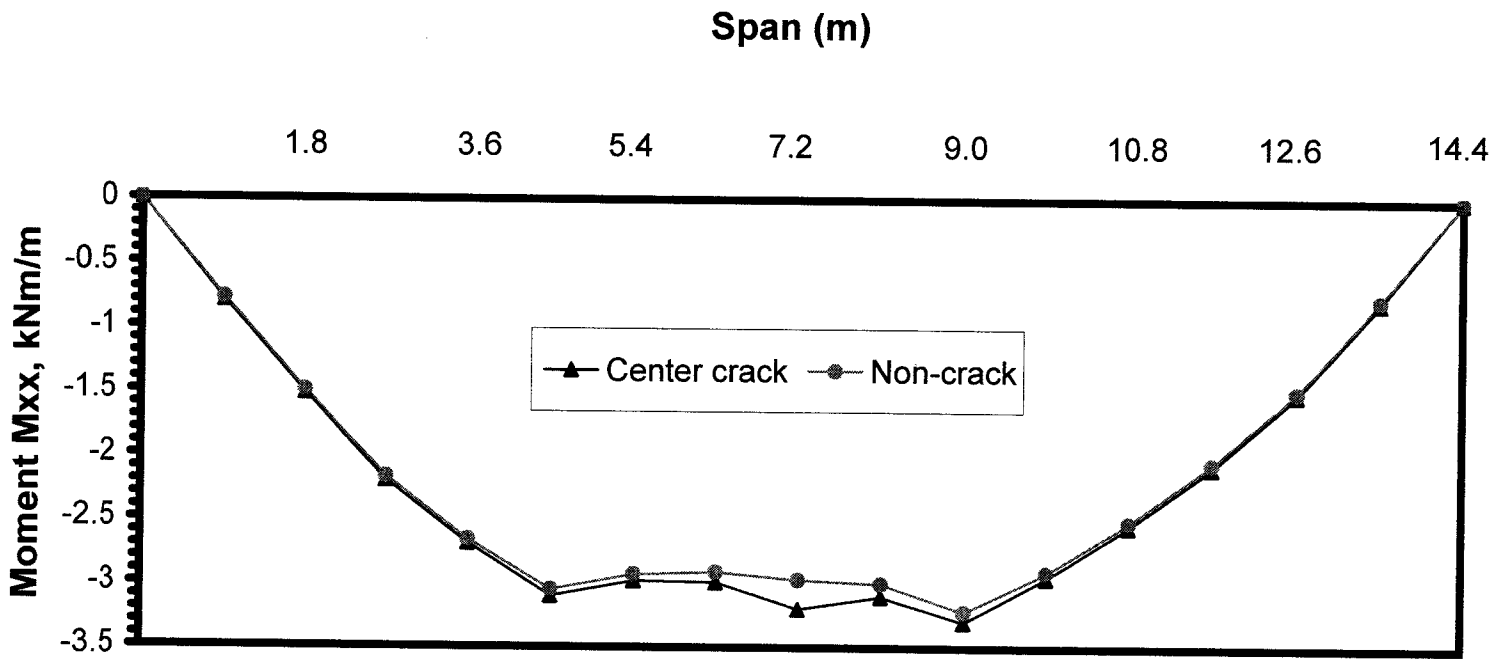

Figure 7.8 Longitudinal moment along A-A, in two-span slab bridge

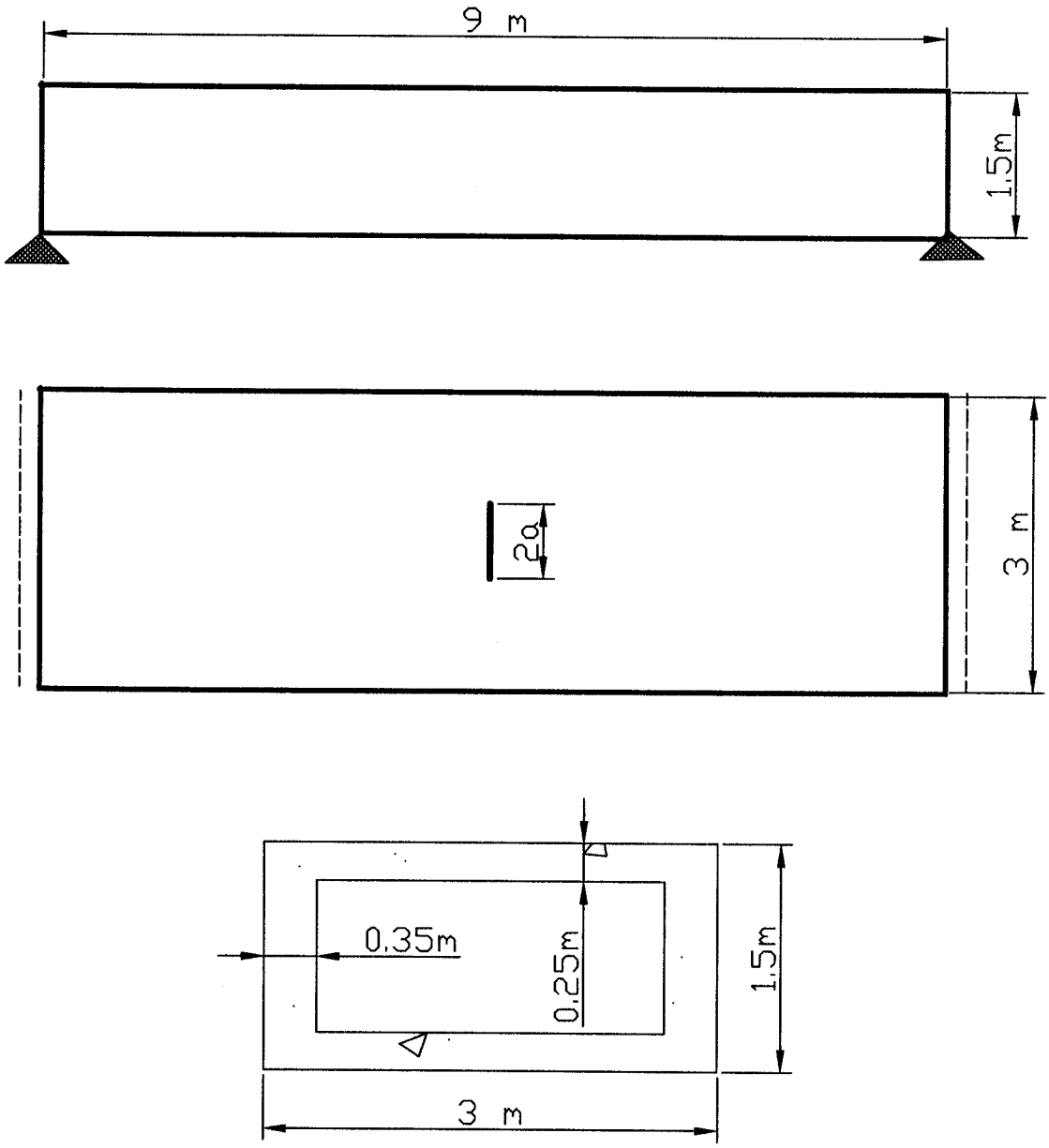

Figure 7.9 Single-cell box girder bridge

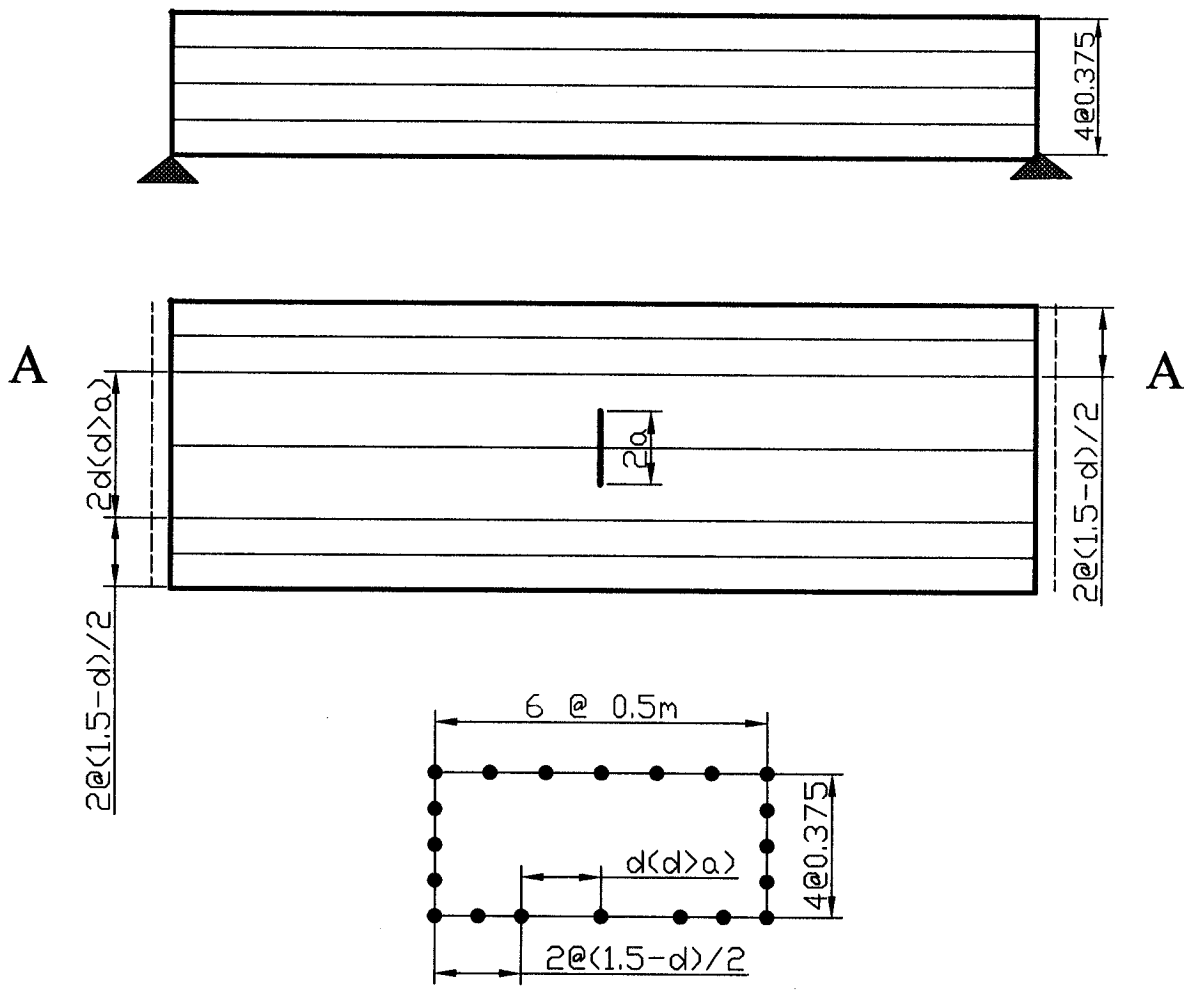

Figure 7.10 Finite strip mesh of single-cell bridge
(If no crack, $a = 0$, then $d = 0.5$)

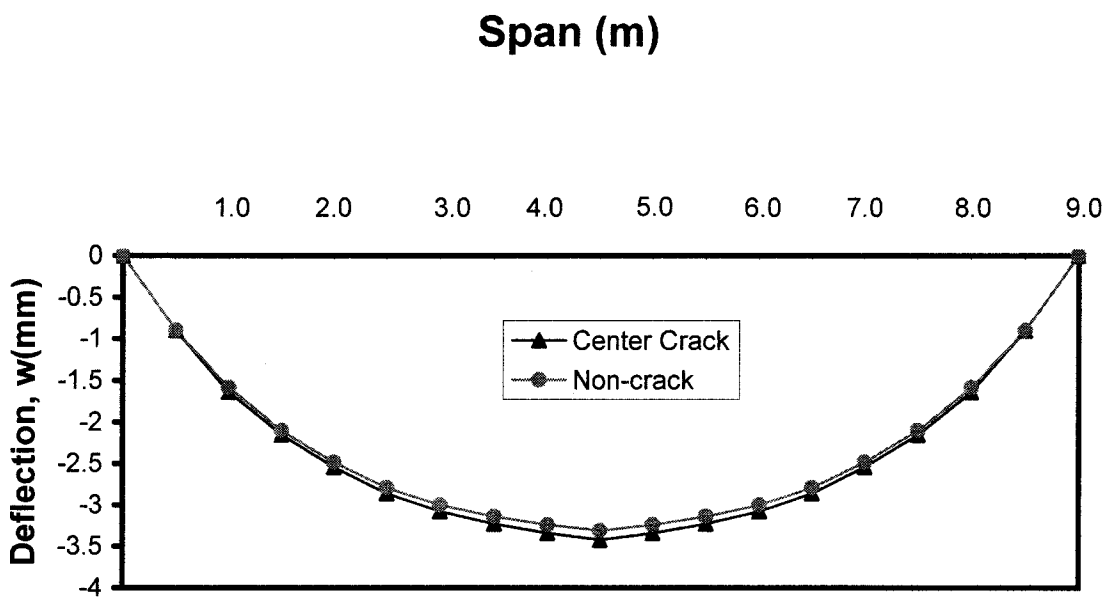

Figure 7.11 Vertical deflection along A-A, on the bottom slab

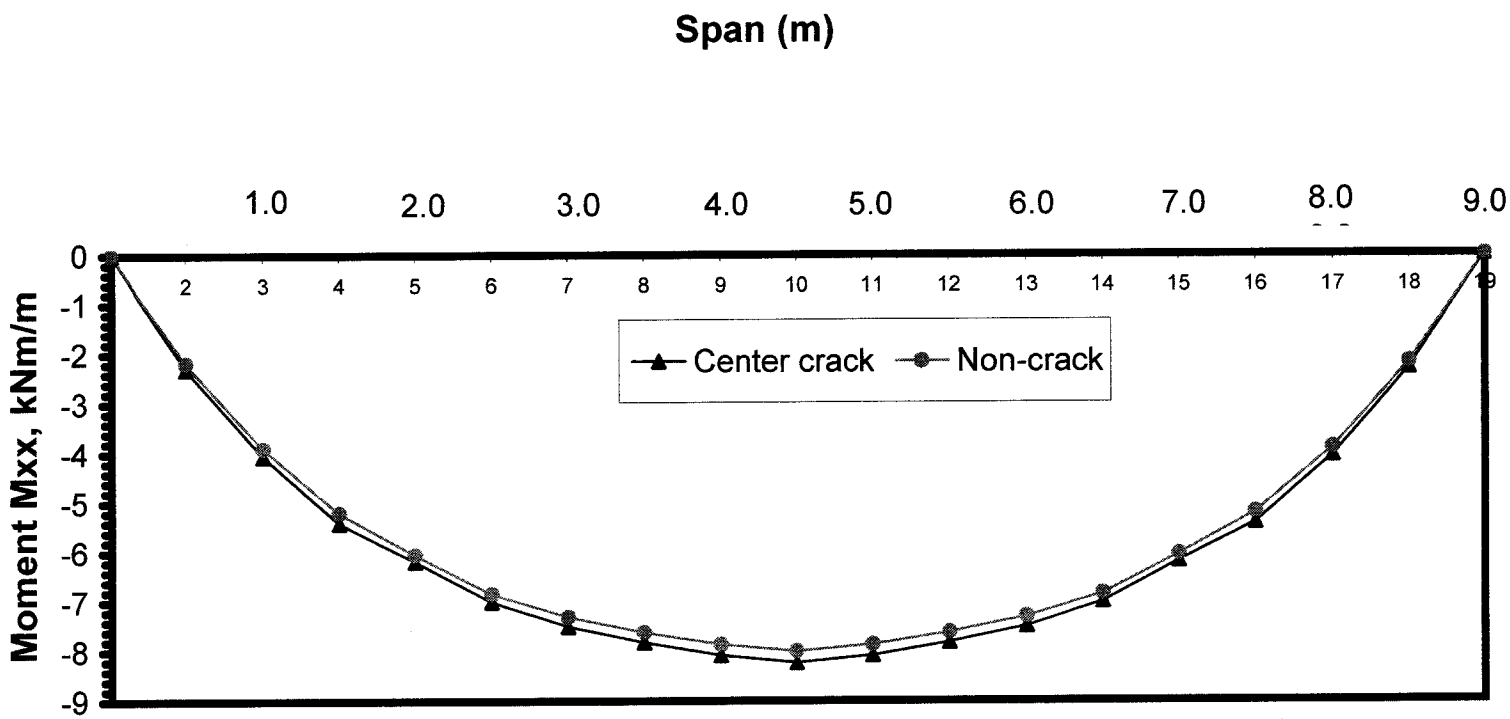

Figure 7.12 Longitudinal moment along A-A, on the bottom slab

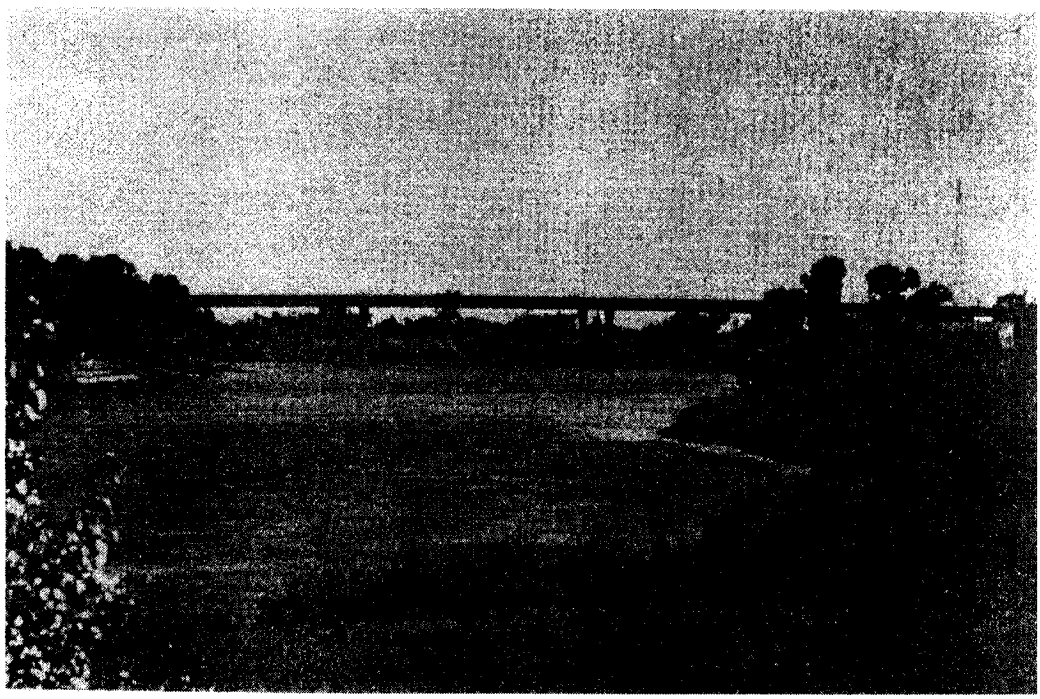

Figure 7.13 Over View of Bryte Bend Bridge

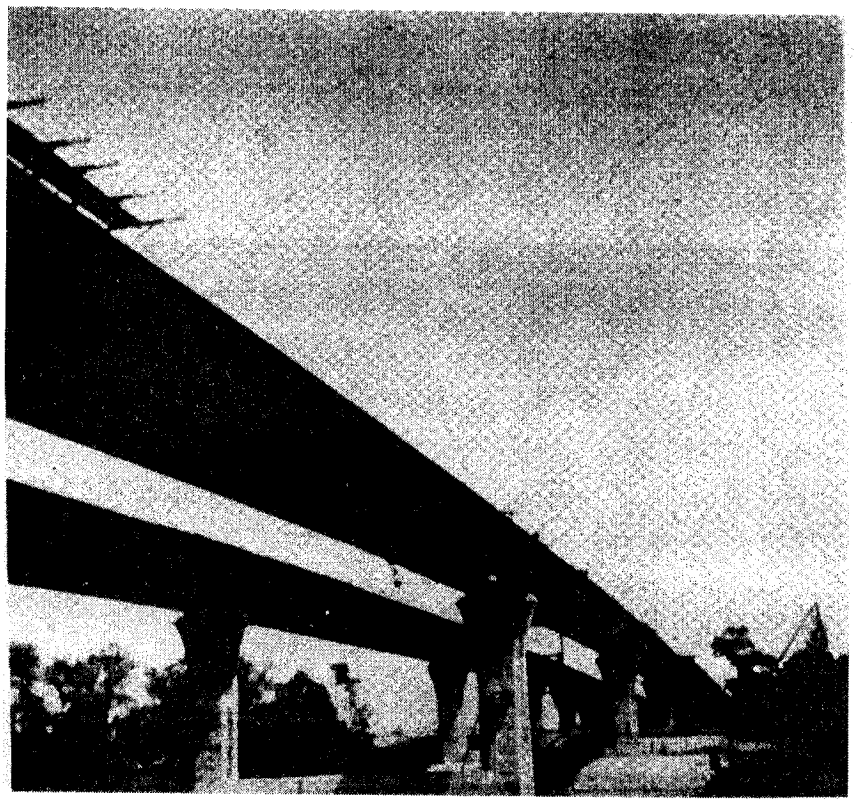

Figure 7.14 View of Twin Structures over River

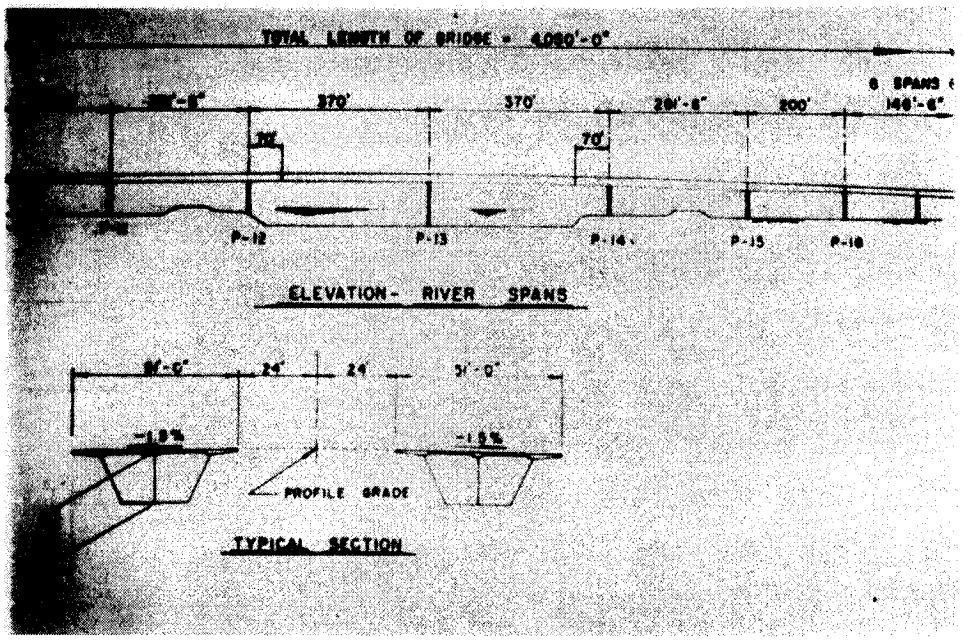

Figure 7.15 Sections and Elevation of 4050 ft. Long Structure

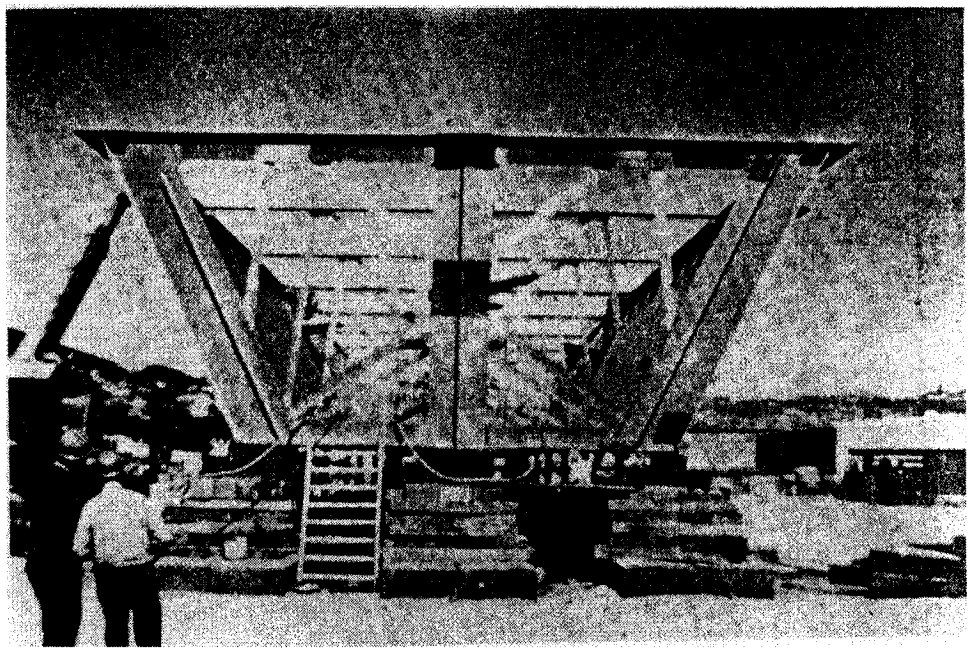

Figure 7.16 Cross-section of Box Girder

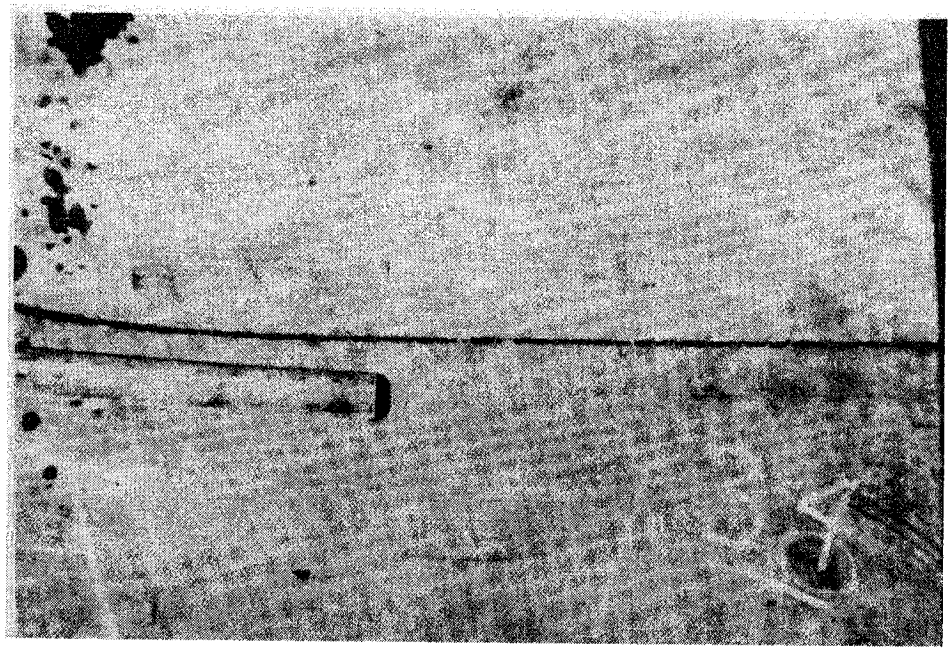

Figure 7.17 Plan View of Brittle Fracture in Flange

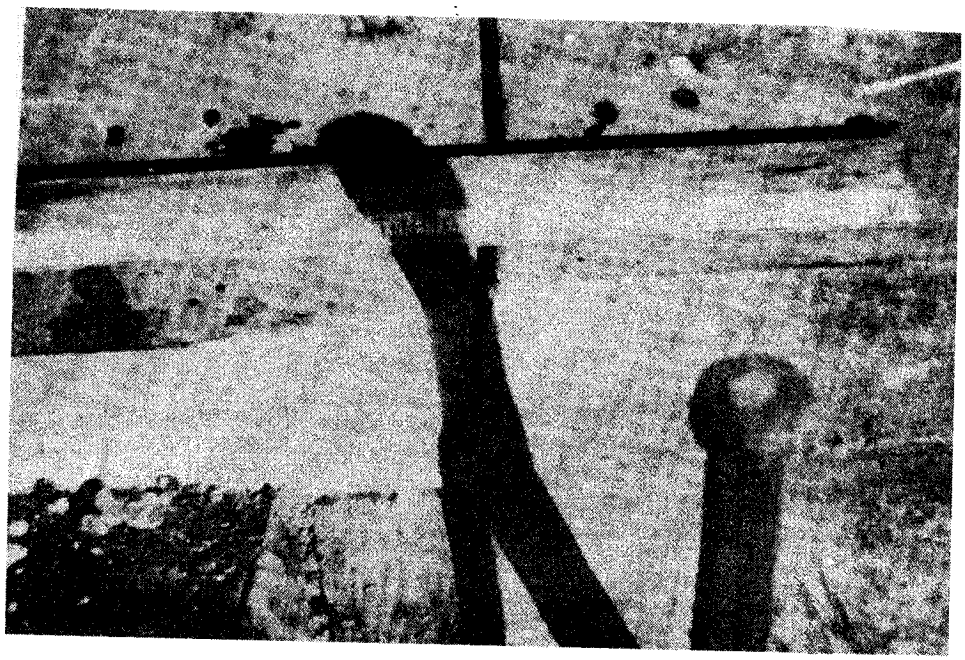

Figure 7.18 Brittle Fracture Origin at Intersection of Lateral Attachment and Flange Plate

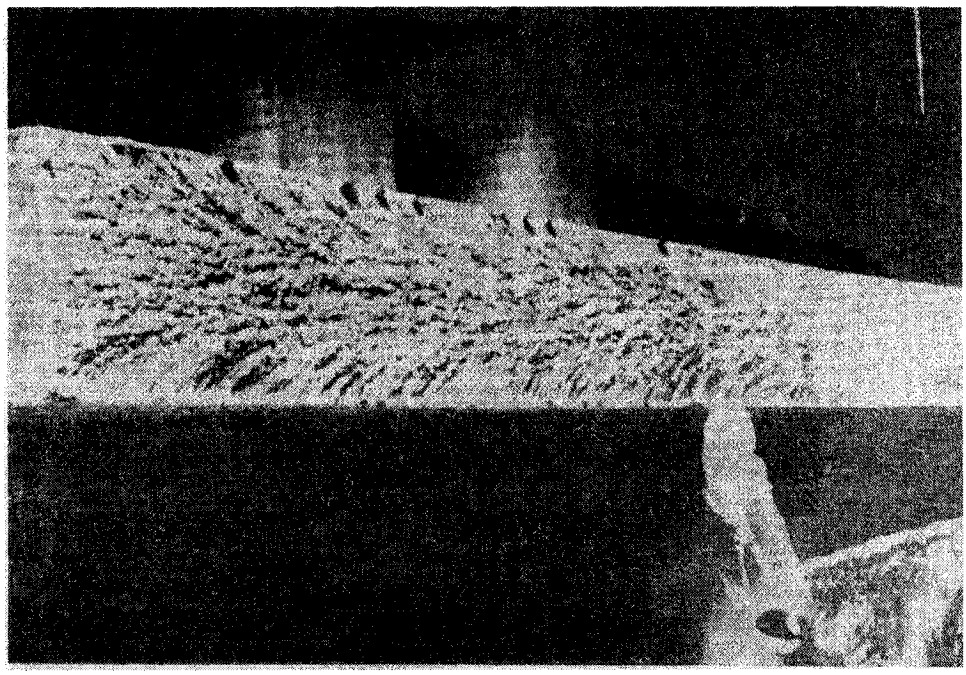

Figure 7.19 Brittle Fracture Surface Showing Classic Herringbone Pattern and Shear Lips

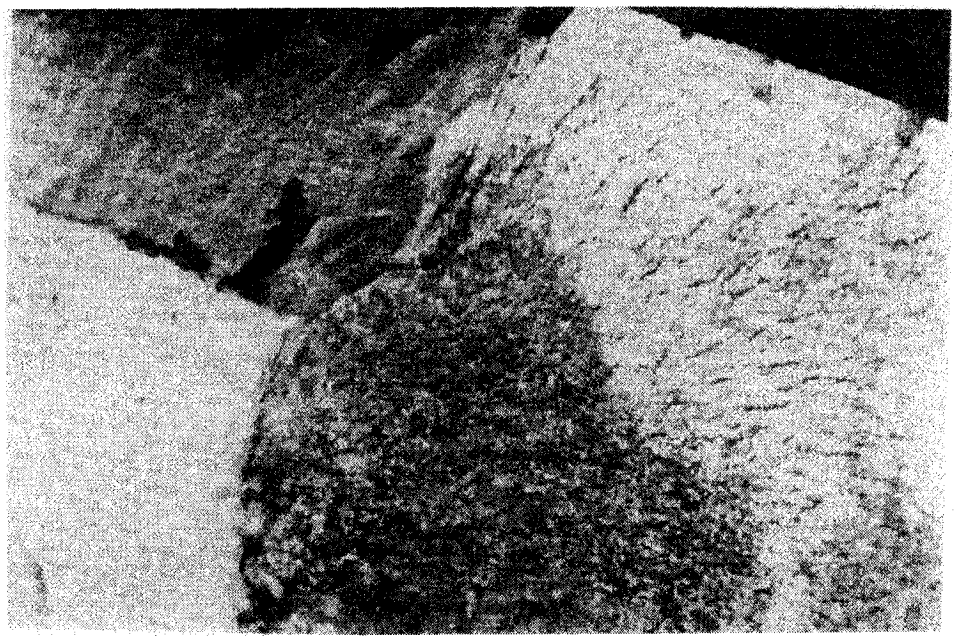

Figure 7.20 Origin of Fracture Showing 0.2 inch Deep Weld Crack and 1.3 inch Deep Crack

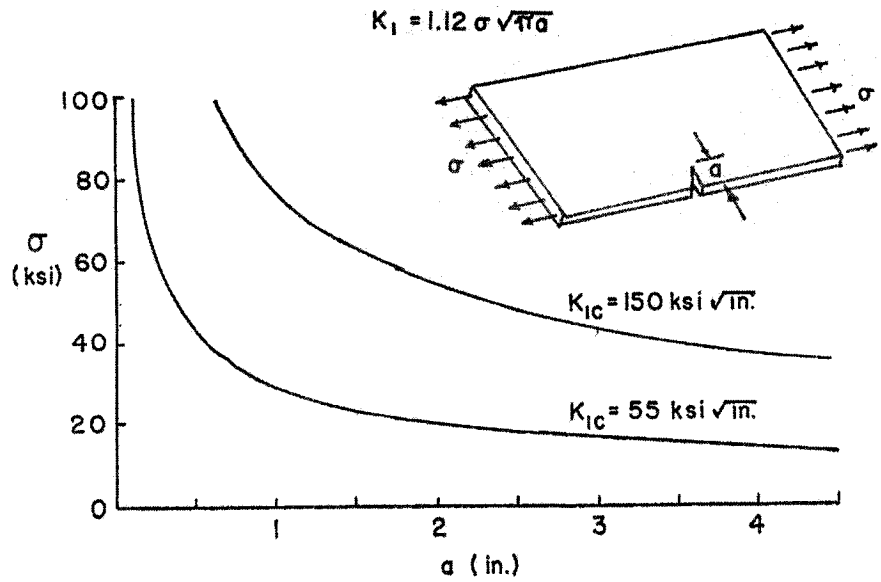

Figure 7.21 Stress-flaw-size Relation for Edge Crack in Steel

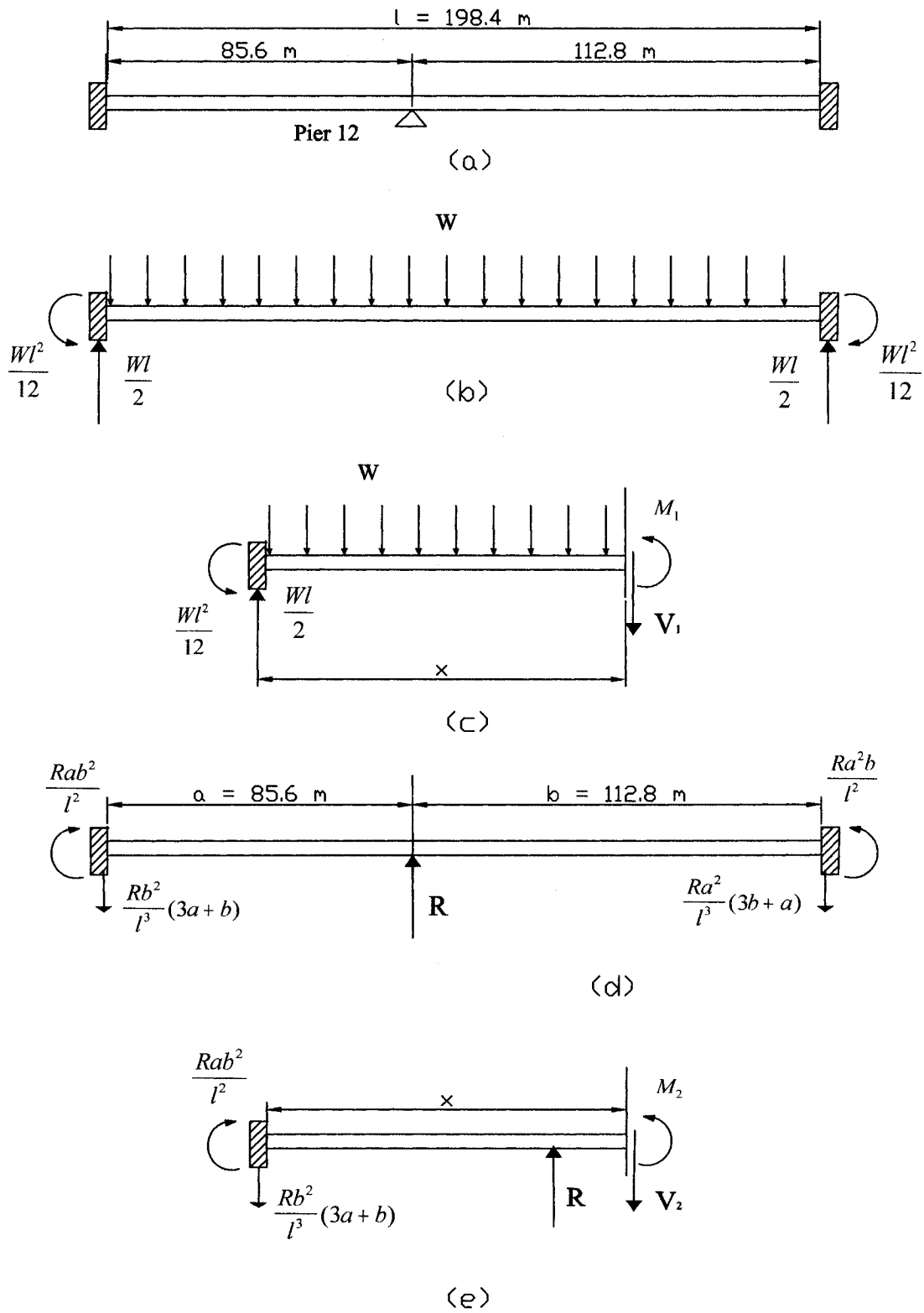

Figure 7.22 Simulation of two spans of Bryte Bend Bridge

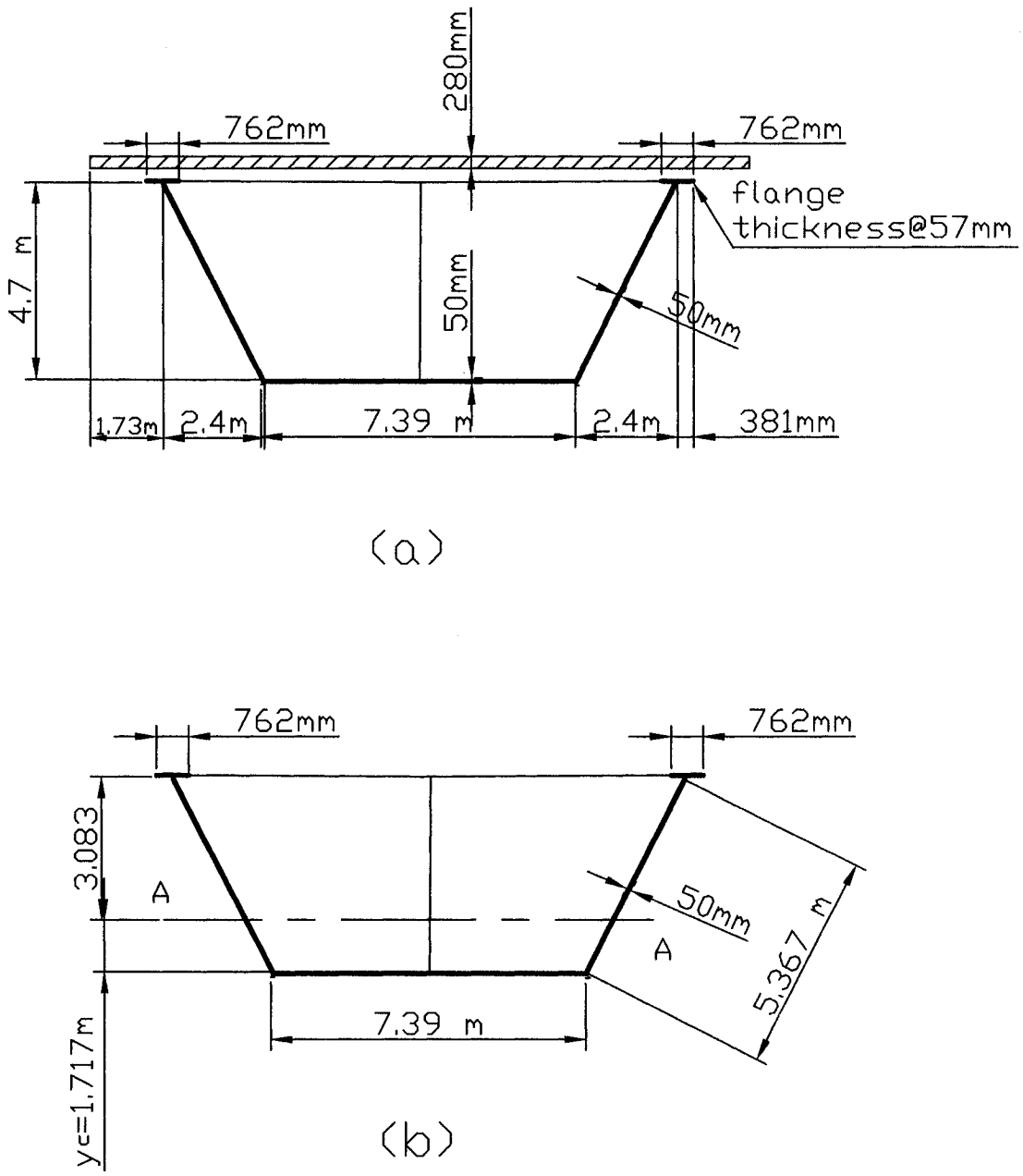

Figure 7.23 Cross-section of top-open box girder

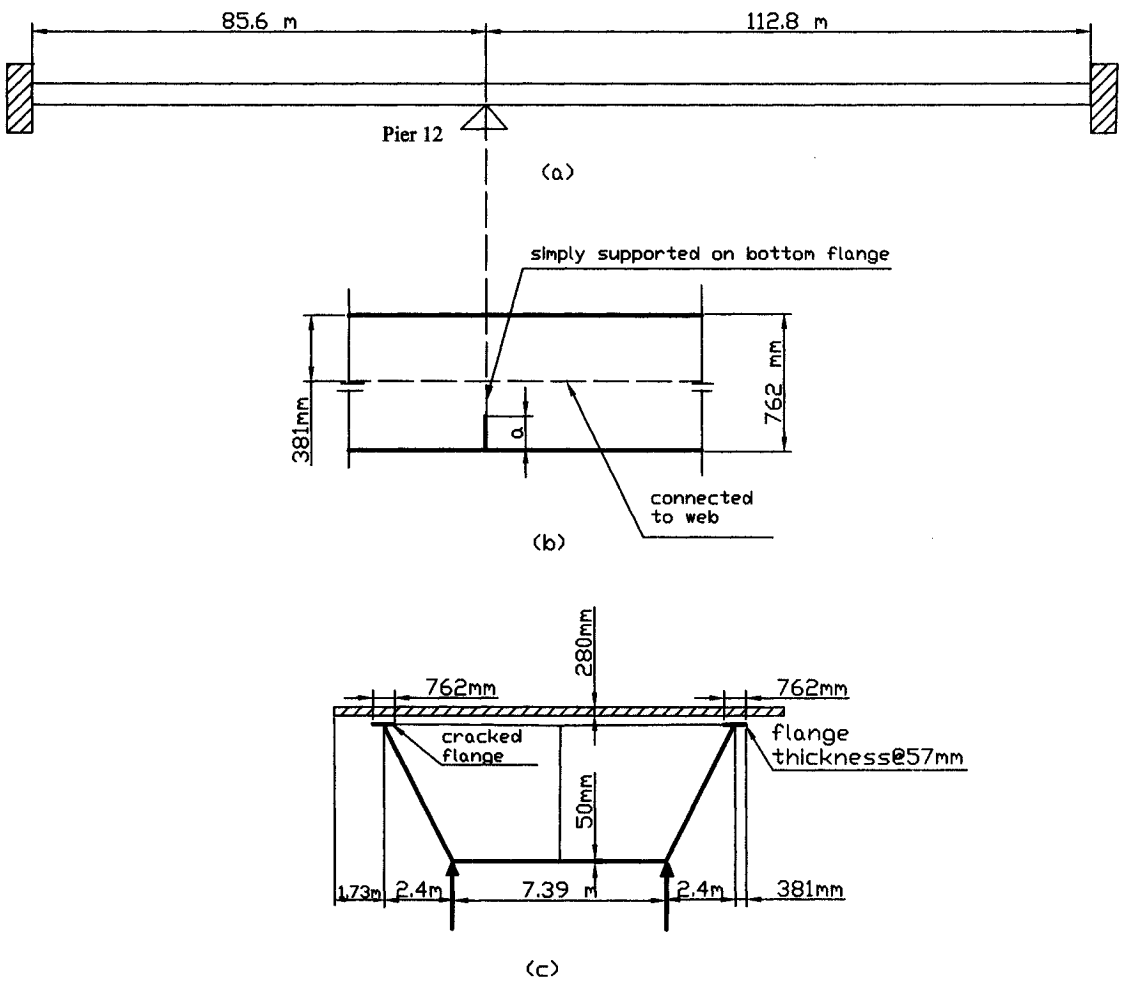

Figure 7.24 Cracked Bryte Bend Bridge
(a) Simulation of two spans
(b) Top flange with crack on edge inside
(c) Cross-section of box girder and deck

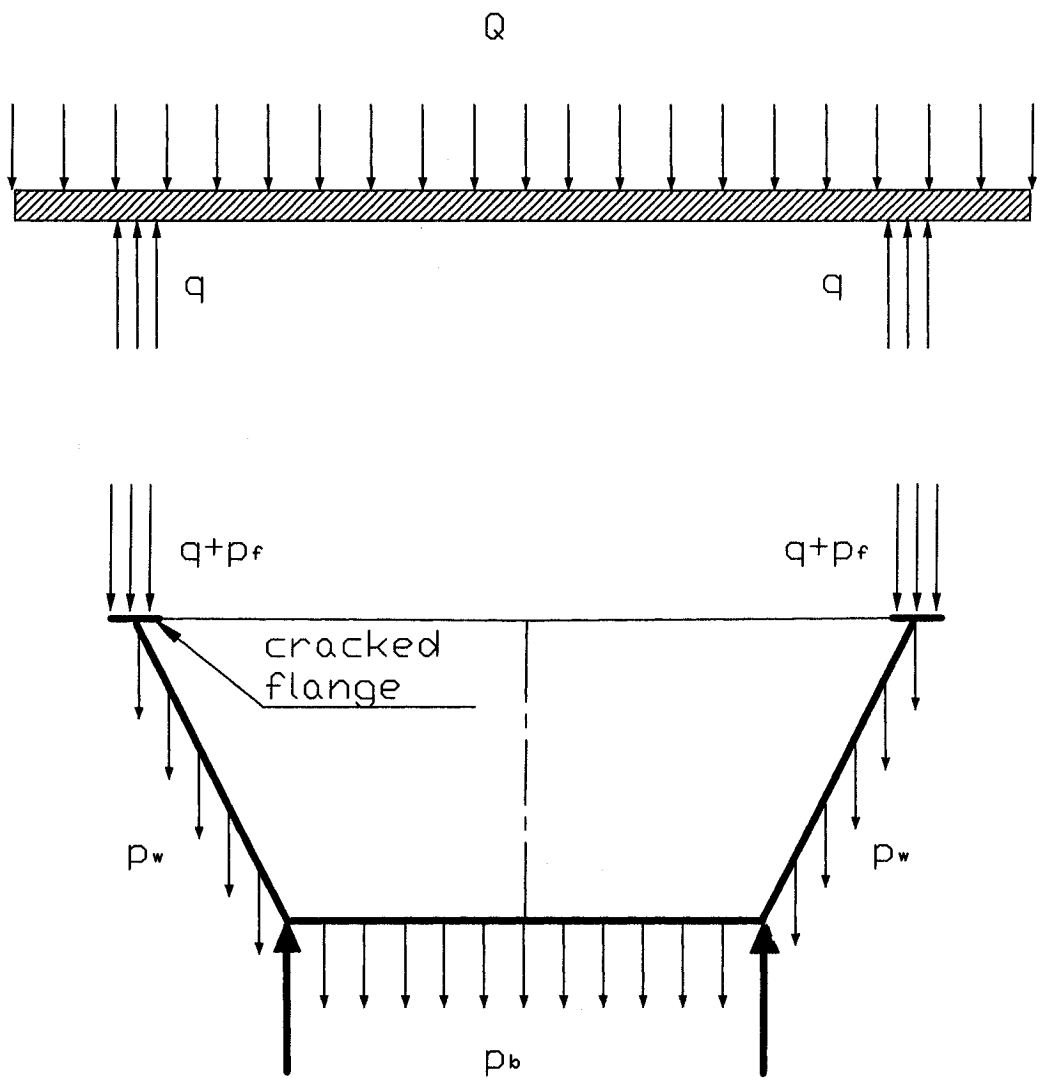

Figure 7.25 Assumption of uniform dead load on the top flange (q = 10.2 Q)

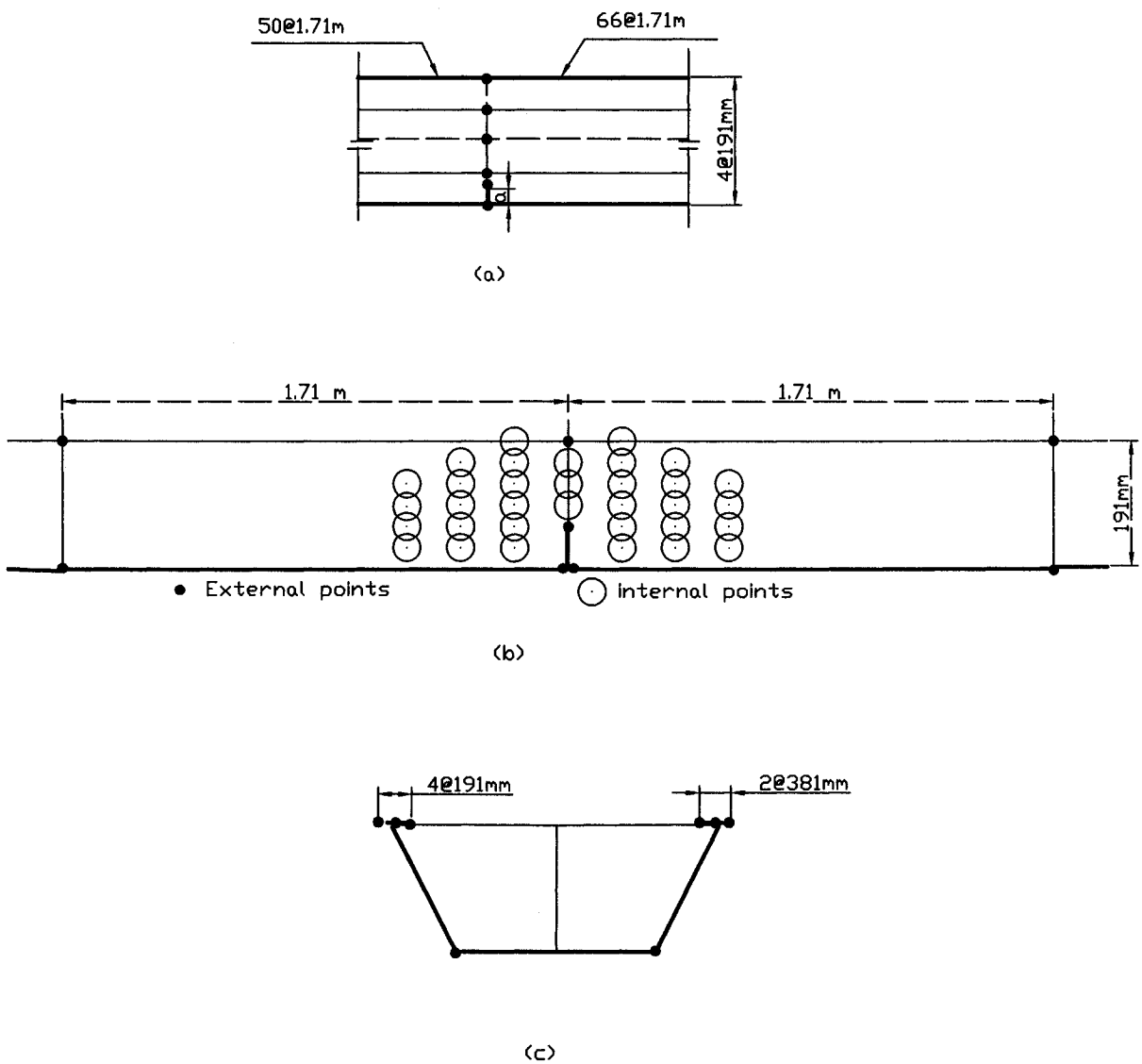

Figure 7.26 Finite strip mesh of the two spans
(a) Crack flange mashed
(b) extra knots surrounding the crack tip
(c) Cross-section of box girder mashed

Chapter 8

Conclusions and Recommendations

8.1 Summary and Conclusions

The primary objective of the present research is to conduct fracture analysis of bridge structures using finite strip method. Combining spline finite strip method with the

eigenfunction expansion at a crack tip, three types of crack strips, namely anti-plane shear crack strip, plane crack strip and bending crack strip, have been developed. The flat shell crack strip, as a combination of the plane crack strip and the bending crack strip, has been developed for the fracture analysis of box girder bridges. Several case studies have demonstrated the satisfactory convergence of the crack strip models. Fracture analysis of different types of bridges have been performed successfully using the proposed crack strips. Based on the results of these analysis, it can be concluded that:

1. The convergence of the crack strip model combined with the spline finite strips is satisfactory, as shown in several case studies.

2. The substructure technique and the extra nodes in the field near a crack tip play great roles in the convergence of the crack strip models.

3. The numerical examples show that, in dealing with the singular integral, Method I in Chapter 3 is more efficient than Method II.

4. Various types of bridges, such as slab bridge, continuous slab bridge, single - cell box girder bridge and continuous bridge with top-open box girder, can be successfully modeled by the crack strips.

5.These proposed crack strip methods are efficient in the fracture analysis of bridge structures

8.2 Recommendations

The convergence and efficiency of the crack strip models in bridge fracture analysis have been demonstrated through several case studies. If a plate structure is subjected to in-plane loading and out-of-plane bending, the flat shell crack strips can be employed, since in these strips the in-plane action and out-of-plane bending are uncoupled, and the related stress intensity factors can be calculated independently. However, if a plate structure is subjected to both bending and torsion, the suitable crack strip has not been developed yet. The reason is that current crack strips include the analytical solution for either anti-plane mode or bending mode, but not both. Both of these two modes include deflection w, making it difficult to determine the contribution of each separately . Thus, the following works are recommended for further studies:

1. To develop the combination of the anti-plane crack model and the bending crack model, and then to conduct the fracture analysis of bridge structures subjected to unsymmetrical deformation, resulted from unsymmetrical loads or angle cracks.

2. The crack strip model can be extended to dynamic fracture analysis of bridge structures.

3. All the methods presented in this study can be extended to more complicated geometries of bridges, such as skew, curved and arbitrary shaped bridges.

8.2.1 Angle Cracks in Bending Plate

In actual bridge structures, most cracks occur in the direction of a principal stress, which may not be parallel to the transverse or longitudinal axis of the bridge. This is the case especially in the webs of a bridge girder. However, in a bending plate or flat shell, the angle crack will result in the coupling of anti-plane mode and bending mode. As a result, the three fracture modes, K_I, K_{II} and K_{III} exist together.

Consider an angle crack in a plate subjected to a bending moment M, as shown in **Fig. 8.1**. This load induces bending moments M_1, M_2 and twisting moment M_{12} in the local coordinate system at the crack tip, as shown in **Fig. 8.2.** By means of the coordinate transformation, the following relationships can be obtained:

$$\begin{aligned} M_1 &= M\sin^2\theta \\ M_2 &= M\cos^2\theta \\ M_{12} &= M\sin\theta\cos\theta \end{aligned} \qquad (8-1)$$

Only M_1 and M_{12}, but not M_2, have contribution to the moment intensity factors k_I, k_{II} and k_{III}. According to Sih (1973), these moment intensity factors can be evaluated as follows:

$$k_I = \Phi(1) M_1 \sqrt{a}$$
$$k_{II} = \Psi(1) M_{12} \sqrt{a} \qquad (8-2)$$
$$k_{III} = -\frac{\sqrt{10}}{(1+\nu)t} \Omega(1) M_{12} \sqrt{a}$$

where the functions $\Phi(1)$, $\Psi(1)$ and $\Omega(1)$ are calculated from integral equations numerically (Sih 1977). Then, the stress intensity factors K_I, K_{II} and K_{III} can be evaluated as

$$K_I = (12z/t^3) k_I$$
$$K_{II} = (12z/t^3) k_{II} \qquad (8-3)$$
$$K_{III} = (3/2t)[1-(2z/t)^2] k_{III}$$

Because anti-plane mode and bending mode are coupled in the fracture analysis of an angle crack in a bent plate, great effort may be required in order to separate bending crack mode and anti-plane shear crack mode, in future studies.

8.2.2 Dynamic Analysis of Cracked Plates in Bending

When applied loads are time dependent, the inertia effect can no longer be ignored in the equilibrium of cracked plates. On the basis of Kirchhoff theory of plate bending, the equation of motion is governed by

$$D\nabla^4 w + \rho t \frac{\partial^2 w}{\partial T^2} = q(T) \qquad (8-4)$$

where ρ is the mass density of the material, t is the thickness of the plate and T is the time. In spline finite strip analysis, equation (8 – 4) can be discretized into:

$$[M]\{\ddot{w}\} + [K]\{w\} = \{p\} \qquad (8-5)$$

Where [M] and [K] are the mass and stiffness matrices separately.

When a vehicle, as a source of impact, passes a bridge with constant velocity as shown in **Fig. 8. 3**, the applied load can be expressed as

$$q = p\delta(x - vT, y) \qquad (8-5)$$

where p is the weight of the vehicle, $\delta(x - vT, y)$ is defined as:

$$\delta(x - vT, y) = \begin{cases} 0 & (x \neq vT \quad or \quad y \neq 0) \\ \infty & (x = vT \quad and \quad y = 0) \end{cases}$$

$$\int_{-\infty}^{\infty} \int_{-\infty}^{\infty} \delta(x - vT, y) dx dy = 1 \qquad (8-6)$$

To form the mass matrix [M] and deal with time derivative of the defections using spline strips and crack strips, great effort is also required in future studies.

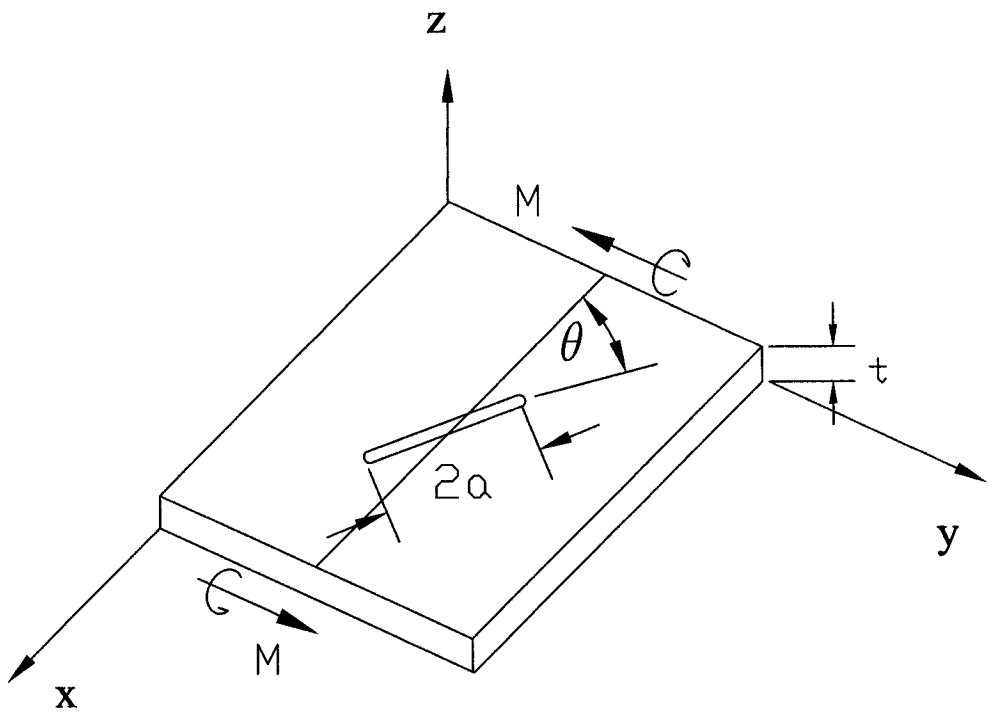

Figure 8.1 Angle crack under bending

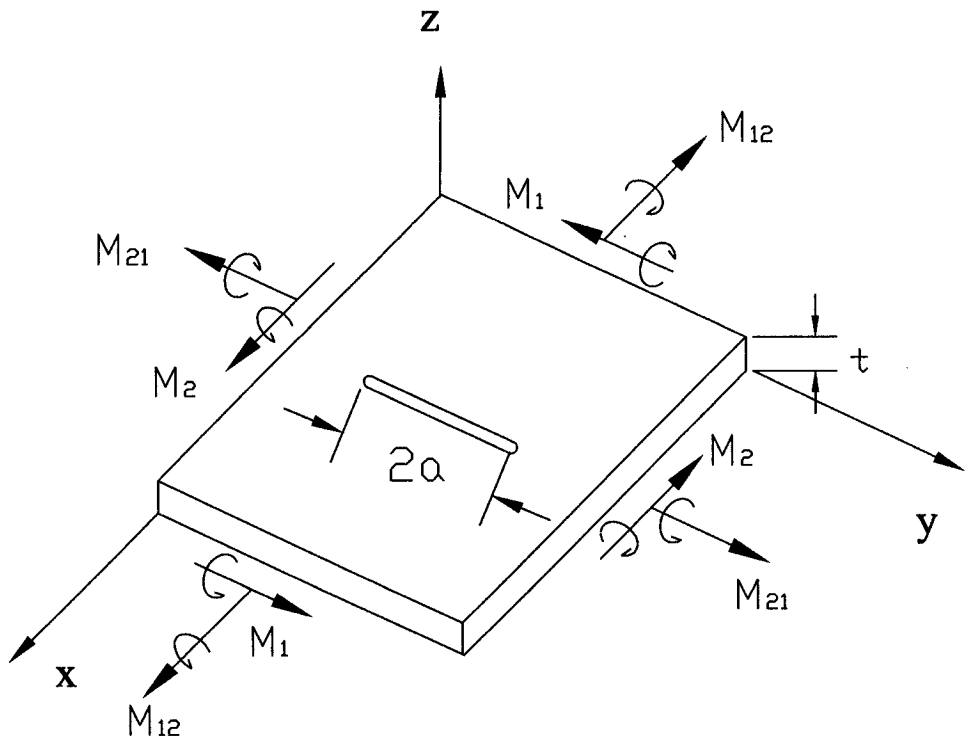

Figure 8.2 Combined bending and twisting

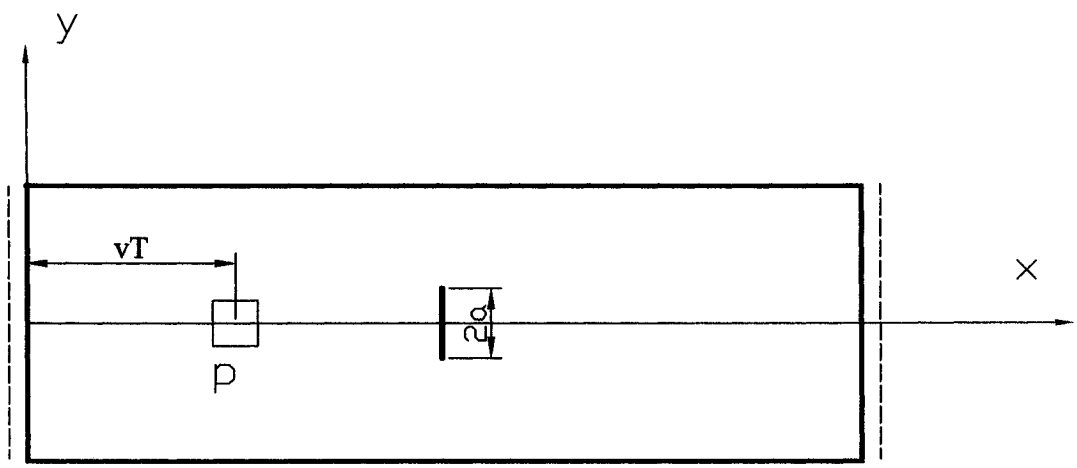

Figure 8.3 A vehicle passes cracked bridge with constant velocity *v*

Appendix

Gaussian Quadrature Formulas

A. $\int_{-1}^{1} f(x)dx \cong \sum_{i=1}^{N} A_i f(x_i)$

N	x_i	A_i
N = 2	0.57735026918962576450	(1)0.10000000000000000000
N = 3	0.77459666924148337703 0.00000000000000000000	0.55555555555555555555 0.88888888888888888888
N = 4	0.86113631159405257522 0.33998104358485626480	0.34785484513745385737 0.65214515486254614262
N = 5	0.90617984593866399279 0.53846931300568309103 0.00000000000000000000	0.23692688505618908751 0.47862867049936646804 0.56888888888888888888
N = 6	0.93246951420315202781 0.66120938646626451366 0.23861918608319690863	0.17132449237917034504 0.36076157304813860756 0.46791393457269104738
N = 7	0.94910791234275852452 0.74153118559939443986 0.40584515137739716690 0.00000000000000000000	0.12948496616886969327 0.27970539148927666790 0.27970539148927666790 0.41795918367346938775

N = 8	0.96028985649753623168 0.79666647741362673959 0.52553240991632898581 0.18343464249564980493	0.10122853629037625915 0.22238103445337447054 0.31370664587788728733 0.36268378337836198296
N = 9	0.96816023950762608983 0.83603110732663579429 0.61337143270059039730 0.32425342340380892903 0.00000000000000000000	(-1)0.81274388361574411971 0.18064816069485740405 0.26061069640293546231 0.31234707704000284006 0.33023935500125976316
N = 10	0.97390652851717172007 0.86506336668898451073 0.67940956829902440623 0.43339539412924719079 0.14887433898163121088	(-1)0.66671344308688137593 0.14945134915058059314 0.21908636251598204399 0.26926671930999635509 0.29552422471475287017

B. $\int_0^\infty e^{-x} f(x)dx \cong \sum_{i=1}^{N} A_i f(x_i)$

N	x_i	A_i
N = 8 e = (-4)0.7770	0.1702796323 0510099979 0.9037017767 9937991219 (1)0.2251086629 8661306893 (1)0.4266700170 2876587936 (1)0.7045905402 3934656972 (2)0.1075851601 0180995224 (2)0.1574067864 1278004578 (2)0.2286313173 6889264105	0.3691885893 4163752992 0.4187867808 1434295607 0.1757949866 3717180569 (-1)0.3334349226 1215651522 (-2)0.2794536235 2256725249 (-4)0.9076508773 3582131042 (-6)0.8485746716 2725315448 (-8)0.1048001174 8715103816

N = 19	(-1)0.7415878375 7205087713	0.1767684749 1591250225
	0.3912686133 1999460733	0.3004781436 0725437948
e = (-10)0.2829	0.9639573439 9795805862	0.2675995470 3817503077
	(1)0.1796175582 0683281255	0.1599133721 3558021678
	(1)0.2893651381 8737839911	(-1)0.6824937997 6149112355
	(1)0.4264215539 6277664743	(-1)0.2123930760 6544324924
	(1)0.5918141561 6440485581	(-2)0.4841627351 1483959672
	(1)0.7868618915 3347337310	(-3)0.8049127473 8136676659
	(2)0.1013242371 6815265925	(-4)0.9652472093 1535017084
	(2)0.1273088146 3842398004	(-5)0.8207305258 0510305440
	(2)0.1569127833 9835888545	(-6)0.4830566724 7307725394
	(2)0.1904899320 9823550153	(-7)0.1904991361 1232856999
	(2)0.2285084976 0829482932	(-9)0.4816684630 9280615576
	(2)0.2716066932 7411448878	(-11)0.7348258839 5511443768
	(2)0.3206912225 1862242322	(-13)0.6202275387 5726163989
	(2)0.3771290580 1219649477	(-15)0.2541430843 0154227237
	(2)0.4431736279 5831496119	(-18)0.4078861296 8257123500
	(2)0.5231290245 7404383165	(-21)0.1707750187 5938370610
	(2)0.6280242315 3500375841	(-11)0.6715064649 9081899599

N = 30	(-1)0.4740718054 0804811461	0.1160440860 2039325561
	0.2499239167 5316022399	0.2208511247 5069602167
e = (-17)0.8456	0.6148334543 9276828461	0.2413998275 8787346416
	(1)0.1143195825 6661007982	0.1946367684 4641672700
	(1)0.1836454554 6225722914	0.1237284159 6688099223
	(1)0.2696521874 5572151957	(-1)0.6367878036 8988269340
	(1)0.3725814507 7795089493	(-1)0.2686047527 3380519411
	(1)0.4927293765 8498824096	(-2)0.9338070881 6042351496
	(1)0.6304515590 9650745228	(-2)0.2680696891 3369005385
	(1)0.7861693293 3702604687	(-3)0.6351291219 4087764640
	(1)0.9603775985 4792620798	(-3)0.1239074599 0688661704
	(2)0.1153654659 7956139700	(-4)0.1982878843 8952961055
	(2)0.1366674469 3064236294	(-5)0.2589350929 1314845837
	(2)0.1600222118 8981066254	(-6)0.2740942840 5360851638
	(2)0.1855213484 0143150124	(-7)0.2332831165 0257961682
	(2)0.2132720432 1783128927	(-8)0.1580745574 7783781036
	(2)0.2434003576 4532693400	(-10)0.8427479123 0570478544
	(2)0.2760555479 6780961027	(-11)0.3485161234 9079771460
	(2)0.3114158670 1111235818	(-12)0.1099018059 7534727279
	(2)0.3496965200 8249069543	(-14)0.2588312664 9592354134
	(2)0.3911608494 9067889121	(-16)0.4437838059 8403008661
	(2)0.4361365290 8484827806	(-18)0.5365918308 2123539536
	(2)0.4850398616 3804200427	(-20)0.4393946892 2917157783
	(2)0.5384138540 6507505617	(-22)0.2311409794 3886493589
	(2)0.5969912185 9235495477	(-25)0.7274588498 2925408322
	(2)0.6618061779 4438489651	(-27)0.1239149701 4482743994
	(2)0.7344123859 5559882239	(-31)0.9832375083 1056357108
	(2)0.8173681050 6727685722	(-34)0.2842323553 4027969143
	(2)0.9155646652 2536838255	(-38)0.1878608031 7495715678
	(3)0.1041575244 3105889451	(-44)0.8745980440 4651875591

C. $\int_0^1 \ln(\frac{1}{x}) f(x)dx \cong \sum_{i=1}^{N} A_i f(x_i)$

N	x_i	A_i
N = 8 e = 0.03465	(-1)0.1332024416 0892465012 (-1)0.7975042901 3894938409 0.1978710293 2618805379 0.3541539943 5190941967 0.5294585752 3491727770 0.7018145299 3909996383 0.8493793204 4110667604 0.9533264500 5635978876	0.1644166047 2800288683 0.2375256100 2330602050 0.2268419844 3191912636 0.1757540790 0607024498 0.1129240302 4675905185 (-1)0.5787221071 7782072398 (-1)0.2097907374 2132978043 (-2)0.3686407104 0276190133
N = 12 e = 0.02118	(-2)0.6548722279 0800587892 (-1)0.3894680956 0449959161 (-1)0.9815026310 6006628862 0.1811385815 9063157735 0.2832200676 6737255470 0.3984344351 6343664370 0.5199526267 9235266272 0.6405109167 1610645430 0.7528650120 5183057837 0.8502400241 6230220067 0.9267496832 2391410104 0.9777561296 8999747917	(-1)0.9319269144 3931324491 0.1497518275 7632236417 0.1665574543 6459300532 0.1596335594 3698765116 0.1384248318 6483562106 0.1100165706 3572116233 (-1)0.7996182177 0828970264 (-1)0.5240695482 4641770650 (-1)0.3007108887 3761187123 (-1)0.1424924558 7998279107 (-1)0.4899924582 3217609390 (-1)0.8340290380 5690336469
N = 16 e = 0.01616	(-2)0.3897834487 1159159240 (-1)0.2302894561 6873239820 (-1)0.5828039830 6240412348 0.1086783650 9105403648 0.1726094549 0984393776 0.2479370544 7057849514 0.3320945491 2991715598 0.4221839105 8194860011 0.5150824733 8146260347 0.6075561204 4772872408 0.6963756532 2821406115 0.7784325658 7326540520 0.8508502697 1539108323 0.9110868572 2227190541 0.9570255717 0354215759 0.9870478002 4798447675	(-1)0.6079171004 3591232851 0.1029156775 1758214438 0.1223556620 4600919355 0.1275692469 3701598871 0.1230135746 0007091542 0.1118472448 5548572262 (-1)0.9659638515 2124341252 (-1)0.7935666435 1473138782 (-1)0.6185049458 1965207095 (-1)0.4543524650 7726668628 (-1)0.3109897475 1581806409 (-1)0.1945976592 7360842078 (-1)0.1077625496 3205525645 (-2)0.4972542890 0876417125 (-2)0.1678201110 0511945150 (-3)0.2823537646 6843632177

References

[1] **Anderson, T. L.** (1995), *Fracture Mechanics, Fundamentals and Applications*, Second Edition CRC Press.

[2] **Azizian, Z. G.** and **Dawe, D. J.** (1985), *Geometrically nonlinear analysis of rectangular Midlin plates using the finite strip method*, Comput. Struct., Vol. 21, No.3, 423-436.

[3] **Beskos, D. E.**(1989), *Boundary element methods in structural analysis,* Prepared under the auspices of the Committee on Electronic Computation of the Structural Division of the American Society of Civil Engineers, New York, N.Y. : ASCE, c1989.

[4] **Bueckner, H. F.,** 1958, *The Propagation of Cracks and Energy of Elastic Deformation,* Trans. ASME, J. of Basic Engineering, Vol. 80, 1225 - 1229.

[5] **Byskov, E.** (1970), *The calculation of stress intensity factors using the finite element method with cracked elements*, Int. J. Fracture Mechanics, Vol.6, 159 - 167.

[6] **Cai, C. W., Liu, M. J.** and **Huang, C. M.** (1983), *An arbitrarily high order singular strain finite element for calculating the stress intensity factor in plane problems,* Acta Mech. Solid. Sinica, Vol.4, 597-605.

[7] **Chajes, A.** (1983), *Structural Analysis,* Prentice-Hall, Inc., Englewood Cliffs.

[8] **Chen, J.L.** and **Chong, K.P.** (1984), *Vibration of Irregular Plates by Finite Strip Method with Spline Function,* Engineering mechanics in Civil Engineering, Proc. of the 5th Engineering Mechanics Div., ASCE, Edited by Boresi, A.P. and Chong, K.P., 1, 256-260.

[9] **Chen, J.L.** and **Chong, K.P.** (1985), *Buckling of Irregular Plates by Finite Strip Method with Spline Function,* Collection of Technical Papers-AIAA/ASME/ASCE/AHS 26th Structures, Structural Dynamics and Material Conference, Part 1, 147-151, AIAA, New York.

[10] **Chen, M.J., Tham, L.G.** and **Cheung, Y.K.** (1984), *Spline Finite Strip for parallelogram Plate,* Proceedings, International Conference on Accuracy Estimates and Adaptive Refinements in Finite Element Computation (ARFEC), Lisbon, Vol.1, 95-104.

[11] **Cheung, M.S.** and **Li, W.** (1990), *Analysis of Haunched Continuous Bridges by Spline Finite Strips,* Comput. Struct. Vol. 36, No. 2, 297-300.

[12] **Cheung, M.S., Li, W.** and **Jaeger, L.G.** (1992), *Spline Finite Strips Analysis of Continuous Haunched Box-Girder Bridges,* Can. J. Civil Eng., Vol.19, 724-728.

[13] **Cheung, M.S., Ng, S.F.** and **Zhao, J.Q.** (1993), *Analysis of Curved Reinforced Concrete Slab Bridges by the Spline Finite Strip Method,* Can. J. Civil Eng., Vol. 20, 855-862.

[14] **Cheung, M.S., Li, W., and Chidiac, S.E.** (1996), *Finite Strip Analysis of Bridge*, London; E & FN Spon.

[15] **Cheung, P., Dade, H.** and **Zongmu, W.** (1987), *Static, Vibration and Stability Analysis of Stiffened Plates Using B Spline Functions,* Comput. Struct., Vol.27, No.1, 73-78.

[16] **Cheung, Y. K.** (1968), *The Finite Strip method in the Analysis of Elastic Plates with Two Opposite Simply Supported Ends,* Proc.Inst.Civ.Eng., Vol. 40, 1-7.

[17] Cheung, Y. K., Fan, S.C. and **Wu, C.Q.** (1982), *Spline Finite Strip in Structure Analysis,* Proceedings, The International Conference on Finite Element Method, Shanghai, 704-709.

[18] Cheung, Y. K., and **Fan, S.C.** (1983), *Static Analysis of Right Box Girder Bridges by Spline Finite Strip method,* Proc. Inst. Civ. Eng., Part 2, Vol.75, 311-323.

[20] Cheung, Y.K., Tham, L.G. and **Li, W.Y.** (1986), *Application of Spline-Finite-Strip Method in the Analysis of Curved Slab Bridges,* Proc. Inst. Civ. Eng., Part 2, Vol. 81, 111-124.

[21] Cheung, Y.K., Tham, L.G. and **Li, W.Y.** (1988), *Free Vibration and Static Analysis of General Plate by Spline Finite Strip,* Comput. Mech., Vol.3, 187-197.

[22] Cheung, Y. K. and **Jiang, C. P.** (1996), *Application of the finite strip method to plane fracture problem*, Fracture Mechanics, Vol.53, No.1, 89-96.

[23] Cheung, Y. K. and **Tham, L. G.** (1998), *Finite Strip Method,* CRC Press LLC.

[24] Chong, K.P. and **Chen, J.L.** (1986), *Bulking of Irregular Plates by Spline Finite Strips,* AIAAJ, Vol. 24, 534-536.

[25] Cook, R.D., Malkus, D.S., and Plesha, M.E., (1989): Concepts and Applications of Finite Element Analysis, 3rd edn. Wiley, New York.

[26] Dawe, D. J. and **Wang, S.** (1995), *Spline finite strip analysis of the bulking and vibration of rectangular composite laminated*, Int. J. Mech. Sci. Vol.37, No.6, 645-667.

[27] Griffith, A. A., 1920, *The Phenomenon of Rupture and Flow in Solids,* Phil. Trans. Roy. Soc., London, Series A, Vol. 221, p163.

[28] Holston, A. (1976), *A mixed mode crack tip finite element.* Int. J. of Fracture 12, p887-899.

[29] Irwin, G. R. (1948), *Fracture Dynamics,* in Fracturing of metals, edited by F. Jonassen et

al., 147-166.

[30] **Irwin, G. R.** and **Kies, J. A.** (1952), *Fracturing of Fracture Dynamics,* The Welding Journal, Res. Suppl., Vol.31, p95.

[31] **Irwin, G. R.** (1957), *Analysis of Stress and Strain near the End of a Crack Transversing a Plate*, Trans, ASME, J. Appl. Mech., Vol.24, p361.

[32]**Kobayashi, A. S.** (1973), *Experimental Techniques in Fracture Mechanics,* SESA Monograph, edited by A. S. Kobayashi, p18.

[33] **Kong, J.** and **Cheung, Y. K.** (1993), *Application of the spline finite strip to the analysis of shear- deformable plates,* Comput. Struct. Vol. 46, 985-988.

[34] **Lau, S.C.W.** and **Hancock, G.J.** (1986), *Buckling of Thin Flate-Walled Structures by Spline Finite Strip method,* Thin-Walled Struct., Vol. 4, No.4, 269-294.

[35] **Leicester, R. H.** (1971), *Some aspects of stress fields at sharp notches in orthotropic materials – I,* CSIRO Div. Forest Products Technique Paper, No. 57.

[36] **Li, S., Reid, S. R.** and **Soden, P. D.** (1994), *A finite strip analysis of cracked laminates*, Mechanics of Materials, Vol.18, 289-311.

[37] **Li, W.Y., Cheung, Y.K** and **Tham, L.G.** (1986), *Spline Finite Strip Analysis of General Plate*s, J. of Eng. Mech., ASCE, Vol. 112, No.1, Jan.

[38] **Luxmoore, A. R.** and **Owen, D. R. J.** (1978), *Numerical methods in fracture mechanics* : proceedings of the First International Conference held at University College, Swansea, U.K on 9th-13th January.

[39] **Luxmoore, A. R.** and **Owen, D. R. J.** (1984), *Numerical methods in fracture mechanics* :proceedings of the Third International Conference held at University College, Swansea, U.K

on 26th-30th March, 1984, Pineridge Press.

[40] Mason, J. C., Smith, R. N. L. and **Thompson, R. M.** (1984), *Stress intensity factor evaluation by boundary element methods for crack at hole,* in Numerical methods in fracture mechanics : proceedings of the Third International Conference held at University College Swansea, Swansea, U.K on 26th-30th March, 1984, Pineridge Press.

[41] Mizusawa, T. (1988), *Application of Spline Strip Method to Analyse Vibration of Open Cylindrical Shells,* Int. J. Num. Meth. Eng., Vol. 26, No. 3, 663-676.

[42] Muskhelishvili, N. (1963), *Some Basic Problem of the Mathematical Theory of Elasticity*, P. Noordhoff, groningen, Neth.

[43] Ohtmer, O. (1984), *Applying analysis functions to define special boundary elements in an elasto- plastic problem with singularity idealized by finite elements*, in Numerical methods in fracture mechanics : proceedings of the Third International Conference held at University College Swansea, Swansea, U.K on 26th-30th March, 1984, Pineridge Press.

[44] Orowan, K. (1949), *Fracture and Strength of Solids.* Report on Progress in Physics, Physics Soc., London, Vol. 12, 185-232.

[45] Paris, P. C., 1957, *The Mechanics of Fracture Propagation and Solutiona to Fracture Arrester Problems*, Document D2-2195, The Boeing Company.

[46] Rice, J.R. (1968), *A Path Independent Integral and the Approximate Analysis of Strain Concentration by Notches and Cracks,* J. of Appl. Mech., Vol. 35, 379-386.

[47] Roberts, R (1977), *Fracture Mechanics for Bridge Design,* v.1, Washington, Federal Highway Administration.

[48] Roberts, R (1977), *Fracture Mechanics for Bridge Design,* v.2, Washington, Federal Highway Administration.

[49] Sih, G. C. (1973), *Handbook of Stress Intensity Factors*, Leheigh University, Bethlehem, Pennsylvania, U. S. A..

[50] Sih, G. C. (1977), *Plates and Shell with Cracks, Mechanics of fracture* v.3, Noordhoof International Publishing, Leyden.

[51] Stroud, A. H. and **Secrest, D.** (1966), *Gaussian Quadrature Formulas*, Prentice-Hall, New York.

[52] Swedlow, J.L. (1972), *Surface Crack: Physical problems and Computational Solutions,* ASME, New York.

[53] Tada, H., Paris, P. C. and **Irwin, G. R.** (2000), *The Stress Analysis of Cracks handbook.* (3rd Ed.), ASME Press..

[54] Tham, L.G., Li, W.Y., Cheung, Y.K. and **Chen, M.J.** (1986), *Bending of Skew Plates by Spline-finite-strip Method,* Comput. Struct., Vol. 22, No.1, 31-38

[55] Tilley, D. R. (1978), *Removal of the singularity from the numerical solution to a crack problem,* in Numerical methods in fracture mechanics : proceedings of the First International Conference held at University College Swansea, Swansea, U.K on 9th-13th Jan..

[56] Walsh, P. F. (1971), *The computation of stress intensity factors by a special finite element technique,* Int. J. Solid Structures., Vol. 7, 1333 - 1342, Oct..

[57] Watwood, V.B. (1969), *The Finite Element Method for Prediction of Crack Behavior,* Nuclear Eng. And Design, Vol. 1, 323-332.

[58] Westergaard, H. M. (1939), *Bearing Pressures and Crack,* Trans, ASME, J. Appl. Mech., Series A, Vol.66, p49.

[59] Westmann, R. A. and **Yang, W. H.** (1967), *Stress analysis of cracked rectangular beam,* J. Appl. Mech., Vol.34, p693.

[60] Williams, M. L. (1957), *On the stress distribution at the base of stationary crack,* J. Appl. Mech., ASME Vol. 24, 109-114.

[61] Williams, M. L. (1961), *The bending stress distribution at the base of stationary crack,* J. Appl. Mech., ASME, Vol. 28, 78-82.

[62] Wilson, W. K. (1972), *Some Crack Tip Finite Elements for Plane Elasticity,* ASTM STP Vol. 513, 90-105.

[63] Wilson, W. K. (1973), *Finite element methods for elastic bodies containing cracks,* in Mechanics of Fracture, Noordhoff International, leyden.

[64] Wu, C. P., Wang, Y. M. and **Hung, Y. C.** (2001), *Asymptotic finite strip analysis of doubly curved laminated shells,* Comput. Mech., Vol. 27, 107-118.

[65] Zhu, D.S and **Cheung, Y.K.** (1989), Postbuckling Analysis of Shells by Spline Finite Strip Method, Computer and Structures, Vol. 31, No. 3, 357-364.